Downloaded from orbit.dtu.dk on: May 05, 2023

DTU Library

Validation and industrial application of AFM

Kofod, Niels

Publication date:
2002

Document Version
Publisher's PDF, also known as Version of record

Link back to DTU Orbit

Citation (APA):
Kofod, N. (2002). *Validation and industrial application of AFM*. IKON Tekst & Tryk A/S.

General rights
Copyright and moral rights for the publications made accessible in the public portal are retained by the authors and/or other copyright owners and it is a condition of accessing publications that users recognise and abide by the legal requirements associated with these rights.

- Users may download and print one copy of any publication from the public portal for the purpose of private study or research.
- You may not further distribute the material or use it for any profit-making activity or commercial gain
- You may freely distribute the URL identifying the publication in the public portal

If you believe that this document breaches copyright please contact us providing details, and we will remove access to the work immediately and investigate your claim.

Validation and industrial application of AFM

Niels Kofod

Ph.D-Thesis
Kgs. Lyngby July 2002

Department of Manufacturing Engineering and Management
Materials and Process Technology
Technical University of Denmark

and

Danish Institute of Fundamental Metrology

Titel:	Validation and industrial application of AFM A Ph.D and industrial researcher project
Keywords:	Surface metrology, Atomic Force Microscopy, Coordinate measuring machine, Instrument construction, Validation, Calibration, Traceability, Integrated systems, Industrial application
Publication:	Ph.D-Thesis
Author:	Niels Kofod
Finished:	July 2002
University	Department of Manufacturing Engineering and Management Technical University of Denmark Produktionstorvet, building 425 DK-2800 Kgs. Lyngby www.ipl.dtu.dk
Company:	Danish Institute of Fundamental Metrology Matematiktorvet, building 307 DK-2800 Kgs. Lyngby www.dfm.dtu.dk
Publication ID:	IPL publication nr: IPL.004.02 MM publication nr: MM02.04 DFM publication nr: DFM-02-phd.01 ISBN 87-90855-36-1 ISSN 1397-0305
Printed by:	IKON Tekst og Tryk A/S, Vedbæk, Denmark

Copyright © 2002 Niels Kofod

PREFACE

This thesis has been prepared as one of the requirements of the industrial researcher and Ph.D- degree. This thesis represented the 2nd version of this thesis.

The work has been carried out from January 1999 to January 2002 at The Danish Institute of Fundamental Metrology (DFM) and The Institute of Manufacturing Engineering and Management (IPL), Technical University of Denmark (DTU). The work has been carried out under supervision from Dr. Jørgen Garnæs, DFM, Dr. Techn. Leonardo De Chiffre, IPL/DTU and Dr. Hans Nørgaard Hansen.

I would like to thank my supervisors for their inspiration and valuable contributions to my work. Furthermore the staff from DFM and IPL/DTU is thanked for their interest and involvement. Image Metrology APS and Dr. Jan Friis Jørgensen in particular are thanked for their support and collaboration within the area of image analysis. Finally I would like to thank Dr. Kai Dirscherl and Mr. René Sobiecki for their big help to my project, and the Myhrwold foundation for financial support.

ADC Denmark A/S has been an informal third part of this project represented by Jesper B. Rasmussen.

The work has been funded by the Danish Academy of Technical Sciences (ATV) and DFM.

Lyngby, July 2002

Niels Kofod

ABSTRACT (ENGLISH)

The scope of this industrial researcher project has been to develop nanometer and micrometer scale characterization of surface topography with AFM methods to a metrological accepted measuring method, with traceability and stated uncertainty, also regarding specimens with a complex geometry.

The present work contains a study of the state-of-the-art in current design and establishment of traceability of transfer standards for SPMs.

A general approach for calibration and a calibration procedure for a metrology AFM (MAFM) is proposed and elaborated / developed. Algorithms for lateral calibration based on an oblique 2D-calibration standard was developed and tested during the work in connection with participation in intercomparisons (Nano4). A vertical calibration based on guidelines described in ISO 5436 was introduced and applied for the MAFM. Three important correction terms developed for the approach were introduced (Nano2). Traceability was established by means of transfer standards covering X, Y and Z. The MAFM was validated during participation in two intercomparisons. Only the results for pre key or key comparisons are reported in this thesis. A key-comparison named Nano4 concerning a determination of an average pitch distance of two line standards. Nano2 is an on-going pre-key comparison for step height measurements. The work has lead to a successful verification and validation of the MAFM. Furthermore the first step for an accredited service for AFM measurement has been established in terms of validated calibration procedures.

The calibration and industrial application of an integrated system for topographic characterization of fine surfaces on large workpieces is presented. The system, consisting of an atomic force microscope mounted on a coordinate measuring

machine, was especially designed for surface mapping, i.e. measurement and tiling of adjacent areas. A calibration procedure was proposed involving a glass artefact featuring different pitch distances giving the possibility to identify the exact position of single surface areas. The calibrated system was used to surface map a hip joint prosthesis consisting of a steel sphere with a polished surface.

ABSTRACT (DANISH)

Formålet med dette erhvervsforskerprojekt er at udvikle metrologisk accepterede metoder for nanometer- og mikrometer karakterisering af overfladetopografi ved brug af AFM. Dette sker igennem sporbarhedsetablering og usikkerhedsberegning.

Det præsenterede arbejde indeholder et litteraturstudie og en beskrivelse af state-of-the-art inden for design og sporbarhedsetablering af overførselsnormaler til SPM.

Der er udviklet og præsenteret en generel beskrivelse af kalibrering og kalibreringsprocedurer gældende for et metrologi AFM (MAFM). Algoritmer for lateral kalibrering baseret på en "skæv" 2D-kalibreringsnormal er udviklet og testet via deltagelse i internationale sammenligninger. En vertikal kalibreringsprocedure baseret på retningslinier beskrevet i ISO 5436 er udviklet og anvendt på et MAFM. Det tre væsentligste korrektionsparametre gældende for denne metode er identificeret og bestemt. Etablering af sporbarhed for X,Y og Z er opnået via brugen af sporbare overførselsnormaler. MAFM er valideret igennem deltagelse i to store internationale sammenligninger. Den første sammenligning (Nano4) omhandlede bestemmelsen af en gennemsnitlig gentagelsesafstand af to 1D-normaler. Nano2 er en igangværende sammenligning til bestemmelse af stephøjder. Arbejdet har ført til en succesfuld verifikation og validering af MAFM. Endvidere er det første skridt taget i forbindelse med etablering af en akkrediteret service for AFM målinger med afsæt i de udviklede procedurer.

Der er blevet udviklet og kalibreret et integreret system for topografisk karakterisering af fine overflader på store emner. Systemet er en sammenbygning af et AFM og en koordinatmålemaskine, og er specielt velegnet til surface mapping (en opmåling og sammenstykning af arealer, der ligger side om side). En kalibreringsprocedure er udviklet med

afsæt i en glasnormal indeholdende et mønster, som gør det muligt at identificere den eksakte position af hvert enkelt areal. Det kalibrerede system er anvendt til karakterisering af et hofte implantat (protese) vha. surface mapping.

PUBLICATION LIST

Following is a list of international publications and technical reports used in the thesis of which I am a co-author. Some of the listed publications concern directly my work while others represent more brief contributions. My own involvement is graduated (G) from 1 to 5 where 1 represents minor contributions and 5 high degree of involvement. In the thesis the involved publications that will be mentioned correspond to the chapter in which they have been used. The publications do not cover in detail all the work presented in this thesis.

Publication	Used in chapter	G
K. Carneiro, L. Nielsen, J. Garnaes, A. Kühle, K. Dirscherl, N. Kofod, "SPM metrology in Denmark" European society for precision engineering and nanotechnology: Proceedings of the 1st Topical Conference on Fabrication and Metrology in Nanotechnology, Copenhagen May 28-30, Vol 1, page 1-9 (2000).	1,2	(1)
J. Garnaes, N. Kofod, J. F. Jørgensen, A. Kühle, P. Besmens, O. Ohlson, J. B. Rasmussen, G. Wilkening, L. Koenders, W. Mirande, K. Hasche, J. Haycocks, J. Nunn, M. Stedman, "Nanometer scale transfer Standards", Vol. 2, pp. 134-137, Shaker-Verlag, 1st EuSPEN conference May-June 1999.	2	(1)
J. Garnaes, N. Kofod, J. F. Jørgensen, A. Kühle, P. Besmens, O. Ohlson, J. B. Ramussen, G. Wilkening, L. Koenders, W. Mirande, K. Hasche, J. Haycocks, J. Nunn, M. Stedman, "Standards for Scanning Probe	2	(1)

Publication	Used in chapter	G
Microscopes", pp.632-633, 10th international conference on Scanning Tunneling Microscopy / spectroscopy and related Techniques, Seoul, Korea, July 1999.		
J. Garnaes, N. Kofod, A. Kühle, P. Besmens, O. Ohlsson, J.B. Rasmussen, G. Wilkening, L. Koenders, W. Mirande, K. Hasche, J. Haycocks, J. Nunn, M. Stedman, "Standards for the calibration of SPMs: design - traceable calibration - application", X. International Colloquium on Surfaces, 31st january to 2nd February 2000.	2	(1)
J. Garnaes, N. Kofod, J. F. Jørgensen, P. Besmens, O. Ohlsson, J. B. Rasmussen, G. Wilkening, L. Koenders, W. Mirande, K. Hasche, J. Haycocks, J. Nunn, M. Stedman, "Transfer standards for scanning probe microscopes", Final report to the EU commission Directorate General 12 for the project SMT-CT95-2018 54 pages (Confidential) (2000).	2	(3)
N. Kofod, J. Garnaes, J.F. Jørgensen, "Calibrated line measurements with an Atomic Force Microscope", Vol. 1, pp. 373-381, 1st Topical EuSPEN conference, Lyngby, Denmark May-June 2000.	3,4	(5)
N. Kofod, J. Garnaes, J.F. Jørgensen, "Method for lateral calibration of Scanning Probe Microscopes based on two dimensional transfer standards", Proceedings of the 4th seminar on Quantitative Microscopy QM 2000 Dimensional	3,4	(5)

Publication	Used in chapter	G
measurements in the micro- and nanometre range, Edited by Klaus Hasche, Werner Mirandé, Günter Wilkening, Semmering, Austria, January 12-14 2000, PTB-Bericht, pp. 36-43 January 2000.		
J. Garnaes, N. Kofod, A. Kühle, C. Nielsen, K. Dirscherl, L. Blunt, "Traceable step height and roughness measurements with atomic force microscopes", 2nd International Conference in Euspen, May 2001 Italy, Vol 1, pp 514-517.	3,4	(4)
J. Garnaes, N. Kofod, A. Kühle, C. Nielsen, K. Dirscherl, L. Blunt, "Traceable step height and roughness measurements with atomic force microscopes" (for publication in Precision Engineering - 2002).	3,4	(4)
R. Breil, T. Fries, J. Garnaes, J. Haycocks, D. Huser, J. Joergensen, W. Kautek, L. Koenders, N. Kofod, K.R. Koops, R. Korntner, B. Lindner, W. Mirande, A. Neubauer, J. Peltonen, G.B. Picotto, M. Pisani, H. Rothe, M. Sahre, M. Stedman and G. Wilkening, “Intercomparison of Scanning Probe Microscopes”, Euspen 2001, Vol 1, pp. 510-513, Turin Italy.	3,4	(3)
N. Kofod, J. Garnaes, “Measurement Report” for participating in WGDM-7: Preliminary comparison on nano-metrology According to the rules of CCL key comparisons Nano4: 1D-gratings.	4	(5)
N. Kofod, J. Garnaes, “Measurement Report” for participating in WGDM-7: Preliminary	4	(5)

Publication	Used in chapter	G
comparison on nano-metrology According to the rules of CCL key comparisons Nano2: Step height.		
H.N. Hansen, N. Kofod, L. De Chiffre, T. Wanheim, "Calibration and Industrial Application of Instrument for Surface Mapping based on AFM", accepted for publication in Annals of the CIRP in 2002.	5	(5)
N. Kofod, H. N. Hansen, L. De Chiffre, "Integration of atomic force microscope on coordinate measuring machine", 3rd seminar on quantitative microscopy Nov.1998.	5	(5)
L. De Chiffre, H. N. Hansen, N. Kofod, "Surface topography characterization using an atomic force microscope mounted on a coordinate measuring machine", Annals of the CIRP, Vol. 48/1/1999 pp. 463-466.	5	(5)
N. Kofod, H. N. Hansen, L. De Chiffre, "Characterization of fine surfaces using an atomic force microscope mounted on a coordinate measuring machine", Vol. 2, pp. 278-281, Shaker-Verlag, 1st EuSPEN conference May-June 1999.	5	(5)

CONTENTS

NOMENCLATURE

SYMBOL	DESCRIPTION	UNIT
γ	The observed angle of 2D-grating	[°]
θ	Certified angle of 2D-grating	[°]
α	Angle deviation caused by the zig-zag motion of MAFM	[°]
(β)	Pitch geometry, flank steepness and vertical noise	
(n_i,m_j)	Number of periodical structures in the pattern.	
ΔZ_{ref}	Reference step height values	[nm]
a, b and γ	Are equal to the certified values L_a, L_b and θ.	
a_x	Unit cell components	[nm]
b_x	Unit cell components	[nm]
b_y	Unit cell components	[nm]
b_y	Unit Cell components	[nm]
a'_x	Uncorrected unit cell components	[nm]
b'_x	Uncorrected unit cell components	[nm]
b'_y	Uncorrected unit cell components	[nm]
b'_y	Uncorrected unit cell components	[nm]
$\underline{\underline{C}}$	Linear transformation matrix	
CC	Cross correlation method	
c_i	Sensitivity coefficient	
C_p	Corresponds to C_x, C_y, C_{xy}	
C_x	Correction factor covering the X-axis of AFM	
C_{XY}	Coupling term between X and Y of AFM	

SYMBOL	DESCRIPTION	UNIT
C_Y	Correction factor covering the Y-axis of AFM	
C_Z	Correction factor covering the Z-axis of AFM	
D_x	Associated with the stability of the measurement for X-direction	
D_y	Associated with the stability of the measurement for Y-direction	
E_N	E_N-value describing the deviation between measurement result of National metrology Institute and reference value compared to stated uncertainties	
K	Coverage factor	
L	Pitch distance of line grating used in Nano4	[nm]
L_a and L_b	Distances of the closest neighbours	[nm]
LMS	Least Mean Square plane	
LMS A	Least Mean Square Average profile	
LWL	Line wise levelling	
Max fl.	Max flatness	
n	Number of measurements	
p_k	Number of pixels in X and Y direction.	[µm]
PMF	Polynomial Fit Method with the order of n	
$S(\Delta Z_m)$	Experimental standard deviation of the observed step height	[nm]
Stdev	Standard deviation	[µm]
U_{Zm}	Expanded uncertainty of the observed step height	[nm]
X	X-coordinate	[mm]
X_PX	Positioning error X-axis	[µm]

SYMBOL	DESCRIPTION	UNIT
X_RX	Roll X-axis	[µrad]
X_RY	Pitch X-axis	[µrad]
X_RZ	Yaw X-axis	[µrad]
X_T	Stylus length in X-direction	[mm]
X_TY	Translatory error of X-axis in Y-direction	[µm]
X_TZ	Translatory error of X-axis in Z-direction	[µm]
XWY	Squareness XY	[µrad]
Y	Y-coordinate	[mm]
Y_PY	Positioning error Y-axis	[µm]
Y_RX	Pitch Y-axis	[µrad]
Y_RY	Roll Y-axis	[µrad]
Y_RZ	Yaw Y-axis	[µrad]
Y_TX	Translatory error of Y-axis in X-direction	[µm]
Y_TZ	Translatory error of Y-axis in Z-direction	[µm]
Z	Z-coordinate	[mm]

Chapter 1
INTRODUCTION

1.1 Introduction to problem identification

It is possible with an Atomic Force Microscope (AFM) to make non-destructive surface morphology measurement (up to 0.2 mm x 0.2 mm) with a resolution better than 1 nanometre. Nearly all kinds of surfaces can be measured with an AFM, but for the time being AFM is not a metrological accepted measuring method. The main reason for the missing metrology acceptance, is the aspect regarding establishment of traceability into the technology and a better documentation for the metrology performance as for example reproducibility, accuracy and calibration etc.

Since the middle eighties more the 5000 AFM's have been installed worldwide, among others in many companies, research institutes and universities, where the use has been focused on the quality control e.g. measurement of critical dimensions on semiconductor components and workpieces with fine surface having roughness in the micron and sub micron range.

The number of AFMs for quality control in companies is estimated to be in the order of 500 and this number is strongly increasing. As a consequence of this situation more restrict demands are set to the performance of the AFM. These demands include reproducibility, accuracy, calibration procedures and establishment of traceability as known for other measurement instruments for large dimentions. This tendency seems to accelerate in the coming years partly pushed by the development of the production of smaller parts with finer tolerances.

The majority of national metrology institutes worldwide have AFM facilities for research in the field of nano- and micrometer

scale metrology. The national metrology institutes for example in USA, Japan and Germany have many groups working with AFM microscopes and traceability of measurements.

Many private companies offer AFM-measurements as a service, especially in the USA. These companies can perform traceable measurement but the traceability does not fulfil the European demands according to accreditation and certification.

The number of companies performing and selling calibration artefacts is increasing, but until now most of the calibration artefacts are sold without certificate.

In the international literature only few authors have stated an uncertainty for parameters which have been measured with AFMs, and until now only very few comparisons between laboratories and industry have been performed. Comparisons are used to determine the measuring capability of the AFM. At the moment no metrology institute offers accredited services involving AFM.

In the area of research and industrial development there is a strong interest for nanometre science and nano technology. As a consequence a number of international conferences and societies[1] within the area have been established.

1.2 Problem identification

The scope of this industrial researcher project is to develop nanometer- and micrometer scale characterization of surface topography with AFM methods to a metrological accepted measuring method with traceability and stated uncertainty, also regarding specimens with a complex geometry.

[1] *Nanotechnology, The European Society for Precision Engineering and Nanotechnology, etc.*

The challenge of establishment of traceability in AFM measurements is approached following two related investigations:

A. Calibration methods for a metrology AFM

B. Development, test and calibration of a new system for measurement of specimens with a complex geometry and fine surfaces.

The objectives of the investigations are:

A. The metrology AFM has to be calibrated by transfer standards and by developing measuring procedures, which take in to account the interaction between the calibration object and the instrument. The accuracy of the measurement will be tested by comparing own results with results obtained by others (participation in international key-comparisons).

Expected outcomes of this part of the project (A):

- DFM will have developed calibration and measuring procedures to a metrology AFM and knowledge about the calibration by using transfer standards. By participating in international key-comparisons DFM will build up reliability regarding its measurements.
- DFM will create knowledge about industrial application of the metrology AFM and thereby recognize tasks where the instrument is relevant to use. Through these tasks knowledge of stating uncertainties for to AFM measurements is establish.
- Development of knowledge into the field of applications, measuring procedures, international comparisons and uncertainties will create the necessary basis for DFM to establish an accreditation of AFM measurements. An accredited service is a way to transfer traceability into industry.

B. Development and calibration of a measuring system, where an AFM is integrated into a metrological reference system in form of a coordinate measuring machine. This integrated system gives the opportunity for arbitrary positioning of the probe in the measuring volume resulting in a high degree of flexibility. Establishment of traceability of the integrated system will be a focus area of the investigations.

Expected outcomes of this part of the project (B):

- IPL will have developed an integrated system dedicated for performing surface mapping on products which normally not are measurable for AFMs.
- To investigate the behaviour of the integrated systems a calibration procedure has to be developed. Furthermore a suitable calibration artefact covering the integrated system has to be developed.

1.3 Scanning Probe Microscope (SPM) technology

The SPM is an image tool with a vast dynamic range, spanning the realms of optical and electron microscopes. It is a profiler with an unprecedented 3-D resolution. The use has a wide variety of disciplines, including fundamental surface science, routine roughness analysis, and spectacular three dimensional imaging from atoms of silicon surface to micron size of protrusions on the surface of a living cell [1].

The first suggestion for a “super-resolution microscope” can be traced back to the British scientist Synge as far back as 1928. He introduced the concept for a scanning probe near-field optical microscope. The first demonstration of a near-field super-resolving scanning microscope was performed by Ash and Nicholls in 1972 using microwave radiation at 3 cm wavelength; they achieved a resolution of 150 µm. The scanning tunneling microscope (STM) is of course a great example of a super-resolution scanning probe microscope; the

wavelength of the electrons that scan the sample is in the order of 1 nm and atomic (0.2 nm) resolution images are routinely obtained. Following the technology of the STM, several novel scanned probes emerged [1].

The STM has revolutionized the field of microscopy being the foundation for an entire family of microscopes generally referred to as scanning probe microscopes which are capable of measuring a range of physical and/or chemical properties on nanometer scale. One of the key points is that it is possible to stabilize and scan a fine probe tip over a sample surface to nanometer accuracies in (x,y,z) by using piezoelectric scanners coupled with electronic feedback techniques.

In order to achieve such precise control of the tip-sample spacing, it is necessary to derive an electronic feedback signal that varies rapidly as the tip-sample distance is varied. All microscopes have the characteristic that their resolution is not determined by the wavelength of light that is involved in the interaction as in conventional microscopy (the so-called Abbe limit), but rather by the size of the interacting probe that hovers over the sample surface to scan the image. As the resolution achieved is far superior to the wavelengths involved, these microscopes come under the general class of super-resolution or near-field scanning probe microscopes [1].

Until the 1990s researchers had relied upon other instruments for imaging and measuring the morphology of surfaces, like optical microscopes and scanning electron microscopes. Table 1 contains some parameters that illustrate the general performance of some instrument types. Table 1 is not exhaustive, and the instrument types can by subdivided.

Characteristics of Common Techniques for Imaging and Measuring Surface Morphology			
	Optical Microscope	**SEM**	**SPM**
Sample operating environment	Ambient air, liquid or vacuum	Vacuum*	Ambient air, liquid or vacuum
Resolution: x,y	1.0 µm	5nm	2-10nm for AFM 0.1nm for STM
Resolution: z	N/A	N/A	0.1nm for AFM 0.01nm for STM
Effective Magnification	$1\times$-$2\cdot10^3\times$	$10\times$ - $10^6\times$	$5\cdot10^2\times$ - $10^8\times$
Sample preparation requirement	Little	Little to substantial	Little
Characteristics required of sample	Sample must not be completely transparent to light wavelength used	Surface must not build up charge and sample must be vacuum compatible*	Sample must not have local variations in surface height >10µm
* Environmental SEMs can be operated at higher pressures and low eV, but resolution is lost			

Table 1: Example of the characteristics of common imaging and measurement technologies. N/A indicates Not applicable [3].

1.4 The Scanning Probe Microscope

SPMs are a family of instruments used for studying the surface properties of material from atomic to micrometer level. An upper limit of the scan range can be stated as 200µm $\times$ 200µm for the x - y axes and 15 µm for the Z-axis.

All SPMs contain the same basic elements illustrated in Figure 1.

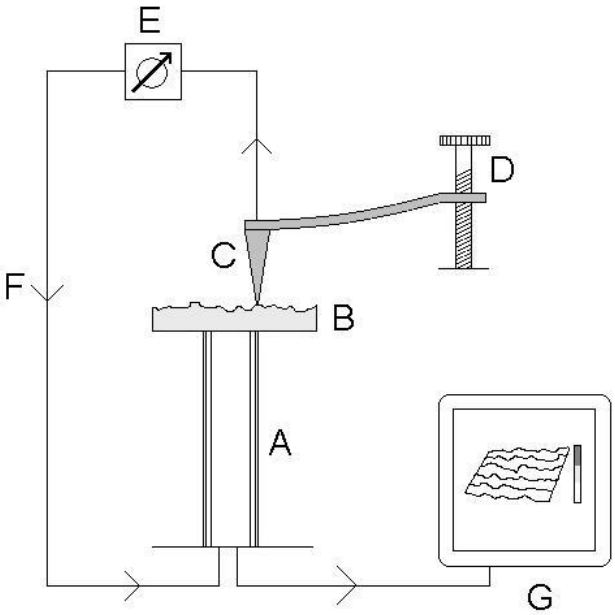

Figure 1: Schematic of a SPM. ***A)*** *A piezoelectric scanner which moves the sample under the tip (or the tip over the sample) in a raster pattern.* ***B)*** *The sample.* ***C)*** *A probe tip.* ***D)*** *A coarse positioning system to bring the tip into the vicinity of the sample* ***E)*** *Means of sensing the vertical positions of the tip.* ***F)*** *A feedback system (closed control loop) to control the vertical position of the tip.* ***G)*** *A computer system that drives the scanner, measures data and converts the data into an image. [1]*

All SPMs share the same basic operating principle. The surface (B) to be imaged is probed by a sharp tip (C). The tip is moved in the same scan motion (often in a bi-directional- or zig-zag pattern) over the surface. This scan motion of the tip produces an image (G) by recording the tip position (E) and its deflection, vertical and / or lateral [4]. Quite often an image consisting of 512×512 pixels (sample points) is sampled, but

images with more then 1024×1024 pixels are possible. The resolution depends on the scan range and can be down to a sub-nanometre level. Yet it is not only the distribution of height over the sample that can be recorded. Several different physical characteristics of the sample can be explored, depending on the nature of the probing tip and its interaction with the surface and the instrument configuration. Some examples of other SPM techniques are given [1], [8]:

- Scanning Thermal Microscope (SThM),
- Near-field Scanning Optical Microscope (NSOM),
- Scanning Capacitance Microscopy (SCaS).
- Scanning ion conductance microscopy (SICM),
- Scanning electrochemical microscopy (SECM) etc..

1.5 Atomic Force Microscope technology

This thesis is concerned mainly with atomic force microscope (AFM). Therefore the remaining part of this section will attempt to explain the working principles of AFM. There will be many analogies to the rest of the scanning probe microscopies, since AFM is a part of the SPM family, and properly the most used technique. The AFM uses the atomic force interaction between cantilever tip and sample surface to detect the surface topography or surface properties.

1.5.1 Working principle of AFM

Most commercial AFMs currently on the market, detect the position of the cantilever with optical techniques (D,E,F,G) in the most common scheme is shown in Figure 2. A laser beam (E) bounces off the back of the cantilever (C) onto a position sensitive photo detector (PSPD) (G). As the cantilever bends (or twists) (H), the position of the laser beam on the detector shifts [4]. The PSPD can be two- or four segmented depending on which cantilever position it has to detect. Two

segments are used for the vertical position four segments are needed to get information about the cantilever twist.

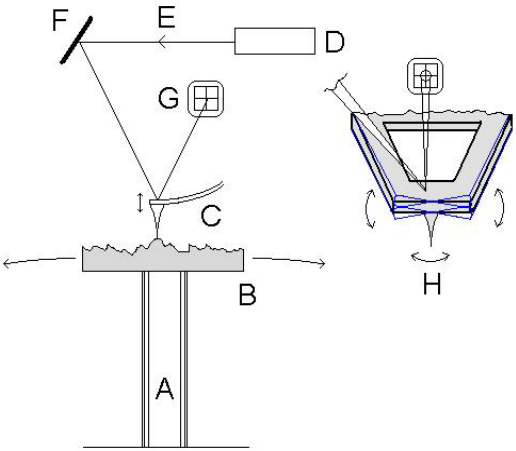

Figure 2: Schematic of generalized AFM. ***A)*** *A piezoelectric scanner* ***B)*** *Sample* ***C)*** *A probe tip and cantilever* ***D)*** *A laser diode* ***E)*** *A laser beam* ***F)*** *A mirror* ***G)*** *A position sensitive photo detector (PSPD)* ***H)*** *Close up look at the cantilever, illustrating the lateral movements and a four segmented PSPD [4].*

The signal from the PSPD is typically applied as a feedback control signal (Figure 1, F). It indicates the motions of the cantilever. Thus it can be applied to control the contact between tip and sample during the process of scanning. The piezo scanner is responsible for both the scan motion in the lateral direction and the feedback response for the tip in Z-direction. Within the last couple of years, it has been possible to buy AFMs equipped with linear sensors on the three measuring scales, often called “metrology AFMs”. For those metrology systems the linear sensors are responsible for the feedback response particular position of the three axes.

The most common design of the drive mechanism or scanner is based on the use of PZT-ceramics (lead-zirconium-titanate), which is a piezo electrical material. Piezo electrical materials

are characterized by changing dimension in response to an applied voltage (see Figure 3, A). With various dopants added it is possible to create specific material properties [5]. Piezo-electrical scanners are often designed to move in X, Y and Z direction and the design follows two principles. The first uses piezo stacks (see Figure 3, B), which are aligned perpendicular to each other. Thus each euclidean direction X, Y, Z is controlled by a single independent piezo stack. The second arrangement consists of a hollow cylindrical tube with four outer- and one inner electrode (See Figure 4, A). The reverse order is also possible. By biasing voltages to a pair of electrodes the tube will bend and create a movement in the lateral direction. Z-movement can be created by biasing the same voltages on all electrodes and the tube extends in Z-direction [6].

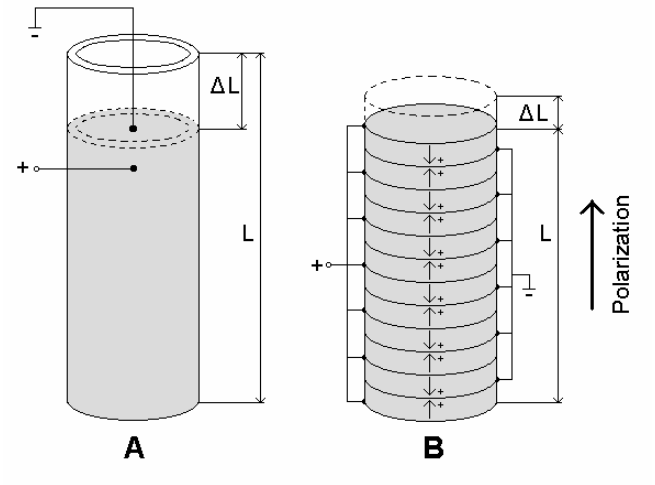

*Figure 3: **A)** Design and definition of a piezo electrical scanner based on PZT. Biasing a voltage to the electrode will effect in an extention ΔL of the tube with the length L. **B)** A piezo stack scanner is constructed with alternating polarization. The electodes set in between the discs are connected as shown. An applied voltage thus can prolong the length L of the stack by ΔL.*

The tube scanner design can also contain multi-tube configurations (Figure 4, B). The tube is designed with one tube part performing the lateral movement and another tube part for the vertical movement. This gives the opportunity for the use of materials with different properties for optimizing the scanner performance [3].

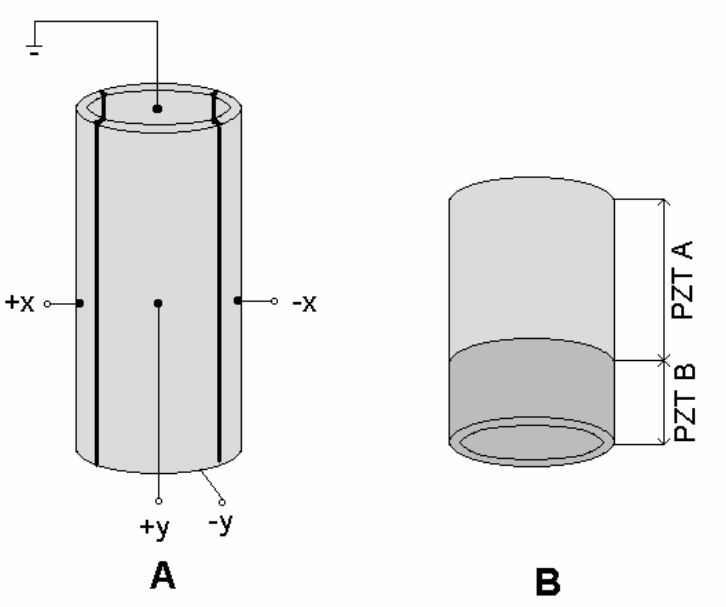

Figure 4: ***A)*** *A four-segmented PZT tube scanner. Applying an opposite voltage on the opposing electrodes can create the lateral bending movement of the tube scanner (x,y).* ***B)*** *A multi tube PZT scanner. The "PZT A" tube part performs the lateral movement. The "PZT B" creates the vertical movement. Often multi tube scanners are manufactured in different materials. A soft PZT for the lateral movement and a hard PZT for the vertical movement.*

The first AFMs used a small diamond fragment glued to an aluminium foil cantilever as the sensor probe [7]. For several years after its invention, these hand-cut cantilevers or bent wires etched to a fine point were the only stylii available. Since the first crude implementation, microfabrication techniques for

cantilevers have made dramatic advances. All commercial AFMs now use microfabricated cantilevers based on processes developed in the semiconductor industry [8].

There are several interaction modes between tip and sample by which the microscope can trace the sample surface. They take advantage of different forces when tip and sample approach (see Figure 5).

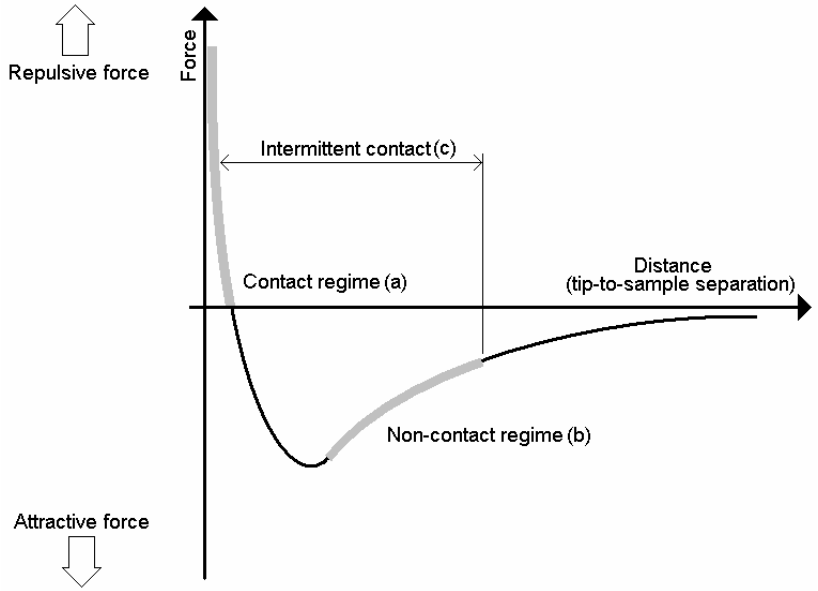

Figure 5: The dependence of the van der Waals force upon the distance between the tip and the sample. In contact regime (a) (repulsive force), the cantilever is held less than a few nm/10 from the sample surface. In the non-contact regime (b) (attractive force), the cantilever is held on the order of one to tens of nanometer from the sample surface [4]. The intermittent contact mode (c) operates in both contact and non-contact regimes with the cantilever held from few to tens of nanometer from the sample surface [8]. The illustration is modified after [1]

Three main operating modes are generally used in AFM depending of the tip-sample interaction and the use of

oscillating (AC) or non-oscillating (DC) cantilevers (See Figure 6).

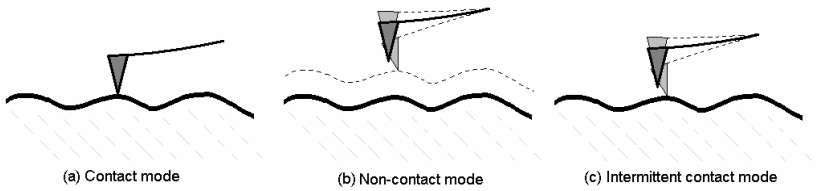

Figure 6: The three primary imaging modes in AFM. ***(a)*** *contact mode, where the tip-sample interaction is repulsive,* ***(b)*** *non-contact mode where the long-range attractive forces dominate the interaction, and* ***(c)*** *intermittent contact mode (often call tapping mode) where the tip comes into contact with the sample at the lowest point of the oscillation cycle.*

When the AFM operated in non-oscillatory DC manner and the tip-sample interaction is in the repulsive regime, the operation is in contact mode. The cantilever is bent slightly upwards from the surface as it scans across the sample (see Figure 6, a).

Several oscillatory modes (AC) are available for AFMs. These methods rely on the change in the oscillation amplitude or phase angle resulting from the force gradient perpendicular to the surface. In the non-contact mode (see Figure 6, b) the cantilever is vibrated near the surface of the sample. The free cantilever can be excited to oscillate close to its resonance frequency, typically about 100-500 kHz. Intermittent contact mode (see Figure 6, c) is similar to non-contact mode except that for intermittent contact mode the vibration cantilever is brought closer to the surface so that in the bottom of its travel it just barely hits or “taps” the sample.

A final remark will be a list containing the general information for the scanners used in this project (see Table 2).

Used in thesis	Metrology AFM (MAFM)	Tubescanner AFM (AFM)
Instrument	Dimension 3100 AFM mounted with Dimension metrology head.	DualScope DS5
Manufacturer	Digital Instruments	DME A/S
Piezo geometry	Linear PZT elements mounted into a parallelogram moving stage.	Medium tube, 4cm made of soft PZT
Max scan range (X, Y, Z)	70µm×70µm×6µm	40µm×40µm×2.7µm
Scan freq.	No specified limit	0.1 – 2.0 Hz
PZT voltage	± 75 V	± 230 V
Online control mechanism	Hardware feedback in x,y from capacitive sensors	Software controlled
Further description	See chapter 5	See chapter 6

Table 2: Specification of applied AFM used in this project. The Metrology AFM (MAFM) concerns the work carried out on DFM. For the work at IPL, AFM has been used.

1.6 Measurement uncertainty

Uncertainty estimation has been used as a general tool for quality identifications of calibrations and measurements carried out in this project. Therefore a short summary of the principle for uncertainty estimation is given in this chapter.

When reporting the result of a measurement of a physical quantity, it is obligatory that some quantitative indication of the quality of the result is given. In this way it is possible to assess

the reliability of the measurement results. Without such an indication, measurement results can not be compared, either with themselves or with reference values given in specifications or standards [9].

Depending on the measurement system many influence components have to be taken into account before reporting the final result and uncertainty.

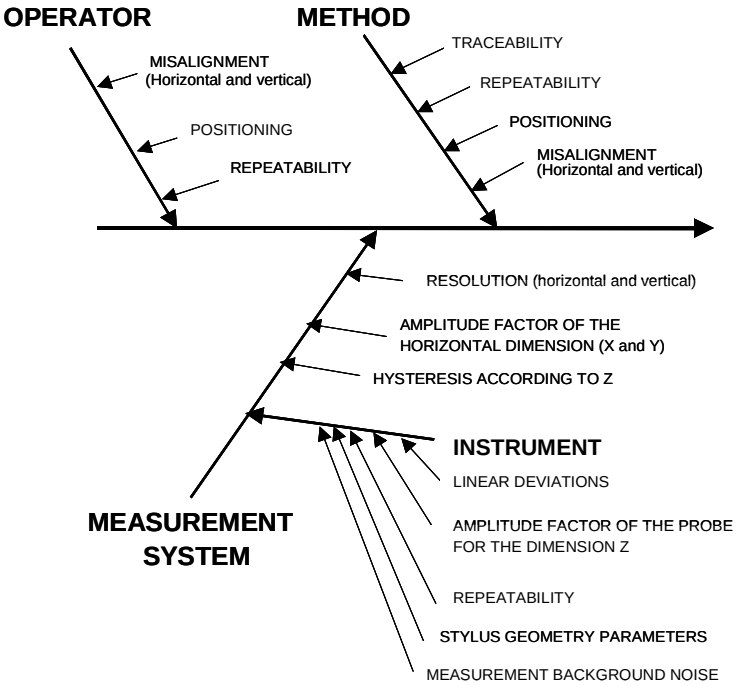

Figure 7: Examples on influence parameters for calibration of roughness tester [11].

Figure 7 gives an example of influence components for calibration of a 2D roughness tester. The components for a complete measuring setup can be divided into three parts:

- Operator

- Method
- Measurement system

Many of the components are identical in other systems.

For this particular project participation in intercomparison is an important part and the result has to be compared to references, therefore uncertainties have to be stated following the rules described in Guide to Expression of Uncertainty in Measurement (GUM) [9], [10].

In this chapter the general approach regarding uncertainty estimation will be presented as a short resume of the guidelines presented in GUM.

The uncertainty estimation procedure is divided into three major parts:

A. Evaluating standard uncertainty (modelling the measurement)

B. Determining combined standard uncertainty (uncorrelated or correlated input quantities)

C. Determining expanded uncertainties (coverage factor)

1.6.1 Evaluating standard uncertainty (A)

The first step in the process to evaluate the standard uncertainty is to express mathematically the functional relationship *f* between the measurand *Y* and the input quantities X_i on which *Y* depends:

$$Y = f\left(X_1, X_2, ...X_N\right) \tag{1}$$

The function *f* should contain every quantity, including all corrections and correction factors that can contribute to a significant component of uncertainty to the result of the measurement.

x_i, the estimated value of the quantity X_i, must be determined either on the basis of a statistical analysis of series of observations or by other means.

The set of input quantities $X_1, X_2, \ldots X_N$ may be categorized as:

- Quantities whose value and uncertainties are directly determined in the current measurement.
- Quantities whose value and uncertainties are brought into the measurement from external sources.

Each input estimate x_i and its associated standard uncertainty $u(x_i)$ are obtained from a distribution of possible values of the input quantities X_i. They can be categorized into two types of contributions:

- Type A standard uncertainties (statistically determined)
- Type B standard uncertainties (scientific judgements)

The covariances associated with any input estimates that are correlated are then evaluated.

The result of the measurement is calculated, that is, the estimate y of the measurand Y, is determined from the functional relationship f using for the input quantities X_i the estimates x_i.

1.6.2 Combined standard uncertainty (B)

The combined standard uncertainty $u_c(y)$ is the quadratic sum of the standard uncertainties of the input quantities $u(x_i)$ each weighted by a sensitivity coefficient c_i.

$$u_c^2(y) = \sum_i c_i^2 \cdot u^2(x_i) \qquad (2)$$

with

$$c_i = \frac{\partial y}{\partial x_i} \tag{3}$$

1.6.3 Expanded uncertainty (C)

It may be necessary to give an expanded uncertainty U whose purpose is to provide an interval *y - U* to *y + U* that may be expected to encompass a large fraction of the distribution of values that could reasonably be attributed to the measurand *Y. U is obtained by* multiplying the combined standard uncertainty $u_c(y)$ by a coverage factor *k*, typically in the range 2 to 3, to obtain

$$U = k \cdot u_c(y) \tag{4}$$

k is selected on the basis of the level of confidence required of the interval.

1.6.4 Discussion regarding uncertainty

Uncertainty estimation plays an important role for the comparability of a measuring result. There are many “standard” methods of evaluating and combining components of different methods for uncertainty [12].

The ISO/BIPM standard has been adopted as a general guideline by many calibration laboratories worldwide. The purpose of this action is to ensure a harmonised way of estimating uncertainty. In the European cooperation for accreditation of Laboratories (EA) the first edition following GUM arrived in 1997, EAL-R2 [13]. Also the National Institute of Standards and Technology (NIST) in USA has endorsed the method and implemented it into their work [14].

The major challenge of using the method presented in GUM is to create an adequate mathematical expression for a certain measuring system. As a consequence, a supplement [15] to the existing guide containing practical examples has been

developed. Other initiatives are courses held by National Metrology Institutes in expressing uncertainties.

The GUM method is a general approach for uncertainty estimation for all systems, normally dedicated in cases where a high level of accuracy is needed (mostly used by accreditated laboratories). A more practical and industrial approach for uncertainty calculation and quality management is described in the ISO 14253 part 2, Procedure for Uncertainty Management (PUMA) [16].

The PUMA method follows the principles described in GUM, but in a simplified way. It has been developed for the use in industrial applications, and is based on an iterative process to estimate uncertainty for an economy optimum rather than a technical optimum [17].

1.7 Summary

This introduction Chapter 1 gives a brief description of the fundamentals and the working principle of the Scanning Probe Microscope technology. As expressed in the problem identification, there is a need for establishment of traceability into the field of SPM to ensure reliable results.

Therefore Chapter 2 contains a description of the state-of-the-art methods for establishment of traceability into AFM by the use of transfer standards and an introduction to the most common design of calibration artefact.

Chapter 3 gives a theoretical description of algorithms for lateral and vertical calibrations of AFMs developed in this project. Furthermore calculation methods for determination of the correction parameters used for the particular algorithms are introduced. Other methods for determination and estimation of correction parameters are presented as well.

In Chapter 4 the calibration methods used during the participation in three intercomparisons are described. The

participation in intercomparisons also leads to the final validation of the metrology AFM.

The work presented in Chapter 3 and Chapter 4 was carried out at the Danish Institute of Fundamental Metrology (DFM).

Chapter 5 describes the work carried out at the Technical University of Denmark at the Department of Manufacturing Engineering and Management. This part of the thesis describes an integrated system containing an AFM integrated on a manual driven coordinate measuring machine (CMM). The Integrated system is dedicated for performing surface mapping on fine surfaces where areas are tilted and stitched together. A calibration procedure for the integrated system is suggested.

Chapter 6 contains a summary and final conclusions of this project. After summary and conclusions are References and Appendix placed.

Chapter 2
ESTABLISHMENT OF TRACEABLE ARTEFACTS FOR CALIBRATION AND PERFORMANCE TESTING OF SPM

The aim of this chapter is to give a short description of state-of-the-art within the area of establishment of traceable standards regarding calibration and performance test of SPMs. The focus will be held on the most common artefacts and methods developed in the last couple of years mainly in Europe and USA.

2.1 Definitions

Traceability is by the International Organisation of Standardization (ISO) defined as [18]:

> *"….the property of the result of a measurement or the value of a standard whereby it can be related to stated references, usually national or international standards, through an unbroken chain of comparisons all having stated uncertainties….."*

An example of an unbroken traceability chain for an SPM is illustrated in Figure 8.

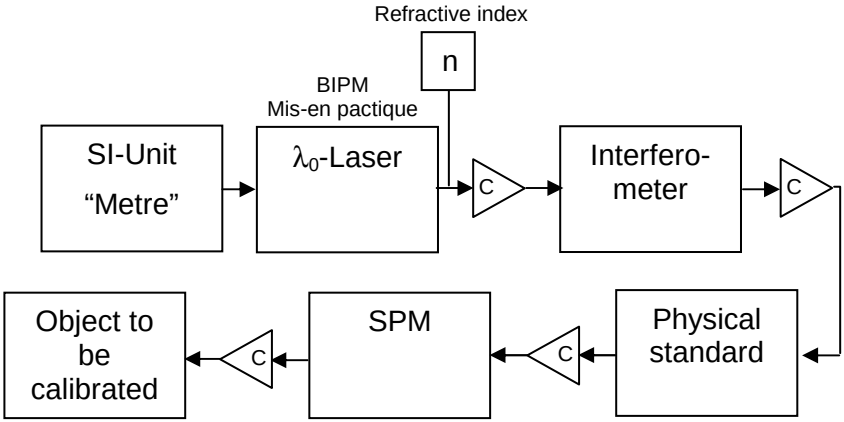

Figure 8: A principle example of a unbroken traceability chain for a SPM. The C inside the triangle is the symbol for calibration that links one standard or instrument to the next.

The traceability is transferred from the calibration standard to the instrument or measuring system by performing a calibration. By definition a calibration is [18]:

> *"….a set of operations that establish, under specified conditions, the relationship between values of quantities indicated by an instrument or measuring system….and the corresponding values realized by standards….."*

At each level of the traceability chain a calibration has been performed using methods with a metrological quality already determined on a higher level. Therefore a calibration hierarchy [18] as shown in Figure 9 exists.

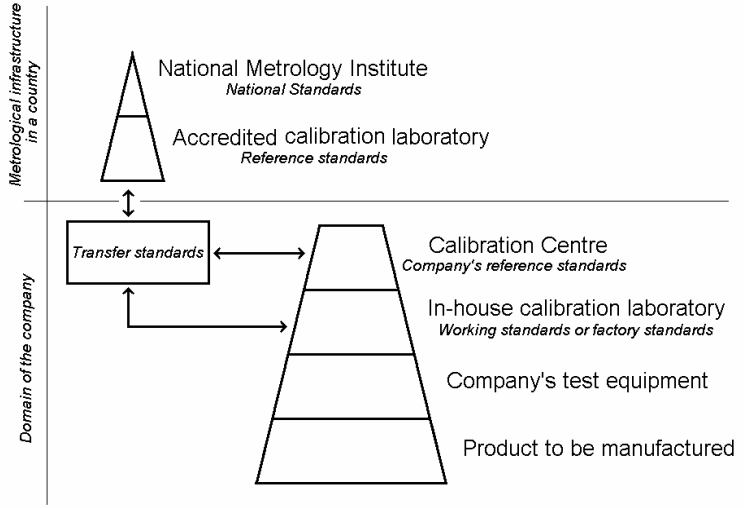

Figure 9: Calibration hierarchy from national standards to the finished product [18].

2.2 Traceability and SPM-technology

The SPM-technology has come to a level where it is not only used for research but also as an important tool to develop high technology parts and quality control in industrial companies. This has led to increasing demands for a better documentation and understanding of the capability of SPMs [20].

Most of the instruments traditionally used in dimensional metrology can be calibrated by standards to ensure the traceability to the SI unit of length. Consequently, the high resolution instruments as for example SPM are now subject to the needs of calibration [20]. At present there is no method available to establish the traceability directly into the AFM instrument design[3]. Calibration must be performed by measurements on standards [21].

[3] *Some metrology AFMs has established traceability by built-in a laser interferometer on the axes.*

There are a number of different commercial artefacts on the market[4] which are used as calibration standards. In most cases they are not specifically designed for the use with SPMs [22] but originally designed for SEM, roughness measurement instruments or CD (line width) measurement in microelectronics technology. In some cases this may be feasible, however one has to bear in mind that these artefacts are designed for instruments with coarser resolutions. Therefore, the quality of the structure is often not adequate for the use with SPMs.

Another aspect is whether the standards are calibrated and the calibration result documented in a certificate. In general, mean values for the parameters of the artefact are reported. They are based on an area which is much larger then the scan range for SPMs. Therefore these standards can only be used with caution [23]. If the standards have to be calibrated by AFMs this situation is unsatisfactory because of both economic and metrological reasons. First, the calibration by SPM is time consuming and therefore expensive, and secondly, the calibration uncertainty achieved by reference SPMs still has to be improved [24]. The uncertainties for SPM measurement are from national institutes stated to lie [23]:

X,Y-range:

$$u_{95} \sim (1.5 – 3)\ \text{nm} + (1 – 2)\ 10^{-4}\ L$$

Z-range

$$u_{95} \sim (1 – 1.5)\ \text{nm} + (0.5 – 1)\ 10^{-4}\ L.$$

[4] From companies like: VLSI [25], Moxtek [26], NT-MDT [27], Nanosensors [28]. Also some national institutes and universities are developing standards.

[6] DFM has been active partners in these EU-Projects.

This is still unsatisfactory. Therefore others techniques are used to calibrate these standards in order to achieve lower uncertainties [23].

2.3 Design of standards

The design of standards is normally related to their main purpose and the manufacturing technique. Some artefacts cover only one calibration or performance facility, e.g. flatness standards, other several e.g. x,y,z magnification standard (See Figure 10).

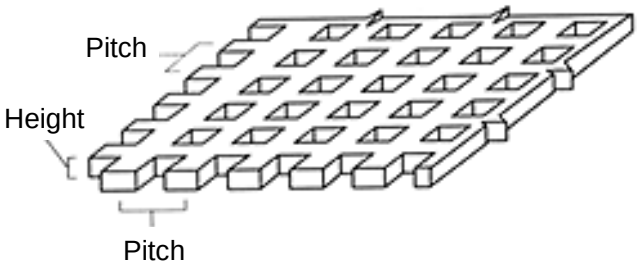

Figure 10: A principle sketch illustrating the design of a VLSI magnification standard.

An important design criterion for the standards has been to cover the whole range of the scan areas of SPM microscopes, but also to possess dimensions suitable for classical measurement techniques for the possibility to obtain traceability.

The standards that are normally used for SPMs can be classified into three groups depending on what they are dedicated for. The first group of standards cover the lateral calibration, the second group vertical calibration and the third group standards for other performance tests (See Table 3).

	Axes	Used for	Expected parameters
Group 1 lateral calibration	X, Y	Calibration of X,Y.	Correction parameters for X (C_x), Y (C_Y), the coupling between X and Y (C_{xy}).
		Determination of orthogonality between X and Y	The orthogonality between X and Y(γ).
		Non-linearity in the lateral movement	An expression or value describing the non-linearity for X and Y
Group 2 vertical calibration	Z	Calibration of Z	Correction parameters for Z (C_z).
		Non-linearity vertical movement	An expression or value describing the non-linearity for Z.
Group 3 Performance test	X,Y,Z	Flatness standard	The remaining image bow of measurements regarding instrument design.
	--	Tip characterization standard	From the image a deconvolution process can be performed to determine the tip shape.

Table 3: Classification of the most used standards for validation and calibration of SPMs. Expected parameters for the use are presented.

2.3.1 Lateral calibration standards

Standards for lateral calibration are in general designed with patterns which are periodic along their surfaces, with a known characteristic pitch for one or two axes. The geometrical structure of the pitch can have different shapes: square, sinusoidal, cylindrical or other shapes close to the mentioned forms. Also the periodical pattern changes, from line wise, only 1D - standard, to “chessboard”, “waffle” for the 2D - standards. The pattern can be an edge to edge structure or stand alone piles (see Figure 11).

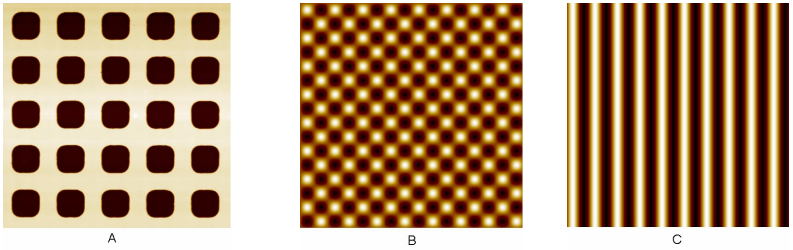

*Figure 11: The most common designs for lateral standards. **A)** Waffle pattern. **B)** Chessboard pattern. **C)** Line pattern.*

1D gratings are normally manufactured by holography techniques and 2D patterns by lithographical techniques. The general values for vertical and lateral calibration standards can be seen in Table 4.

2.3.2 Vertical calibration standards

The general problem for Z-calibration is to create a standard with a reliable reference plane. Different layouts, e.g. micro spheres and inclined planes have been introduced but step height artefacts are used in general.

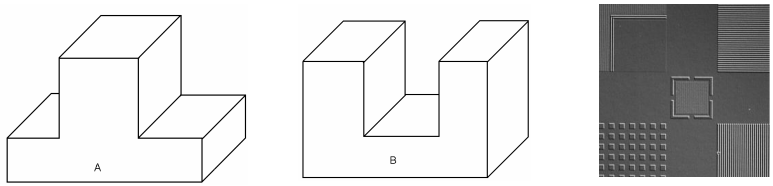

*Figure 12: The most used design for Z-calibration is a step height. The step height can be a **A)** rib or **B)** groove. Example of a step height standard with the reference field in the centre can be seen on the right hand side [31].*

Two designs are used for step heights standards. Single step like thickness of layer standards or step height arrays with a waffle-like arrangements of pits in a plane (as shown in Figure 10).

	Axes	Layout	Nominal pitch distances [nm]
Standards for lateral calibration	X, Y	Lines (1D or 2D) Ridge lines (1D or 2D)	10, 30, 300, 700, 3000
		Waffle like (2D) or (3D) Cylindrical posts (2D) Flat-topped pyramid-like posts(2D) Chessboard (2D) Diamond shaped posts (2D) Array of negative pyramids (2D)	100, 200, 300, 500, 700, 1000, 1500, 1800, 3000, 5000, 10000, 20000.
			Nominal step height [nm]
Standards for vertical calibration	Z	Single steps – 1 single bar	8, 18, 44, 88, 180, 450, 940.
		Step arrays: Waffle like (2D or 3D) Lines(1D or 2D)	3, 8, 18, 20, 24, 44, 80, 100, 180, 240, 500, 800, 2400.

Table 4: Examples of nominal values of pitch distance and step heights. The list covers only the major manufacturer of calibrations standards [23]. Therefore the list is not exhaustive.

2.3.3 Other standards

Some SPMs use piezo tubes as X-Y-scanners. The tip moves like a "dog tail" and deviation in all directions evolve [4]. A reference plane helps correcting for the "bowl shape" deviations. At the moment, no special SPM flatness reference artefact is commercially available. SPM users take pieces of Silicon wafers, mica or other atomically flat surfaces. Also, optical flats may be used [23]. In [42] a flatness standard for SPM was developed. The flatness standard is prepared by structuring chromium layers on high-quality glass substrates, with a peak-to-peak value, in the certified area, below 10 nm (see Figure 13).

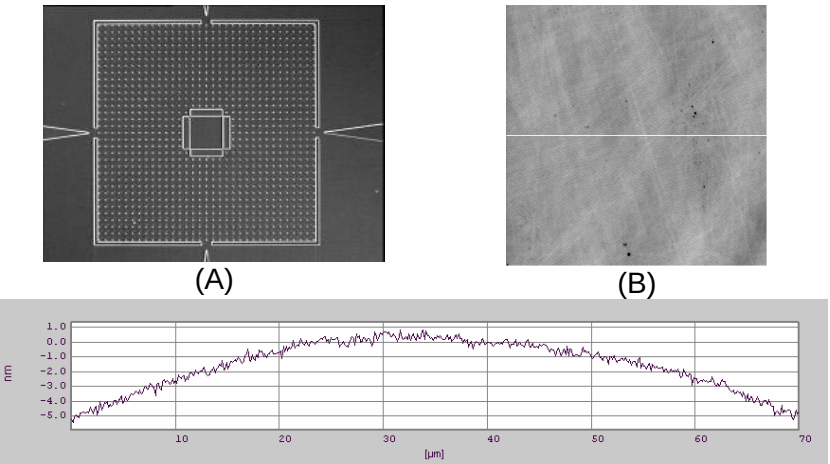

*Figure 13: Example of a flatness standard **(A)** with the reference field in its centre **(B)** Is an example of a measurement on the flatness standard. **(C)** A profile of image (B), illustrating the remaining "bowl shape" after a 1st order alignment.*

SPM measurements are limited by the shape of the tip used to probe the sample surface. As the tip wears, the finite size of the AFM tip may not allow the tip to accurately probe narrow or sharp features on a sample, resulting in underestimation of surface roughness and/or rounding/broadening of sharp surface features. For this reason, it is often desirable to discard a tip when it is no longer sufficiently sharp. To obtain the knowledge abut the tip shape a "tip characterization standard" can be useful. These standard can have different design (example, see Figure 14), but the main purpose is to have a structure that can separate the tip shape from the structure.

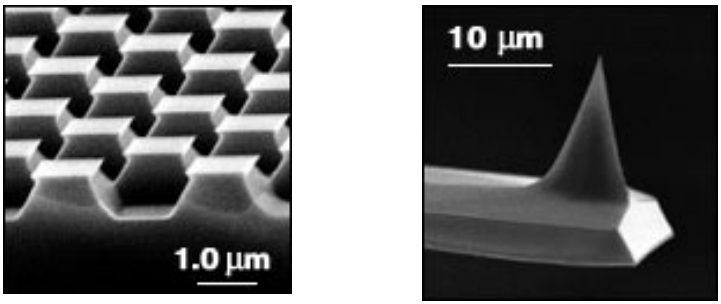

(A) (B)

*Figure 14: Example of a standard **(A)** that characterizes the shape of a tip **(B)**. Pictures are from [29].*

Another technique to find the tip shape is through "blind reconstruction" where the shape / form is calculated on the basis of already existing information in each single measurement [33], [34].

2.4 Establishment of traceability of artefacts

To create the link between the measurements and the scale on the images, the metre definition has to be introduced into the SPM-technology. In this chapter the most common methods for creating traceable transfer standards for SPM will be described.

2.4.1 Traceability for the lateral direction

The calibration of gratings and periodic structures is often based on optical diffraction. The technique consists of directing a laser beam onto the surface of the standard and aligning the surface of the standard so that the diffracted orders are directed back towards the laser (see Figure 15). The measurement obtained is the weighted mean period of the part of the standard illuminated by the Gaussian intensity distribution of the laser beam [35].

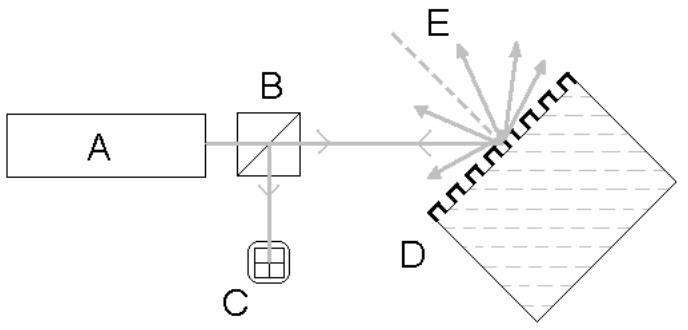

*Figure 15: Schematic diagram of the basic principle in optical diffraction. **A)** Laser, **B)** Beam splitter, **C)** Detector, **D)** Periodical sample, **E)** Diffraction orders. Modified after [36].*

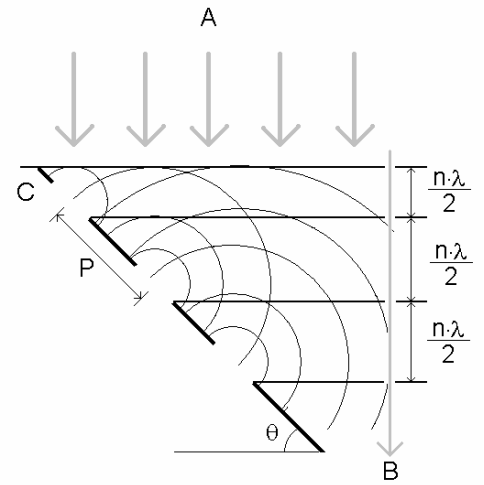

Figure 16: Schematic diagram of diffraction method used to calibrate a standard. A indicates the incident beam, B the wave front. Modified after [35].

Figure 16 shows the condition when the first diffracted order is directed back towards the laser. The angles θ_n at which this condition occurs can be used to calculate the period of the grating using Eq. 1 [35].

$$P = \frac{n \cdot \lambda}{2 \cdot \sin(\theta_n)} \quad (5)$$

Where P = period, n = diffraction order, λ = wavelength, θ_n = angle of n^{th} diffraction order.

The traceability of optical diffraction relies entirely on two components: the wavelength of the laser and the calibration of the angular table [35].

The expanded uncertainties typically achieved in pitch measurement and the determined orthogonality of various gratings can be seen in Table 5 [35], [36].

Measurement	Uncertainties
Pitch (X,Y)	$> 5 \cdot 10^{-5}$ - 10^{-6} (relative)
Orthogonality	10 – 0.1 arc minutes*

*Table 5: Typical achieved expanded uncertainties of optical diffraction. *The orthogonality uncertainty depends much on the grating period; a small period gives a small uncertainty [35].*

2.4.2 Traceability for the vertical direction

One of the most well known technologies to establish traceability for standards covering the vertical axes is interference microscopy [37].

A wide variety of microscope and objective designs have been implemented for interference microscopy, many following the basic principles of the Michelson, Mach-Zehnder, or Jamin interferometers.

A traditional technique is white-light interferometry in which a pattern of bright and dark lines (fringes) result from an optical path difference between a reference and a sample beam [38]. The mechanism is as follows: incoming light is split inside an interferometer, one beam going to an internal reference surface and the other to the sample. After reflection, the

beams recombine inside the interferometer, undergoing constructive and destructive interference and producing the light and dark fringe pattern. The fringe pattern can be translated into an expression of the height distribution, of the particular surface from the knowledge of the wavelength of the light [38].

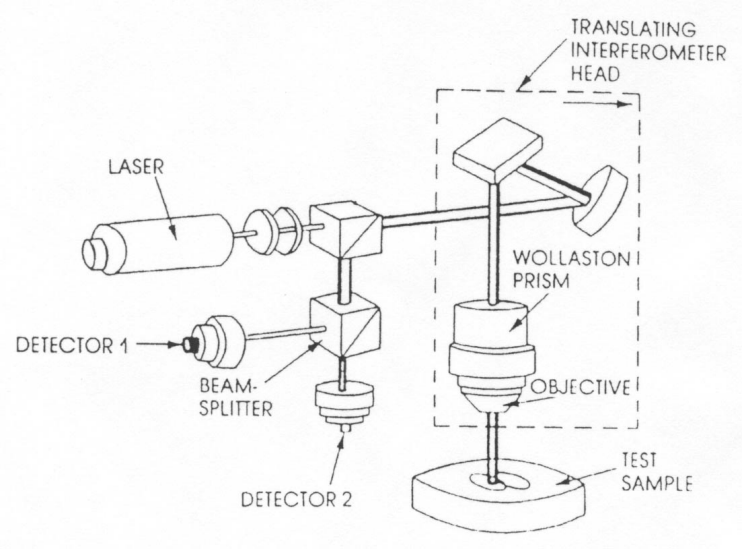

Figure 17: Schematic diagram of a scanning differential interferometry instrument [40].

Examples of the achievable expanded uncertainty on step height standard calibrations based on interference microscopy are listed in the Table 6.

Nominal (*certificate value*) step height [nm]	Uncertainty U(k = 2) [nm]
24 (*13.2*)	3.2
80 (*81.4*)	4.6
240 (*258.7*)	5.4
800 (*759.7*)	8.2
2400 (*2322*)	17

Table 6: Examples of achievable expanded uncertainty on step height standards [41].

2.5 Summary

This chapter contains a short description of state-of-the-art within the area of establishment of traceable standards regarding calibration and performance test of SPMs.

In order to create a link between the measurements and the scale on the images, the metre definition has to be introduced into the SPM-technology. At present there is no method available to establish the traceability directly into most commercial AFM instrument design. Therefore calibration must generally be performed by measurements on standards. There are a number of different commercial artefacts on the market which are used as calibration standards. In most cases the standards are not specifically designed to be used with SPMs. The design of standards is normally related to their main purpose and the manufacturing technique. Some artefacts cover only one calibration or performance facility, e.g. flatness standards, other several e.g. x,y,z magnification standards. An important design criterion for the standards has been that they should cover the whole range of the scan areas of SPM microscopes, but also possess dimensions suitable for classical measurement techniques for the possibility to obtain

traceability. The standards that are normally used for SPMs can be classified into three groups depending on their purpose. The first group of standards cover the lateral calibration, the second group vertical calibration and the third group standards for other performance tests. The methods used to calibrate transfer standards are normally based on optical principles. Lateral calibration standards are calibrated by optical diffraction, vertical calibration standards by interference microscopy.

As a consequence of the increasing demands of traceability in SPM-measurements, a number of EU-projects[6] like [42], [43] have been carried out. The topics for these projects are in the field of:

- Design and manufacturing of calibration- and performance standards for 3D-surface roughness measurements.
- Measurement and calibration procedures.
- Establishment of traceability to the SI-system.
- Creation of suitable algorithm for calculation of all necessary parameters (for software implementation).

Chapter 3
CALIBRATION OF AFMS

The calibration of AFM is a central activity in this industrial researcher project. Therefore this chapter will give a general approach to calibration of AFMs and describe the corresponding theory developed under this project.

The method described in this chapter is mainly developed for a metrological atomic force microscope equipped with distance sensors. However, the method can be applied to most other metrology AFM systems.

The chapter is divided into two major parts, one concerning the lateral calibration, and one concerning the vertical calibration. The focus will mainly be held on the theoretical description of expressing the correction parameters. Some of the results are presented in separate papers (see the PUBLICATION LIST in the beginning of this thesis). All illustrations and results presented in this chapter are generated from work within this project.

The purpose of performing calibrations is to ensure the reliability of a particular measurement result. Calibration of an instrument means determining the instrument reading error by checking it against a calibration standard with known values.

All image analysis performed in this project is carried out using the same software called Scanning Probe Image Processor (SPIP) developed by ImageMetrology [54],[55].

3.1 Lateral calibration

To perform a lateral calibration of an AFM a certain number of steps has to be considered to get the optimal outcome. It concerns three main elements:

- The calibration artefact
- The measurement to be performed
- Data analysis

A more detailed description is shown in Figure 18 and in the text below.

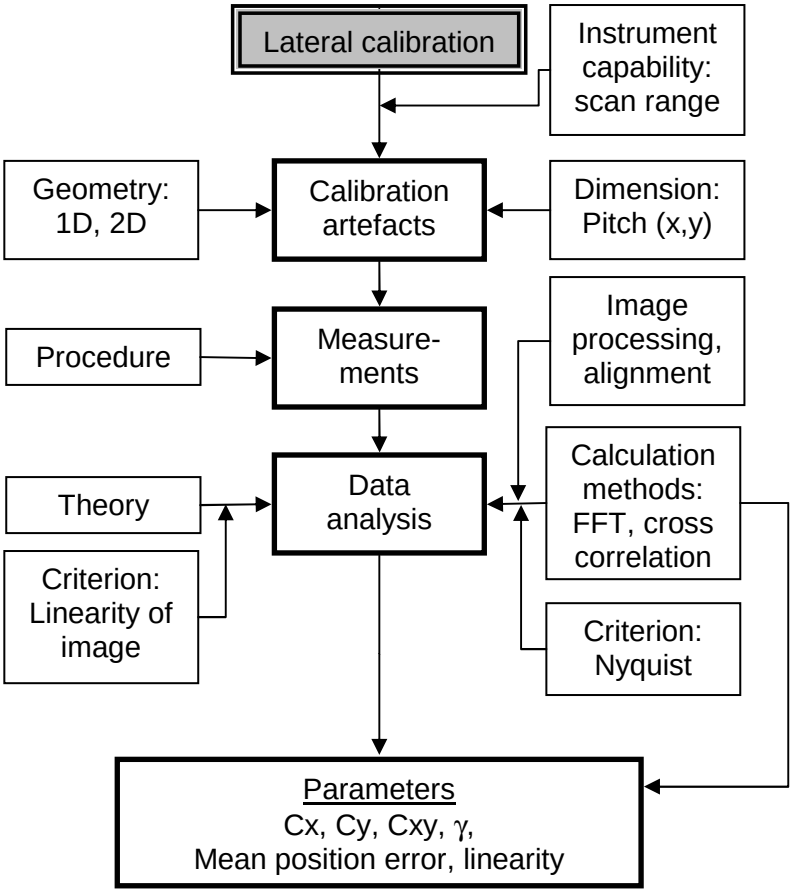

Figure 18: The main operations for lateral calibration of AFM.

3.1.1 Calibration artefacts

From the knowledge of the instrument capability (scan range in x,y,z) the dimension and geometry of the calibration artefact should be chosen. For most of the instruments a pitch in the range from 0.5 µm to 3 µm is suitable for the main part of the calibrations. In general the 2D-calibration artefact is preferable

due to the fact that the calibration procedure and the analysis methods are faster and easier to use.

3.1.2 Calibration and measuring procedure

Depending on the purpose of the calibration and accuracy level different procedures can be chosen:

- *A sequence* for periodical inspection of AFM by using reference standard (A).
- *A-B sequence*[8] for transferring traceability from A (reference) to B (unknown specimen).
- *A-B-A sequence*[9] for transferring traceability from A (reference) to B (unknown specimen) and back to A (reference) for verification of system stability.

The A-B-A sequence is illustrated in Figure 19 and Figure 20.

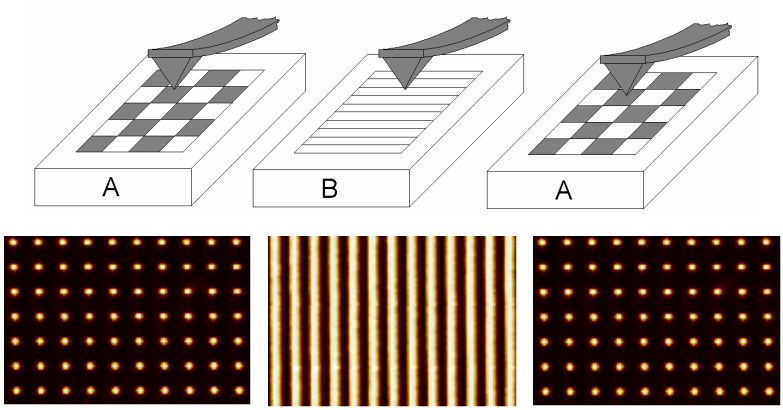

[8] *This method is used as a subroutine for surface mapping. Further description can be found in Chapter 5 Integration of AFM on CMM.*

[9] *This method is used for the pre-key comparisons Nano4 and Nano2. Further description can be found in Chapter 4 Validation of metrology AFM.*

Figure 19: An illustration of an A-B-A measuring sequence. First on A (reference standard), then on B (unknown specimen), and back to A.

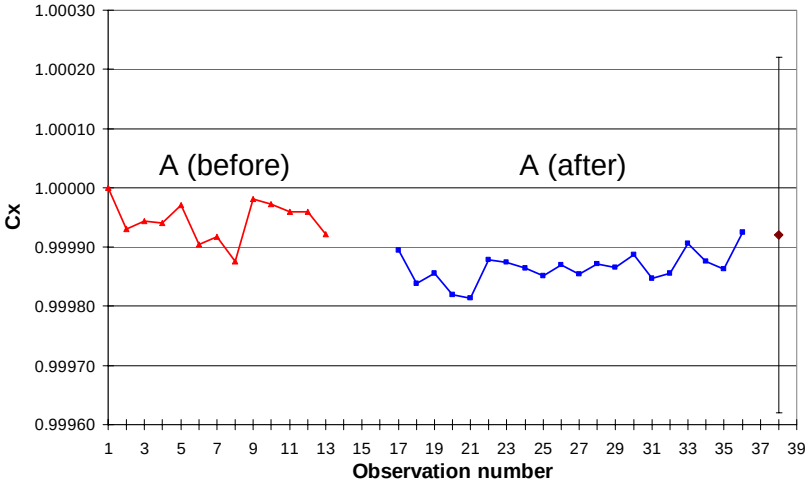

Figure 20: The graph is an example there shows the differences on C_x for measurements on a reference 2D-standard in a A-B-A measuring sequence (before and after measurement). The diamond markers in the right hand side of the graph indicates the reference value and the bars the expanded uncertainty (2σ) [47].

The A and A-B sequences are normally the most used.

In systems where the long term stability has been proven in a long calibration historic, an A-sequence is useful for maintaining traceability. For these systems the traceability can be transferred to unknown specimens without a direct comparison on a reference standard.

In newer systems, where the long term stability has not been proven yet, it can be necessary to perform an A-B sequence for establishment of traceability to an unknown specimen.

To ensure and increase the accuracy of the calibration an A-B-A sequence can be useful. The system stability can be

monitored almost directly, and this can be helpful for example when participating in intercomparisons. This method is the most time consuming of the three (measuring time and analysis time).

3.1.3 Theory for lateral calibration

The fundamental theory and the methods for data analysis are based on the nature of the calibration artefact, which has periodical structures.

The lateral calibration method developed and described in this thesis is based on a two dimensional ***oblique*** grid characterized by its lattice constants in the X and Y direction along with the angle between the two directions.

A linear transformation of the scanned and uncorrected image into a corrected image can be defined by a correction parameter C_x for the X-direction, a correction parameter C_y for the Y-direction and a coupling term C_{xy} between the scanned X and Y axes. Exact expressions for these correction parameters are given for an oblique reference grid.

In earlier work the expression for the correction parameters C_x, C_y and C_{xy} based on a scanned image in the special case of a square lattice [44], and a hexagonal lattice [45] have been deduced.

3.1.4 The reference frame and the transformations

The observed image is considered as linear, as the residual non-linearity of the image is much less than one pixel for the applied measurement conditions [47]. The remaining non-linearity can then be treated as a contribution to uncertainty[10]. Several correction parameters can be determined from the data analysis.

[10] *This criteria can only be stated for the metrology AFM.*

The reference standard is defined by three parameters L_a, L_b and θ (see Figure 21).

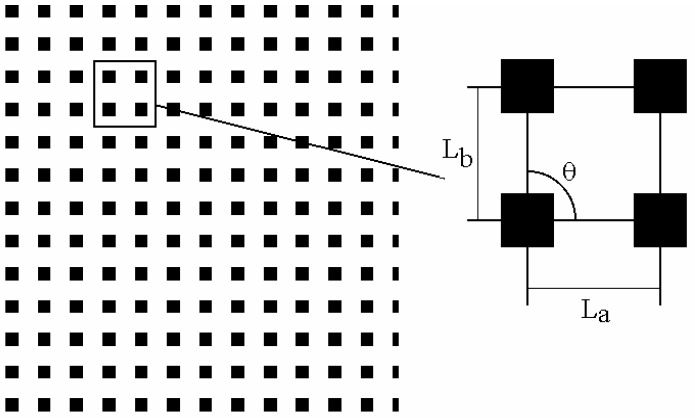

Figure 21: Definition of the oblique ($|\underline{a}| \neq |\underline{b}|$, $\theta \neq 90°$) reference structure of the traceable standard. L_a and L_b are the distances of the closest neighbours.

In order to describe the correspondence between the observed image and the grating it is necessary to define a linear transformation matrix $\underline{\underline{C}}$. The uncorrected image recorded by the microscope is denoted the scanned image *z(x´, y´)*, with the scanned coordinates *(x´, y´)* (see Figure 22). The linear transformation $\underline{\underline{C}}$ of the distorted plane into a corrected plane, $(x', y') \rightarrow (x, y)$ is then given by [46].

$$\begin{pmatrix} x \\ y \end{pmatrix} = \begin{pmatrix} C_x & C_{xy} \\ 0 & C_y \end{pmatrix} \begin{pmatrix} x' \\ y' \end{pmatrix} \tag{6}$$

This thesis treats the general case and expresses the correction parameters based on an image of an oblique lattice. These expressions are often required as the certified dimensions of a standard are rarely exactly square and the expressions are always needed to calculate the uncertainty of the correction parameters [47],[48].

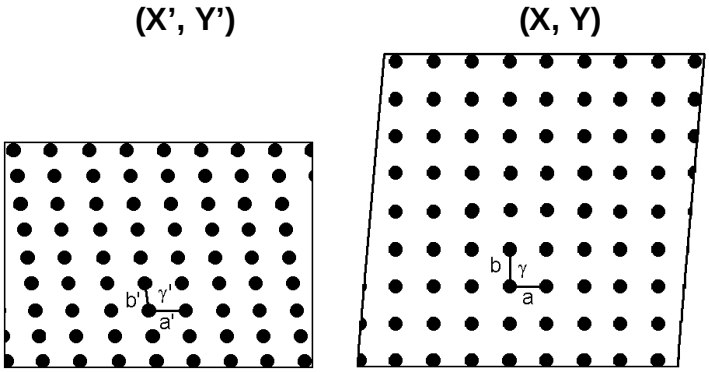

Figure 22: Left: is the uncorrected image were a', b' and γ' is the observed unit cell vector which is different from the certified values L_a, L_b and θ, that is, $|\underline{a'}| \neq L_a$, $|\underline{b'}| \neq L_b$, and $\gamma \neq \theta$. Right: A corrected image where a, b and γ are equal to the certified values L_a, L_b and θ.

The linear transformation of the observed unit cell vector $\underline{a'} = (a'_x, a'_y)$, $\underline{b'} = (b'_x, b'_y)$ (see Figure 22) can be written as

$$\begin{pmatrix} a_x \\ a_y \end{pmatrix} = \begin{pmatrix} C_x & C_{xy} \\ 0 & C_y \end{pmatrix} \begin{pmatrix} a'_x(1+d_x) \\ a'_y(1+d_y) \end{pmatrix} \quad (7)$$

$$\begin{pmatrix} b_x \\ b_y \end{pmatrix} = \begin{pmatrix} C_x & C_{xy} \\ 0 & C_y \end{pmatrix} \begin{pmatrix} b'_x(1+d_x) \\ b'_y(1+d_y) \end{pmatrix} \quad (8)$$

where C_x, C_y and C_{xy} are the unknown parameters to be estimated and d_x and d_y are associated with the stability of the measurement (e.g. due to thermal drift). The accuracy of a'_x, a'_y, b'_x, *and* b'_y is influenced by: the number of recorded pixels, the number of observed pitches, the remaining non-linearity and the tilt of the sample relative to the scanning plane.

3.1.5 Calculation of correction parameters

For the unit cell vectors of an oblique lattice in the corrected plane the following apply:

$$\left|\vec{a}\right| = L_a \tag{9}$$

$$\left|\vec{b}\right| = L_b \tag{10}$$

$$\vec{a} \cdot \vec{b} = L_a \cdot L_b \cdot \cos(\theta). \tag{11}$$

By inserting (7) and (8) into (9), (10) and (11) a restraint between the unknown matrix elements C_x, C_y and C_{xy}, and the certified dimensions L_a , L_b and θ is obtained resulting in three equations with three unknown parameters. The solutions are

$$C_x = \frac{A}{\left(a'_y \cdot b'_x - a'_x \cdot b'_y\right) \cdot \left(1 + d_x\right)} \tag{12}$$

$$C_y = \frac{L_a \cdot L_b \cdot \sin(\theta)}{\left(1 + d_y\right) \cdot A} \tag{13}$$

$$C_{xy} = \frac{b'_x \cdot b'_y \cdot L_a^2 + a'_x \cdot a'_y \cdot L_b^2 - \left(a'_y \cdot b'_x + a'_x \cdot b'_y\right) \cdot L_a \cdot L_b \cdot \cos(\theta)}{\left(a'_y \cdot b'_x - a'_x \cdot b'_y\right) \cdot \left(1 + d_y\right) \cdot A} \tag{14}$$

where

$$A = \sqrt{b'^2_y \cdot L_a^2 + a'^2_y \cdot L_b^2 - 2 \cdot a'_y \cdot b'_y \cdot L_a \cdot L_b \cdot \cos(\theta)} \tag{15}$$

3.1.6 Test of new algorithm

To determine the accuracy of the new algorithms (12), (13), (14) and (15) a large test was performed (see Figure 23). More than one hundred different combinations of calibration layout (e.g. 1D and 2D, pitch distances etc.) and calibration methods have been tested. The new algorithm is implemented into the SPIP software [54], which allows a faster image analysis and the use of already existing calculation facilities.

The purpose of testing the behaviour of the algorithms analytically or numerically is to validate the outcoming values. Furthermore an important step in uncertainty estimation is to

determine the sensitivity coefficient c_i which is based on partial differential calculations, which can be performed analytically[11] or numerically.

The basis for the testing is to compare the result obtained with the different calculation methods and principles with the exact value known from artificial test input to the algorithm.

The results presented in this thesis are only a fragment of all the results obtained during the testing due to a reasonable limitation of this thesis. Besides the results shown in this chapter a few graphs are placed in the Appendix 2.

The test has two different approaches:

- Change of features of virtual calibration artefact.
- Different calculation methods, for example Fourier transformation including examination of the behaviours of the analytical and numerical solution (especially according to differentiation of the equations).

The foundation of the testing is the final value of the unit cell vectors and the corresponding pitch distance.

Special software[12] was developed to create artificial test surfaces with a pattern as a virtual calibration artefact (see Figure 26).

[11] All analytical tests have been performed in the software Mathematica. The analytical solution was also implemented in SPIP.

[12] The software was developed in collaboration with Dr. K. Dirscherl

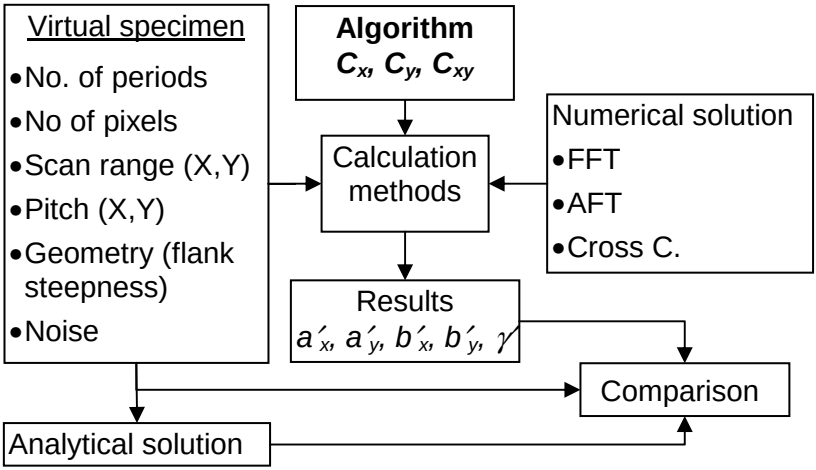

Figure 23: Overview of software test. Data from a virtual calibration standard used as input to the calculation method based on the numerical estimation principle[13]. The same data are used directly to perform the analytical solution. The result obtained by the different calculation methods is compared with the exact value known from the virtual calibration standard.

With the software the characterization of the virtual calibration standard could be changed, like (see Figure 24 and Figure 25):

- Scan range in X,Y-direction.
- Pitch distances in X and Y (L_a, L_b).
- The angle θ.
- Number of pixels p_k in X and Y direction.
- Number of periodical structures (n_i,m_j) in the pattern.
- Pitch geometry, flank steepness (β) and vertical noise.

[13] *Further description of the different methods used for calculation of the test result can be seen in section 3.1.7.*

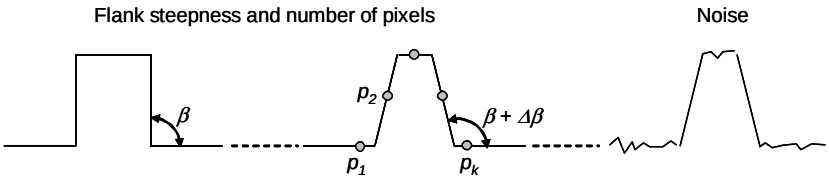

Figure 24: Illustration of flank steepness β. Number of pixels P_k and applied vertical noise.

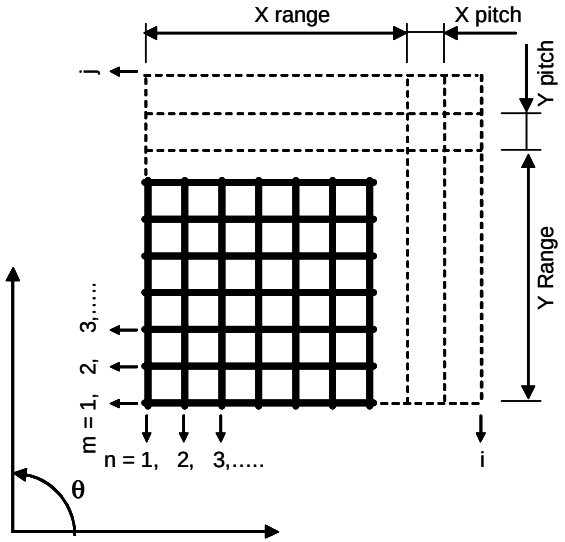

Figure 25: The changeable parameters of the virtual calibration standard. The number of periodical structures n_i,m_j. The pitches in X and Y-direction. Scan range for X and Y and the angle θ between X and Y.

The nominal values used for the virtual standards are comparable to a real traceable 2D transfer calibration standard and line standard used for the pre-key comparisons Nano4 (see section 4.4). The entire series of test image has no misalignment in the lateral plane. Example of the virtual calibration standard is shown in Figure 26.

By introducing a flank angle $\beta \neq 90°$ and applied vertical noise, the virtual surface becomes more realistic and comparable to real measurements.

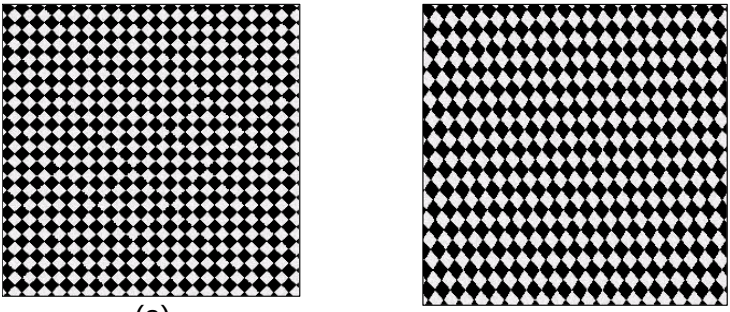

(a) (b)

Figure 26: Examples on virtual 2D test surfaces. ***(a)*** *A 25µm × 25µm chessboard pattern containing 20 pitches for x and Y direction 512 × 512 pixels.* ***(b)*** *A 25µm × 25µm chessboard pattern containing 20 pitches for x and 15 pitches for Y direction with 512 × 512 pixels.*

The algorithms have to work properly in the software SPIP. Therefore should the existing calculation methods for correction parameters (Fourier transformation and Cross correlation, see section 3.1.7) be used on the algorithms. Examples of test conditions for a 2D pattern are shown in Table 7.

Scan range in X,Y-direction	5µm - 80µm
Pitch distances (L_a, L_b).	L_a = *895nm*, $L_b \approx$ *895nm*
The angle θ	88° - 92°(0°-180°and 91.106°)
Number of pixels p_k	64 pixels - 1024 pixels
No of period. struct. (n_i,m_j)	5.59 - 89.39
Flank steepness (β) and vertical noise	Clip[14] between 0 - 1 On or off

Table 7: Test conditions for the virtual standard during the test in SPIP.

For all obtained results the deviation between the nominal and observed pitches distances have been isolated versus the different combinations. The examples shown in Figure 27 and Appendix 2 represent the tendency of all test results. There is no significant deviation between the nominal and observed pitches (generally below 0.3 pixels). There are some differences between the used calculation methods, but that might be expected according to the working principle (see section 3.1.7) and it is not giving any problems in the further work.

[14] Clip 0 - 1 represents 1 or 2, 2.3, 2.5, 3, 6, 7 pixels from top to button (see Figure 24).

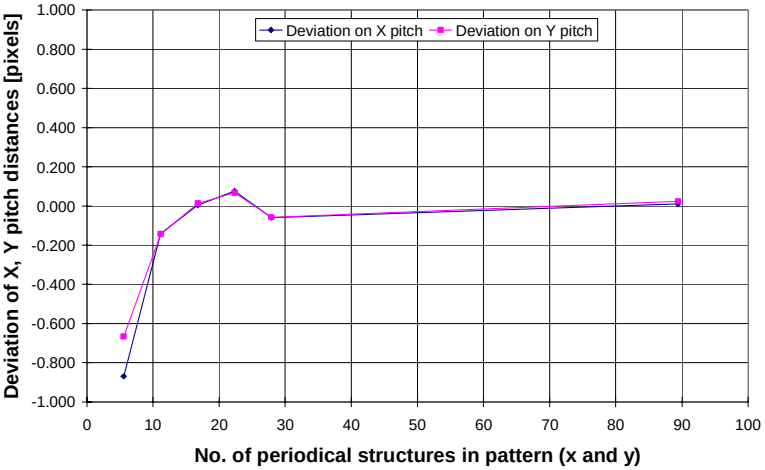

Figure 27: Deviation in pitch distance while changing the number of periodical structures in the virtual 2D-surface. The result is obtained by using cross correlation methods.

The test shown above has mainly been concentrated on the numerical principle. To ensure the validity of the numerical solution the analytical solution was tested and compared against the results obtained by the numerical principle. The purpose of this test was to investigate the differences of the differentiation of the equations because of the complexity of each equation. This has interest for the uncertainty calculation of the calibrations. A representative example of the result is shown in Table 8, Table 9 and Table 10.

By using a set of parameters (Table 8) in the analytical solution (as obtained by performing a partial differentiation of equations (12), (13), (14) and (15)) a result is obtained. When this result is compared with the results of the numerical solution a maximum deviation in the order of 3-4 per thousand (see Table 9) is observed.

Parameters	
Certified value of calibration standard	
L_a	895 nm
L_b	895 nm
θ	91.106°
Stability	
D_x	0
D_y	0
Unit cell componentes	
a'_x	-893.402 nm
b'_y	3.427 nm
b'_x	6.543 nm
b'_y	792.323 nm

Table 8: Test conditions for the performed analysis.

	Analytical solution relative to numerical solution		
	$\left\|\frac{C_x(a)}{C_x(n)}\right\|$	$\left\|\frac{C_y(a)}{C_y(n)}\right\|$	$\left\|\frac{C_{xy}(a)}{C_{xy}(n)}\right\|$
$\partial C_p / \partial L_a$	0.999973	0.999605	0.999905
$\partial C_p / \partial L_b$	1.003500	1.001294	0.999266
$\partial C_p / \partial \theta$	1.000204	0.999442	0.999995
$\partial C_p / \partial D_x$	1.000000		
$\partial C_p / \partial D_y$		0.999996	1.000000
$\partial C_p / \partial a_x$	0.999955		0.999929
$\partial C_p / \partial a_y$	1.000568	0.999119	1.003218
$\partial C_p / \partial b_x$	1.000212		1.003548
$\partial C_p / \partial b_y$	0.999632	0.996587	1.000160

Table 9: Differences on the partial differentiations of the equation used for dertermination of correction parameters. The results are obtained by the use of Matematica and DFM-GUM. Index P is either X, Y or XY.

Finally the deviations between the numerical and analytical results can be seen in Table 10.

	$\left\|\frac{C_x(a)}{C_x(n)}\right\|$	$\left\|\frac{C_y(a)}{C_y(n)}\right\|$	$\left\|\frac{C_{xy}(a)}{C_{xy}(n)}\right\|$
Analytical solution relative to numerical solution	1.000000	0.999996	0.999999

Table 10: The relative differences between analytical (a) and numerical(n) solutions.

As a general summary the obtained result during the test shows a very fine agreement between the known artificial values and the result obtained by different calculation methods.

The first test approach was to change features of the calibration standard to investigate the behaviour of numerical methods based on Fourier analysis and Cross correlation. The results obtained by these tests showed deviations in the order of one pixel or better, especially the cross correlation methods have extremely small deviations, in general better than 0.2 pixels.

Furthermore by comparing results obtained from the analytical and numerical solution a negligible deviation is observed. It can therefore be concluded that the algorithms work properly for virtual calibration artefacts and the observed deviation is mainly caused by the different calculation principles (see section 3.1.7).

3.1.7 Evaluation methods for lateral calibration and linearity

In this paragraph the calculation methods which are implemented in SPIP are described. Furthermore the test performed in this section is generated from real measurements and not artificial values.

From the equations described above the a'_x, a'_y, b'_x, *and* b'_y have to be determined to detect the unit cell. The unit cell is the basis for this lateral calibration and which describing the equidistant distances of the periodic lattice used for the calibration. As mentioned earlier calibration artefacts used for SPM in general contain a periodical structure for the determination of the correction parameters (see Figure 28, (a)).

Fourier transform is a powerful tool for image analysis, in particular for analysis of repeated patterns such as pitch

standards and molecular or atomic structures. Fourier images reflect repeated patterns as narrow peaks, the co-ordinates of which describe their periodicity and direction. Such peaks are easy to detect by image processing without any pre-knowledge of the features form or periodicity.

Furthermore, the repeat distances can be measured very accurately by determining the Fourier peak co-ordinates at sub-pixel level[15]. The discrete Fourier transform is calculated by the formula [54]:

$$F(u,v) = \frac{1}{N_x N_y} \sum_{x=0}^{N_x-1} \sum_{y=0}^{N_y-1} z(x,y) e^{-i2\pi\left(\frac{ux}{N_x}+\frac{vy}{N_y}\right)} \qquad (16)$$

where N_x, N_y are the number of pixels in the X,Y directions and u,v the discrete Fourier indexes: u = 0,1,2,..N_x-1 and v = 0,1,2..N_y-1. The Fourier transform (see Figure 28, (b)) can also be regarded as a sum of sinusoidal functions, each described by a frequency, amplitude and a phase. The number of computational operations can be reduced dramatically by Fast Fourier Transform (FFT) algorithms that break the calculation down to a sequence of smaller Fourier transforms. The highest efficiency is obtained when the side lengths N_x and N_y are powers of 2. Therefore typical images consist of are 256 × 256 or 512 × 512 pixels. The chosen size is a compromise between a high pixel density and the cost in form of extra acquisition time, storage demands and calculation time [54].

Another very useful method is cross correlation. The accuracy level for the correction parameters can be improved by combining FFT and cross correlation. The correlation averaging techniques improve the signal to noise ratio.

[15] *Further reading of the principle can be found in [54] and especially in [55].*

The correlation method, which is designed for measurements containing regular structures, uses an averaging procedure. A section (see Figure 28, (d)), containing at least one period of the lattice pattern is marked. The cross correlation function is then calculated by use of the Fourier method. The generated cross-correlation image (see Figure 28, (c)) contains several correlation peaks that identify matching areas. From certain mathematical criteria the real peak is found and the averaging image is obtained by superposition of the regions around the peak position [55]. From both methods the unit cell can be detected.

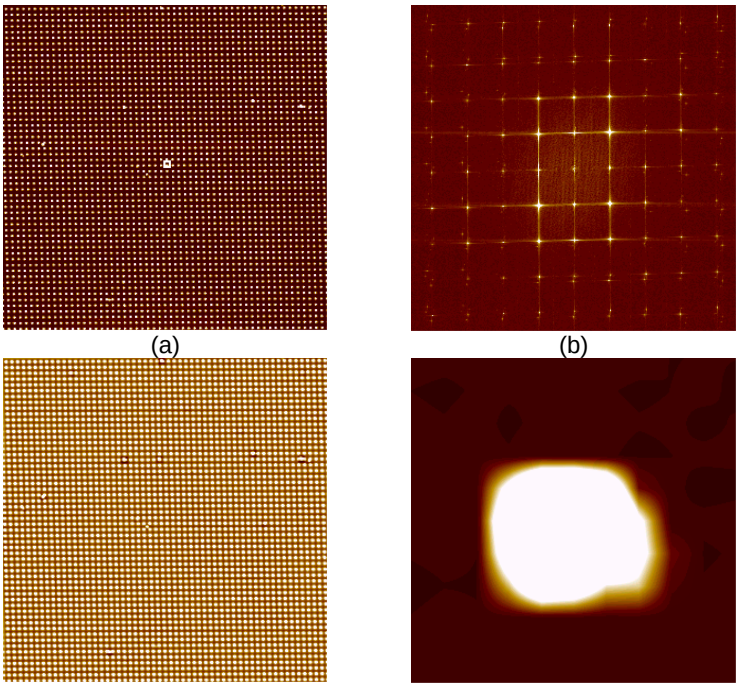

Figure 28: ***(a)*** *A 50 µm × 50 µm measurement obtained from a 2D-calibration artefact, with a x and y pitch of 895nm. The white square indicates the unit cell.* ***(b)*** *The Fourier transformation of the same measurements. The fundamental peaks are located around the centre. Other peaks represented in the transformation are higher*

harmonically peak and aliasing. ***(c)*** *The cross correlation image obtained and* ***(d)*** *the section used for generation of the cross correlation.*

The software to calculate the correction parameters uses three different methods [54].

Fast Fourier Transformation (FFT), based on detection of the fundamental (dominant) peaks in the Fourier spectre to express the unit cell.

Accurate Fourier Transformation (AFT) uses the fundamental (dominant) peaks and the higher harmonical peak. Depending on the peak number there is a relationship between the fundamental peak and n^{th}-peak. For example by dividing the observed wavelength of the fundamental peak with the wavelength of the second order peak the ratio will be in the order of two. The ratio between the fundamental peak and the third order peak will be in the order of three and so forth. In this way it is possible to ensure that the fundamental peak found is “the right one”, and furthermore it is possible to get a better estimate of the wavelength by averaging all wavelengths belonging together (a weighted average wavelength).

The combined ***Fourier transformation and cross correlation*** as described above.

Furthermore the cross correlation method gives the basis for an estimate of the non-linearity of the particular image[16] and a mean position error as a quality parameter [44],[55]. The estimated non-linearity obtained from the analysis can be expressed in two 3^{rd} order equation covering the X and Y axes,

[16] *Only if there are a equidistant peak distances*

$$X = C_{1x} \cdot x + C_{2x} \cdot x^2 + C_{3x} \cdot x^3 \quad (17)$$

$$Y = C_{1y} \cdot y + C_{2y} \cdot y^2 + C_{3y} \cdot y^3 \quad (18)$$

where C_{ij} are the coefficient to be estimated. From the non-distorted image due to the non-linearity the coefficient $C_{1j} \rightarrow 1$ *and* C_{2j}, $C_{3j} \rightarrow 0$. From the expression (17) and (18), the distorted image can be compensated for the observed non-linearity. It is an iterative process to minimize the non-linearity. Also other parameters can be expressed as maximum or minimum values or individual values from the X or Y axes.

In Table 11 and Figure 29 an example is given on a linearity analysis performed on a measurement carried out on the MAFM and the tube scanner AFM.

Parameters	MAFM	AFM	AFM
No. of iterations	1	1	3
C_{1x} C_{2x} C_{3x}	1.0006 -6.56E^{-7} -7.03E^{-10}	1.1049 -6.57E^{-4} 1.08e^{-6}	1.0007 -1.63E^{-6} -1.12E^{-8}
C_{1y} C_{2y} C_{3y}	0.9998 1.57E^{-7} -2.14E^{-9}	0.9117 8.86E^{-4} -2.66E^{-6}	1.0039, -1.004E^{-6} -2.02E^{-8}
Mean Pos. error [pixels]	0.091(0.16)	2.2 (2.9)	1.1 (1.9)
n	1	1	1

Table 11: Results obtained from a linearity analysis. Measurements are performed on MAFM and AFM.

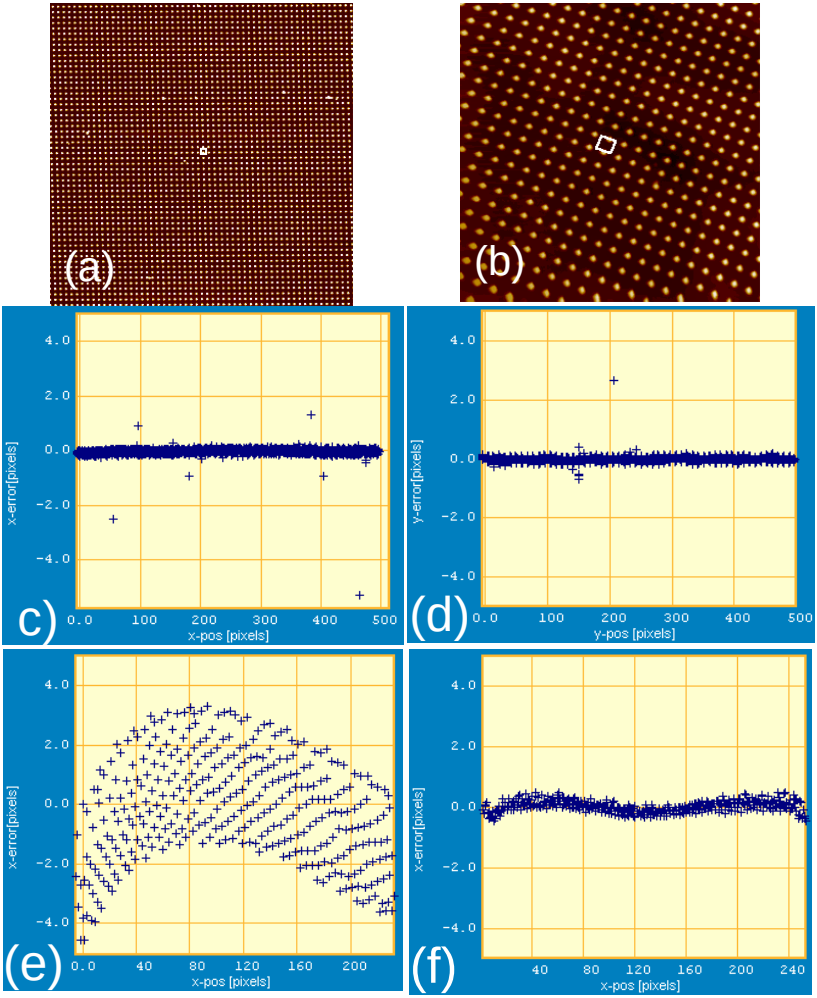

Figure 29: ***(a)*** *MAFM measurement 50 µm × 50 µm (512 × 512 pixels).* ***(b)*** *AFM measurement 35 µm × 35 µm (256 × 256 pixels). Each + in the graphs indicates the positioning error for each detectable unit cell in the measurement.* ***(c)*** *The non-linearity in X-direction for MAFM.* ***(d)*** *The non-linearity in Y-direction for MAFM.* ***(e)*** *The non-linearity in first iteration for AFM.* ***(f)*** *The remaining non-linearity after three iterations for the AFM.*

From the calculation of the correction parameters from the same set of data (as shown in Figure 28, (a)), treated with the same pre-operations, differences between the three methods can be shown. In Figure 30 and Table 12 representative results are presented.

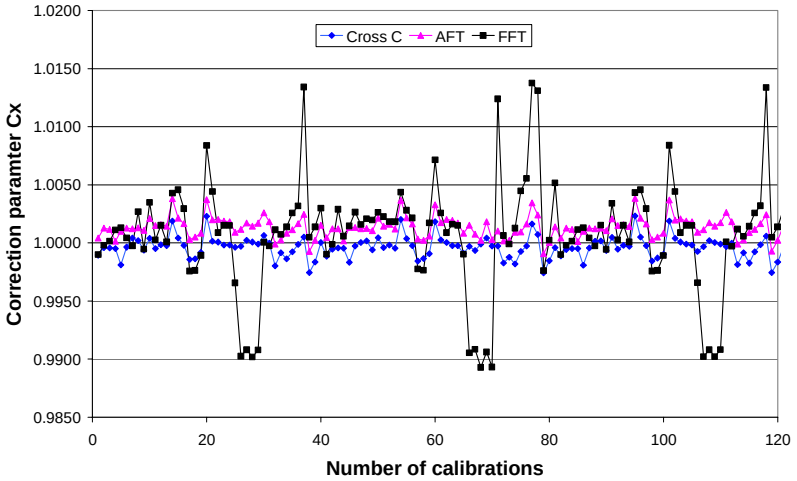

Figure 30: Comparison of the three different calculation methods: FFT, AFT and FFT and Cross Correlation based on estimation of correction parameter C_x. The result is based on the same data set from squared (50µm × 50µm) measurement on a 2D-calibration artefacts with a X pitch of 895 nm ± 1. The calibrations have been performed over a two month period [56].

Correction parameter	FFT	AFT	Combined FFT and CC
C_x	1.0006 (0.0048)	1.0013 (0.0009)	0.9996 (0.0009)
n	121	121	121

Table 12: The average value of C_x obtained by using the three different methods for calculation of correction parameters (as shown in Figure 30). The number in brackets indicates the standard deviation.

Generally the Fourier Transformation methods based methods give systematically higher values compared to the results obtained by the combined FFT and CC method (see Figure 30 and Table 12).

The accuracy of the calibration results can be verified by re-orientation of the calibration artefact differently compared to the one normally used (Figure 31). Normally the standard is oriented parallel to the scanned axes (as shown in Figure 31, top). This will result in the Fourier peaks being placed parallel to the axes near the centre in the Fourier spectrum.

Noise is normally placed in belts nearby the centre mainly in the Y-direction of the Fourier spectrum. The represented noise (1/frequence) is mainly created due to the differences in scan speed between axes (X is fast-, Y is slow scan direction), where the slow scan direction generates low frequency which is more dominant in the Fourier spectrum. Other noise sources, e.g. environment created noise, can also be applied to the measurement and be seen in the Fourier analysis.

Therefore by re-orienting the calibration artefact (see Figure 31, lower illustration) the peaks will move out of the noise belt and thereby ensure a more reliable result [57].

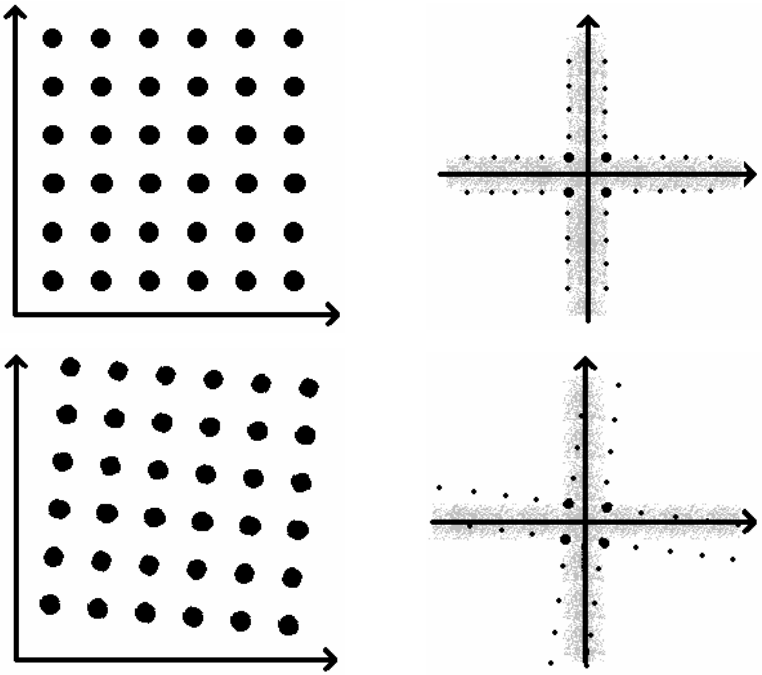

Figure 31: The orientation of calibration artefact can influence the result obtained from the calculation methods for lateral correction parameters. By re-orientating the calibration artefact during the calibration the effect due to the noise problem can be clarified [57]. Top illustrations have structure parallel to the scanned axes. Lower illustrations re-oriented structure.

A test has been performed to investigate different influence parameters on the calibration result, especially the alignment techniques effect on the results can be seen in Appendix 1

3.1.8 Summary lateral calibration

To perform a lateral calibration of an AFM a certain number of steps have to be considered to get the optimal outcome of the work, these include the calibration artefact, the measurement to be performed and data analysis.

Depending on the purpose of the calibration and the accuracy level different procedures can be chosen, e.g. A, A-B, A-B-A sequences or other methods.

The lateral calibration method described in this thesis is based on a two dimensional grid (as shown in section 2.3) characterized by its lattice constants in the x and Y direction along with the angle between the two directions.

A linear transformation of the scanned and uncorrected image into a corrected image can be defined by a correction parameter C_x for the X-direction, a correction parameter C_y for the Y-direction and a coupling term C_{xy} between the scanned x and y axes. Exact expressions for these correction parameters are given for an oblique reference grid.

The developed algorithms have been implemented in SPIP. By creating artificial surfaces with variable properties the new methods have been tested with existing calibration facilities. The obtained results showed very small deviations between nominal and observed values (general much better then 1 pixel) and no significant difference could be proved.

To determine the correction parameters Fourier Transformation is very useful. An extended method based on Fourier transformation or a combined Fourier transformation and cross correlation method can improve the calibration result. The last method can also give an expression of the non-linearity and several parameters expressing the position error (max, min, mean etc) of the lateral plane.

3.2 Vertical calibration

The AFM is often used for height related measurements (like thickness or roughness measurements) mainly because of the very high resolution in Z-direction which is in the order of 0.1 nm or better.

In literature different methods have been introduced to perform vertical calibration by using different calibration

standards or measuring techniques and setups (example see Figure 32). However performing vertical calibration using step height standards still is the most used method.

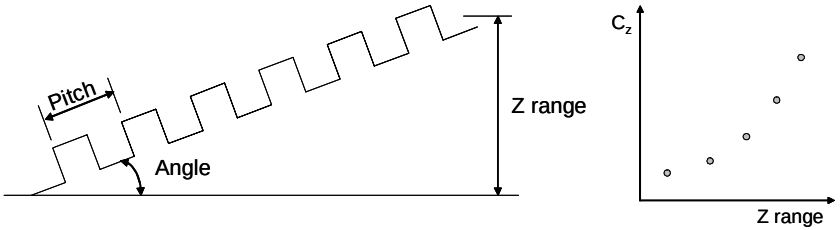

Figure 32: Example of a tilting device for vertical calibration. Left: From the knowledge of pitch and angle the whole vertical axis of an AFM can be calibrated (right).

This thesis suggests how the Z axis can be calibrated on step height standards[17] after a well known principle as described in ISO 5436. Furthermore a correction parameter for the important "out of plane motion" will be introduced. For small step heights this is the dominating error source. The method is based on the use of transfer standards calibrated using well accepted classical techniques as for example interference microscopy [59],[60].

As for the lateral calibration a number of useful steps are suggested that should be considered before performing the vertical calibration (see). The three main steps are:

- The calibration artefact.
- The measurement to be performed.
- Data analysis.

[17] *This method is introduced by PTB for the participation in pre-key comparison Nano 2.*

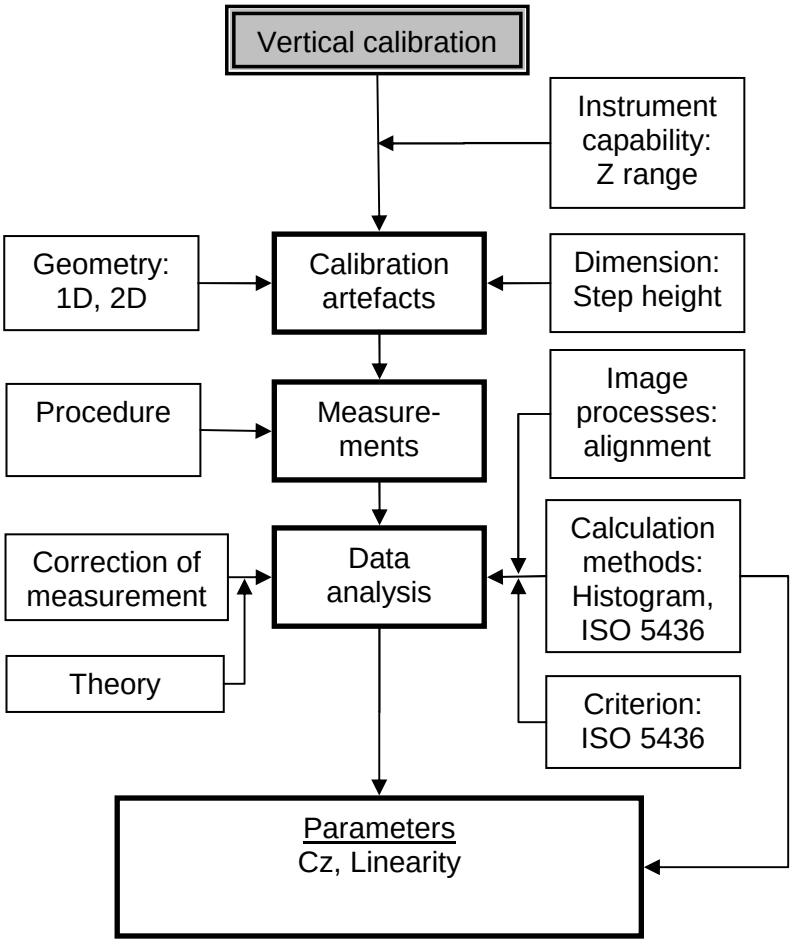

Figure 33: The main operations for vertical calibration of AFM.

3.2.1 Calibration artefacts

For vertical calibration step height standards are typically used. Often a step height standard contains only one step arranged line by line or in a 2D-pattern (see section 2.3.2). This situation can make it difficult to produce proper calibration

curves because in this case the curve would only contain one single point. Another aspect introduced by the same situation is that the step height sometimes differs by orders of magnitude from the height of the surface to be measured [63]. So as opposed to the lateral calibration several standards containing different step heights are needed to cover the vertical range of the instrument. The use of a line by line standard or a 2D-standard is normally not critical, but the geometry must contain well defined upper and lower plateaus for the step height calculations according to [32],[65].

3.2.2 Calibration and measuring procedure

The procedure which is already proposed for the lateral calibration in section 3.1.2 can be recommended as useful calibration and measuring procedure for the vertical calibration as well.

3.2.3 Theory for vertical calibration after ISO 5436

A new approach [50] for calibration of the Z-axis of AFMs is suggested. It is based on the well known principle described in ISO 5436 regarding the depth definition of a groove of a profile. The ISO standard normally is used for classical 2D stylus roughness testers [64]. The standard defines a step height as the vertical distance between the top and bottom plane of a plateau in a certain distance from the edge (Figure 34).

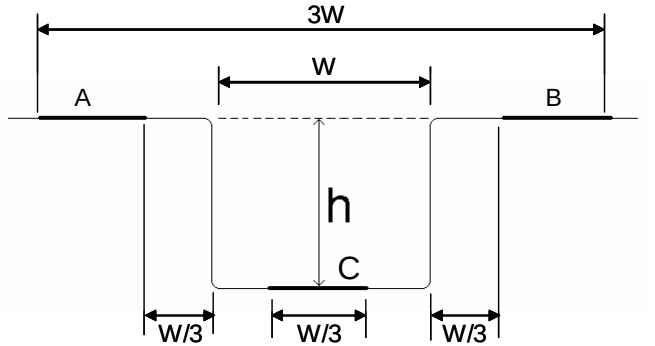

Figure 34: Definition of the depth of a groove according to ISO 5436. The depth h is defined as the vertical distance between the upper plateaus A - B down to the lower plateau C. W is the width of the groove. Modified after [64].

To determine the step height a continuous straight mean line is drawn over the thick line to represent the upper level of the surface and another representing the lower level. Both lines are extending symmetrically about the centre of the line (see Figure 34). The surface at portion C is assessed only over the central part of its width. The height *h* is defined as the perpendicular distance of the mean of the portion C to the line through the mean of portion A and the mean of portion B.

The new approach is only dealing with step heights calculated from a single profile which introduces new aspects of the normal 3D measurement performed by AFM.

In order to implement the ISO 5436 into the field of AFM, it may be needed to modify the definitions of the depth. The main reasons are:

- Only few calibration artefacts for SPM available today are designed to follow the definition after ISO 5436 standard. This concerns the width *W* of the groove compared to the whole length to be measured (*3W)* (see Figure 34).

- The use of conventional standards that follow the definition and which contain step heights measurable by AFMs will often be limited by the relatively small lateral scan range for AFMs.

The major point to be considered when following the definition of the ISO standard is the width of the groove. This will often lead to a reduction of the total length (<3*W*) which has to be measured[18].

To calculate the results after ISO 5436 a special software was developed to identify the three plateaus and calculate the step height. The step height was estimated as the perpendicular distance between the marked part of a continuous straight line fitted by the least square method to the lower level of a profile and a straight parallel line fitted to the upper level, see Figure 35 [60].

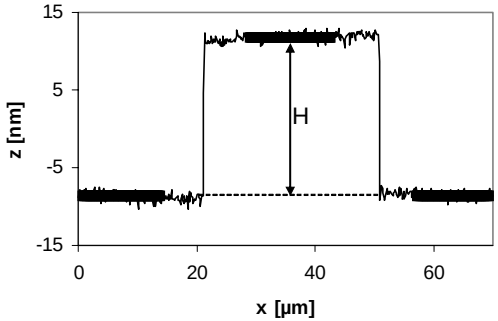

Figure 35: Principle of specification and interpretation of a step height measurement. The thin line is the observed average profile (64 lines) of a small step height (nominal height 20 nm). The perpendicular (vertical) distance between the parallel solid broad lines is the step height H fitted to the AFM measurement using the least squares method [60].

[18] The ISO standard prescribes a total length of 3W where W is the width of the groove or step. In the Nano2 pre-key comparison (see section 4.5) the total length is reduced to 2.5W in order to make AFM measurements possible.

3.2.4 Correction terms for vertical calibration after ISO 5436

In addition to the implementation of ISO 5436, a thorough analysis (described in [60]) was performed to investigate for the sensitivity of this new approached needed and by the analysis find and quantify important corrections terms. It expresses the physical Z-coordinate of an imaged surface as a function of the observed and uncorrected Z-coordinate and the horizontal position based on a Taylor expansion of this function. This method is only valid for MAFM systems where there are corrected hysteresis and creep. The out coming correction terms of the analysis can be very useful as a general approach for all AFM systems.

From the analysis the three most important correction terms were identified and estimated based on a series of measurements on a calibrated step height and a flat reference surface[19] [60]. The correction terms are:

A. Thermal drift, causes the height level of the surface under investigation to shift along the slow scanning Y-axis of the microscope.

B. The Z-axis is coupled to the x and y axes causing a flat surfaces to appear with a superimposed bow.

C. The vertical capacitive distance sensors have a remaining non-linear error for the Z-coordinate.

(A): As long as the measuring technique is based on a scanning principle the thermal drift between scan lines can not be avoided. As it can be seen in Figure 36, the scan lines are bumping up and down mainly because of noise, contamination of the sample and thermal drift. The correction of thermal drift is normally done by performing line wise levelling of each recorded profile.

[19] *Carried out to the pre-key comparison Nano2.*

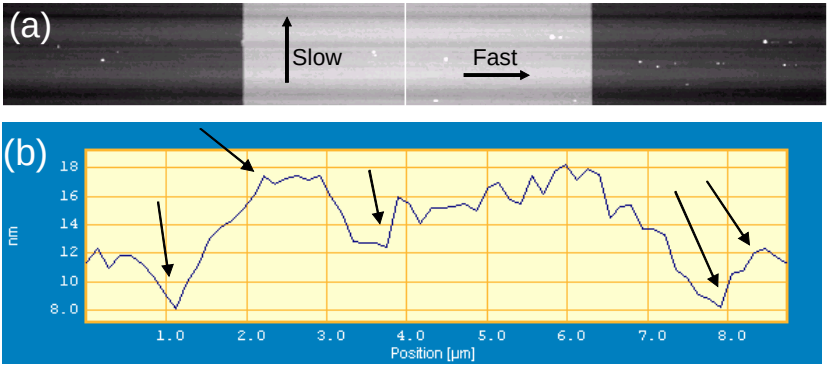

*Figure 36: **(a)** A 70µm × 8.75µm step height measurement with a nominal height of 20nm. The arrows indicated fast and slow direction of the measurement. The white line indicates the position for the profile **(b)**. The arrows on the profile (b) are examples that indicate the different position of the scan lines. Measurement is from [61].*

(B): The coupling between the Z-axis and the X and Y axes is mainly caused by the construction and working principle of AFMs, this is the fact for both tube scanner AFMs or MAFMs. The effect due to this coupling phenomenon has a much stronger influence on the tube scanner AFM than on the MAFM. In scanning sample systems[20] the sample height has influence on the total coupling effect [62].

[20] *Scanning sample systems move the sample relative to the probe otherwise in scanning probe systems where the probe is moving relative to the sample.*

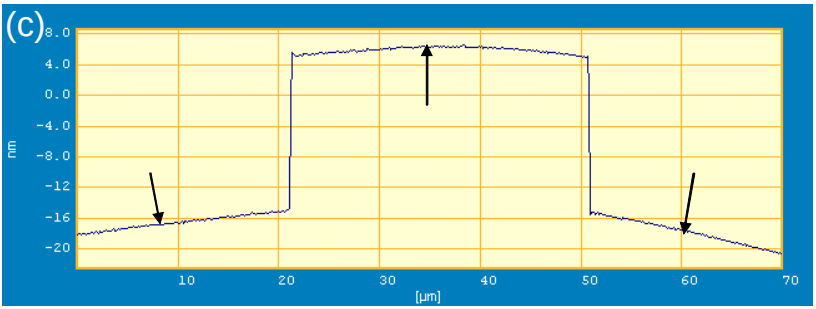

Figure 37: A 70µm × 8.75µm step height measurement with a nominal height of 20nm. The arrows indicate positions where the superimposed bow clearly can be seen

In Figure 37 an example of the coupling effect of the small step height is shown and here the superimposed bow clearly can be identified.

The superimposed bow can be found by measuring on a flatness standard as shown in Figure 13, b and c. To evaluate this “out of plane motion” the measurement has to be corrected for thermal drift (correction term *A*). This is done by subtracting a least mean square fitted first order line from each recorded profile, and an average profile can then be calculated. The remaining curvature of the image can be fitted to a 2nd order polynomium with a good approximation (see (19) and Figure 38).

$$y = a \cdot x^2 + b \cdot x + c \tag{19}$$

where *a* is the coefficient to be determined of the 2nd order term and *x* is the particular position at the aligned profile (see Figure 38).

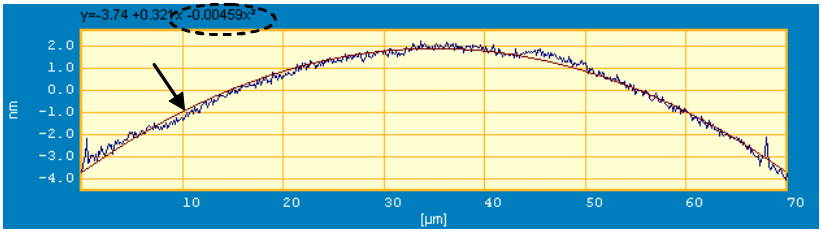

Figure 38: A 70µm × 2.2µm measurement of a flatness standard obtained using the MAFM. The measurement is aligned with a least mean square fitted first order line. The arrow indicates the position of the 2nd order polynomium (thin line) and the value surrounded by dotted circle is the (a) coefficient.

To compensate the step height measurement for superimposed bow or "out of plane motion" the 2nd order term is then subtracted from the image or profile [60].(see Figure 39)

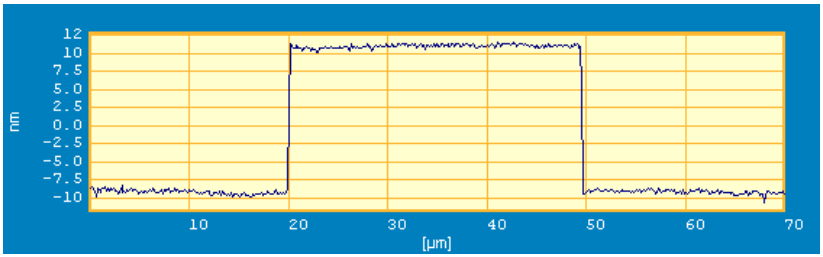

Figure 39: The result obtained by subtract the 2nd order term (Figure 38) from the profile shown in Figure 37

The estimated curvature is sensitive to a change in surface tilt. Therefore it is important to perform the flatness and step height measurements under the same conditions. The contribution of the superimposed bow on the measurement is dependent on the final scan length.

(C): The remaining non-linearity of the vertical distance sensor introduces different correction factors C_z when the average position of the Z-scale is change during scanning. This can have an effect for example on step heights if the positions in

the Z-range are different between measurements or on large step height where the top - bottom distance are in the order of micrometers. The non-linearity can be determined by performing measurements on the same spot at the step height standard and changing the Z - offset between measurements. Afterwards the step height is calculated (see Figure 40).

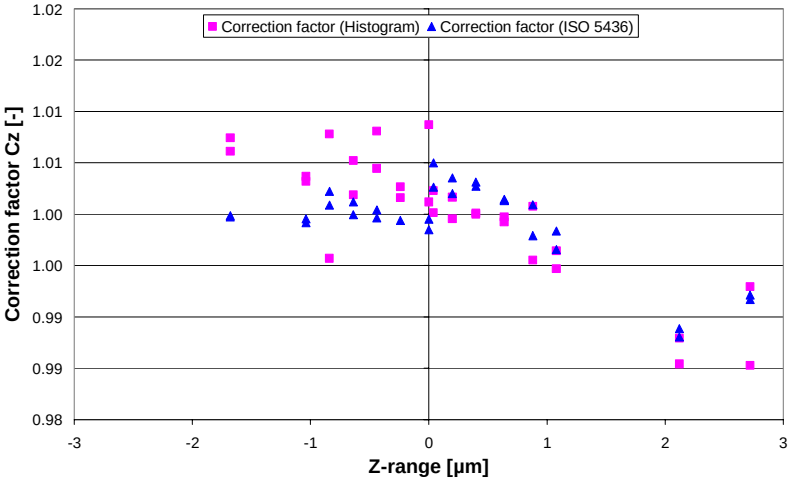

Figure 40: The result obtained during a non-linearity test of the MAFM which has a Z-range at 6µm. The test was performed on a VLSI grating with a nominal value at 180nm. In the graph are result obtained after analogy to ISO 5436 compared to histogram methods (see section 3.2.5).

The graph shown in Figure 40 indicates no significant difference between ISO 5436 and histogram method which belong to the classical methods for step height calculation[21]. Due to the fact that the calibration artefact not is design according to ISO 5436 specifications the calculation is performed using an analogy definition of the ISO standard (see section 3.2.3).

[21] *This method will be described in the next paragraph section 3.2.5.*

3.2.5 Other calibration methods for vertical calibration

AFM images of step heights are often calculated using two different methods [60]:

A. Histogram method[22].

B. A manual point to point measurement.

(A): The Histogram analysis tool calculates individual and cumulative frequencies for a range of data. This tool generates data for the number of occurrences of a value in a data set. The histogram method improves the measurement precision by incorporating the height of many image pixels into the calculation process. Major peaks in the histogram correspond to the top- and bottom plateau of the measurement. The distance between the peak centers gives the step height [65], [66], [67].

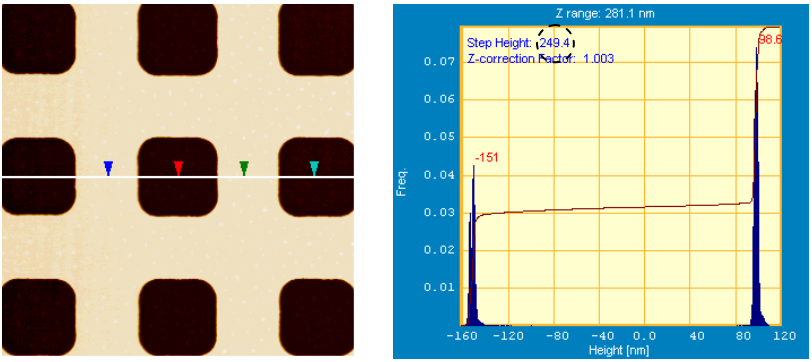

(a) (b)

*Figure 41: A 20µm x 20µm step height measurement **(a)** with a nominal height at 250nm. The line in (a) indicates the position for the profile shown in Figure 43. **(b)** is a height distribution histogram of (a) and the dotted circle in the top shows the observed height [64].*

[22] *This method is used in the comparison arranged under the EU-project SPMet*

The accuracy of the step-height measurement can often be improved by the correlation averaging technique, which will provide an average image with improved signal-to-noise-ratio.

The measured height from the histogram depends systematically upon tilt (see Figure 42). Image bow and hysteresis also cause systematic deviations of the estimated step height. Therefore, the histogram method does not give a unique step height, as there is no common accepted or obvious self consistent method for levelling the observed profile. For calibrations of small step heights this ambiguity may be a problem [60],[65].

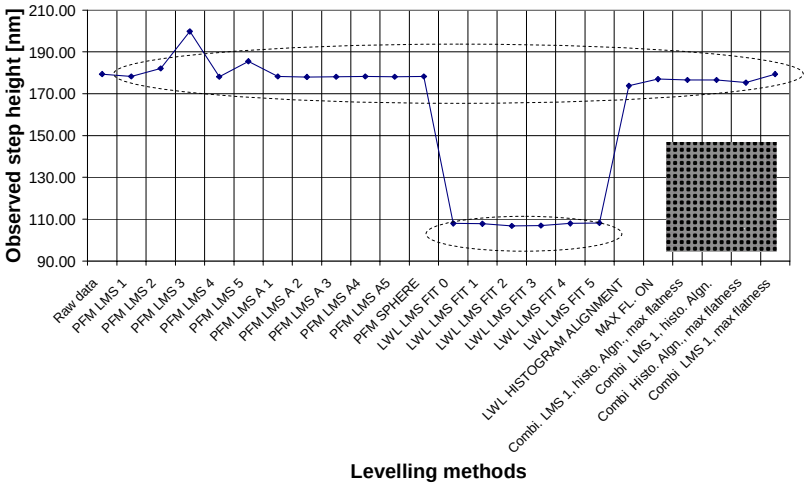

Figure 42: The graph shows the effect of different alignment techniques on the step height (nominal height at 180nm). The majority of the used techniques agree on one value in the order of 180nm, but some levelling methods give significantly lower step heights. PMF = polynomial fit method of least mean square (LMS) n-order. LWL = line wise levelling of least mean square (LMS) n-order

Step-height images will often exhibit overshoot phenomena at the edges, and these overshoots can be explained by combined creep and hysteresis effects of the Z-piezo element

of the scanner. This having effect on the height distribution histogram and the quality of the measurement. To limit this effect it is possible to apply a different filter that results in the best histogram [54].

(B): The manual single-point method is based on recognition of suitable spots at the upper and lower plateaus. This is an extremely sensitive approach for determination of the step height. This method is obviously not satisfactory for calibration, but can give a fast rough “guess” on the obtained step height.

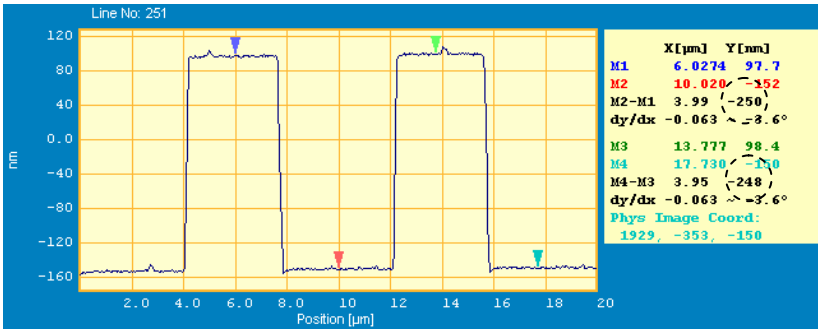

Figure 43: The graph shows a profile of a step height measurement shown in Figure 41. The dotted circles at the right hand side indicate the step height based on a manual point to point measurement (indicated by the markers) [64].

3.2.6 Summary vertical calibration

In this section it is suggested how the Z axis can be calibrated on step height standards after a principle described in ISO 5436. The correction term for the important “out of plane motion” is introduced.

As for the lateral calibration a number of useful steps are suggested that should be considered before performing the vertical calibration.

In order to implement the ISO 5436 it may be needed to modify the definitions mainly because of the design of

calibration artefacts for SPMs and the limited lateral scan range.

In addition to the implementation of ISO 5436, a thorough analysis was performed and the three most important correction terms were identified. There are thermal drift, “out of motion plane” and the remaining non-linearity of the vertical distance sensor.

To perform the vertical calibration after the ISO 5436 all step height measurements have to be corrected for a least these three error contributions before the step height is finally calculated. The correction term can also be useful for other calculation methods.

The histogram and manual point to point methods are some of the most used calculation methods for step heights. The measured height from the histogram depends systematically upon tilt, image bow and hysteresis. Therefore, the histogram method does not give a unique step height. The manual point to point method is only useful for a rough estimate of the step height.

By comparing results obtained after ISO 5436 and histogram methods no significant difference can be observed, mainly because of a strict alignment procedure.

3.3 Summary Calibration of AFMs

To perform a lateral or vertical calibration of an AFM a certain number of steps have to be considered to get the optimal outcome of the work. These include the calibration artefact, the measurement to be performed and data analysis.

Depending on the purpose of the calibration and the accuracy level different procedures can be chosen, e.g. A, A-B, A-B-A sequences or other methods.

The lateral calibration method described in this thesis is based on a two dimensional grid characterized by its lattice constants

in the X and Y direction along with the angle between the two directions.

A linear transformation of the scanned and uncorrected image into a corrected image can be defined by a correction parameter C_x for the X-direction, a correction parameter C_y for the Y-direction and a coupling term C_{xy} between the scanned X and Y axes. Exact expressions for these correction parameters are given for an oblique reference grid. By creating artificial surfaces with variable properties the new methods have been tested with existing calibration facilities.

It is suggested how the Z axis can be calibrated on step height standards after a principle described in ISO 5436. In addition to the implementation of ISO 5436, a thorough analysis was performed to characterize the sensitivity of the approach. From the analysis the three most important correction terms were identified to be: thermal drift, “out of motion plane” and the remaining non-linearity of the vertical distance sensor.

The histogram and manual point to point methods are some of the most used calculation methods for step heights. By comparing results obtained after ISO 5436 and histogram methods no significant difference can be observed.

Chapter 4
VALIDATION OF METROLOGY AFM

The purpose of this chapter is to describe the methods and the results of the performance verification of a MAFM[23].

The starting point for the validation and performance verification test of the MAFM is the participation in intercomparisons. Three comparisons covering the nanometre range of length measurement have been held[24] in the project period in an international forum. Two of the comparisons were arranged by the working group WGDM7 of the Consultative Committee for Length (CCL) under BIPM and are described / defined as pre-key comparison. The last comparison is a part of a EU-project. In this thesis only results obtained in the pre-key comparisons will be presented.

The expected outcome of the validation will be the foundation for an establishment of an accreditated service for AFM measurement performed at DFM. Performance verification of the MAFM leads to increased knowledge about:

- Instrument performance.
- Establishment of traceability - lateral and vertical.
- Calibration- and measuring procedures.
- Uncertainties.
- Calibration artefacts.
- Etc.

[23] For this project the work has been concentrated and limited to verification of the capability of the metrology head, see section 4.2.

[24] DFM has participated in them all.

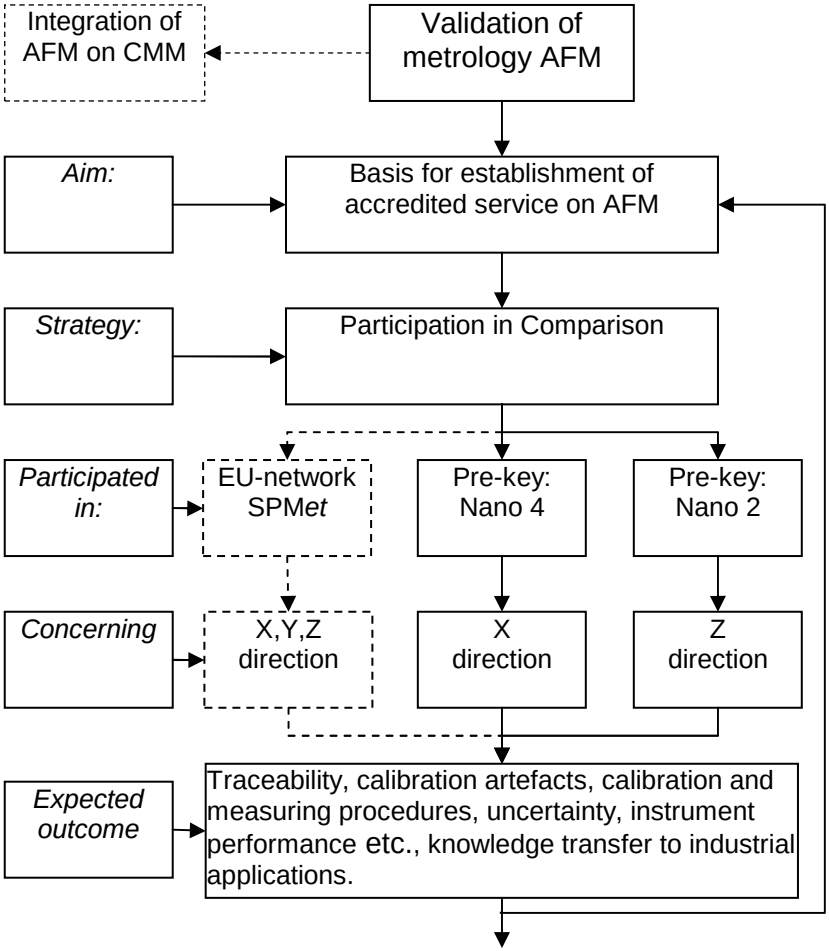

Figure 44: The main objectives for validation of the MAFM. The dotted lines indicate a comparison that will not be described further in this thesis.

The use of performance verification test for AFMs is not limited to a single purpose. Table 13 gives examples of situations where performance verification would typically be carried out [68].

Situation	Necessary action
A. Purchase of AFM	Acceptance testing
B. Service on AFM	Re-verification
C. Periodical inspection (short and long intervals)	Interim testing
D. New hardware or software installation	Re-verification
E. Special or important measurements	Interim testing

Table 13: Typical situations for performance verification of AFMs.

In this project two reasons are obvious for performing verification test.

- DFM has purchased a commercial MAFM in co-operation with Danish Technological Institute (DTI) - *Situation A*.
- Development of a metrological accepted way of performing measurements[25] with the MAFM - *Situation E*.

To develop a metrological accepted way to perform measurements with AFM it is necessary to establish traceability. This can be accomplished by measure on traceable calibration standards [71] and developing calibration- and measurement procedures.

The theories and methods described in the previous chapters will form the basis for the verifications test of the MAFM:

[25] *Establishment of traceability trough calibration on traceable transfer standards.*

- Chapter 2 Establishment of traceable artefacts for calibration and performance testing of SPM
- Chapter 1.6
- Chapter 3 Calibration of AFMs

4.1 Comparisons

Global traceability of units in the SI system is ensured through joint research in the form of international comparison measurements, expert groups and research projects conducted by the various countries national standards laboratories. Comparison measurements on reference standards can provide insight into the state of art of scanning probe microscopy and - if the task is appropriately defined - provide information about weak points.

The working group of the Consultative Committee for Length has decided to start a series of five preliminary key comparisons among National Metrology Institutes in the field of nanometrology [51]. Until now one pre-key comparison is finished (Nano4 with twelve participants). Nano2 (twelve participants) is still running. Nano5 is planned to start in 2002. In the EU network "The Calibration of SPMs (SPM*et*)". 13 partners from five countries have participated[26] [52] and are finished.

The MAFM will be validated trough participation in these intercomparisons.

[26] *There will not be any further presentation or discussion of the result obtained in this particular comparison. The final result can be seen in [52].*

Comparison (Year)	Organized by:	Concerning	Pilot laboratory
SPM*et* (1999)	EU-network	2-D grids Step height Flatness	PTB (DE)
Nano 1	CCL/WGDM7	Line width	
Nano 2 (2001)	CCL/WGDM7	Step height	PTB (DE)
Nano 3	CCL/WGDM7	Line spacing	
Nano 4 (1999)	CCL/WGDM7	1-D gratings	OFMET(SW)
Nano 5 (2002)	CCL/WGDM7	2-D grids	DFM (DK)

Table 14: The planned intercomparisons for nanometrology.

In general the comparison of the results has to comprise both the measured features and the stated uncertainties. A common used way to do this is to calculate an E_N-value.

$$E_N = \left| \left(\frac{\text{Result}_{\text{NMI}} - \text{Result}_{\text{Reference}}}{\sqrt{U_{\text{NMI}}{}^2 + U_{\text{Reference}}{}^2}} \right) \right| \qquad (20)$$

The E_N-value describes the difference between the result obtained by the participant and the reference value compared to the stated uncertainties. If E_N<1 there is good agreement between the two results, and if E_N>1 then the results are significantly different. Of course a very big stated uncertainty U_{NMI} also causes small E_N-values and here the E_N-value might give a wrong picture of the situation.

4.2 The MAFM

A metrological atomic force microscope system is a system where the tip moves along orthogonal axes (not the commonly used tube scanners) and the position of the tip is measured by distance sensors and not just deduced from the voltage input to the scanning device. Such instruments have been built by several scientific groups and have been commercially available for some years. However they are still only used by a limited amount of groups [60].

The MAFM used in this project (see Figure 45, right) is equipped with a special metrology head containing capacitive sensors in X;Y and Z-direction (see Figure 45, right). The MAFM head incorporates a closed loop scanning in the x and Y direction based on signals from capacitive sensors.

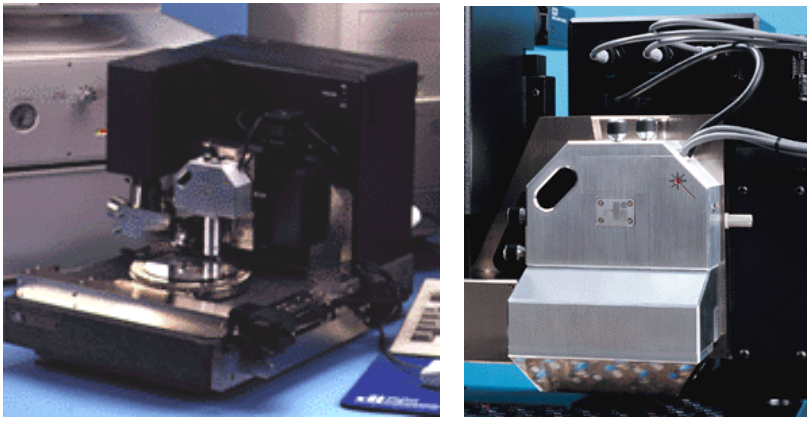

Figure 45: The complete MAFM, left, equipped with a metrology head (right).

The instrument has a nominal horizontal scanning range of 70 µm × 70 µm, and a nominal vertical range of 6 µm [72].

The main parts are: CCD-camera, a semi automatic moving stage for the sample and the mounting facility for the scanner head (see Figure 45, left).

The construction of the scanner head ensures that each axis of the scanning system is straight and mutually orthogonal with minimum amounts of roll, pitch and yaw (See Figure 46).

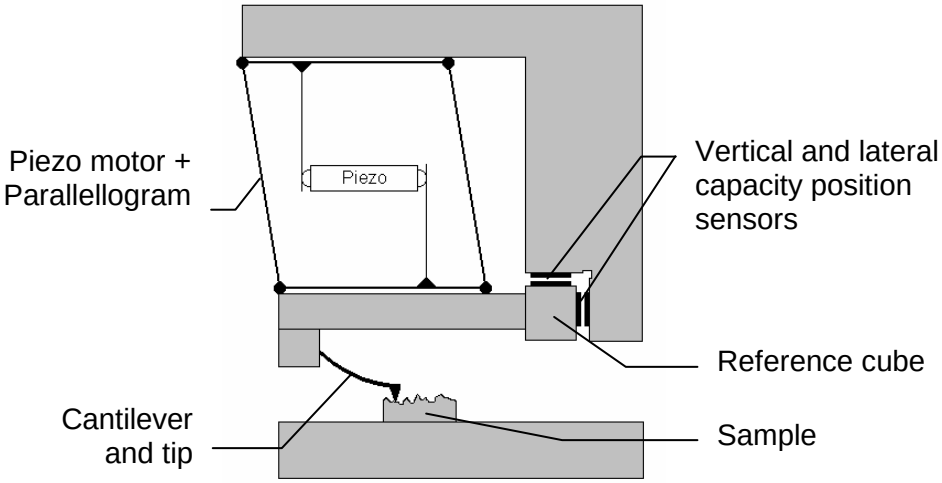

Figure 46: Sketch of the metrology system. The metrology frame is indicated for the x and z axis only. The figure is modified from [49].

In Table 15 the manufacturer's main specifications are listed [72].

Linearity(X,Y)	± 0.10 % for x,y
Linearity (Z)	± 1.2 % for Z
Orthogonally (X,Y)	<0.1° for x,y
Repeatability	1.5 nm(1σ) for x,y 0.25 nm(1σ) for z
Accuracy	± 0.3 % for X,Y ± 1.2 % for Z
Flatness translation	± 5 nm for X ± 10 nm for Y

Table 15: Main specifications of the MAFM [72].

4.3 Experimental setup

4.3.1 Environmental conditions

The laboratory at DFM is temperature controlled, and kept at 20.5° ± 1.5°C. To minimize vibrations the system is placed on a vibration isolation platform. The vibration isolation platform has a continuous stainless steel top and edge, with a core constructed of bonded steel plates and core material. This entire assembly is suspended by compressed air using pneumatic isolators. The specimens are placed in the laboratory at least 72 hours before use in order to assure thermal stability. All the measurements are recorded on a thermally stable AFM ("power on" for a minimum of 48 hours before measurement).

4.3.2 Establishment of traceability

In order to establish traceability for the lateral and vertical directions of the MAFM the following calibration artefacts have been used.

Lateral direction:

To establish the traceability for the lateral direction a 2D-calibration artefact calibrated at NPL was used [73]. NPL calibrating the artefact using a technique based on a diffraction method. The diffraction method gives the mean period of the pitch distance of the 2D calibration artefact. The main calibration results are presented in Table 16.

As seen from Table 16 the lateral calibration artefact has an oblique lattice structure.

The calibration grid is fabricated by a photolithography method. The mask-oxide-layer is patterned by holography. The advantage of the holographic technique is a highly equidistant pattern all over the standard (see Figure 47).

	Certificate value	Uncertainty U(k = 2)
Mean Period for x,Y direction [µm]	0.895	0.001
Mean period, + diagonal [µm]	1.254	0.001
Mean period, - diagonal [µm]	1.278	0.001
Orthogonality Error [deg:min:sec]	+01:06:22	00:02:00

Table 16: The certified values and uncertainties (k=2) for the lateral calibration artefact used for validation of MAFM [73].

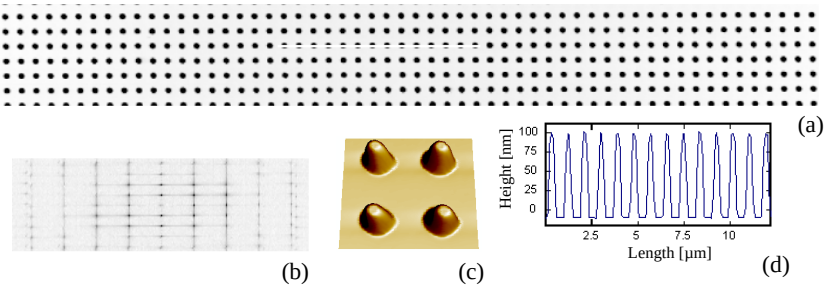

Figure 47: The pictures described in Table 14 show a typical measurement of the 2D-reference standard. The height of the pitch is ≈100 nm. ***(a)*** *50 µm x 6.25 µm scanned area.* ***(b)*** *Fourier transformation of (a).* ***(c)*** *3D-view of zoomed pitch structure.* ***(d)*** *Profile along the line in (a).*

Vertical direction

Establishment of traceability for the vertical direction was achieved using a series of step height artefacts calibrated at PTB [41]. They were calibrated by fringe evaluation in an interference microscope. The main calibration results are presented in Table 17.

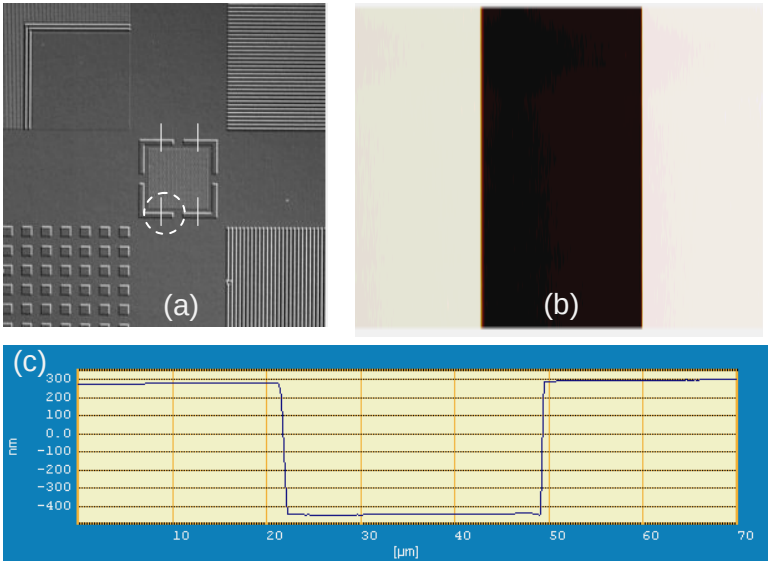

Figure 48: The traceable step height standard used for vertical calibration in the pre-key comparison Nano2. The step height standard has a certified height of 759.7 nm, and a nominal width of the step height of 20 µm. ***(a)*** *is an image of the standard. The white line indicates the certified areas. The dotted circle indicates the spot which is used for all calibrations.* ***(b)*** *is a measurement obtained on (a) and* ***(c)*** *is an average profile of (b).*

ID and nominal step height [nm]	Certificate value [nm]	Uncertainty U(k = 2) [nm]
H24 - 24	*13.2*	3.2
H80 - 80	*81.4*	4.6
H240 - 240	*258.7*	5.4
H800 - 800	*759.7*	8.2
H2400 - 2400	*2322*	17

Table 17: The certified values and uncertainties (k=2) for vertical calibration artefacts used for validation of MAFM [41].

The standard has a nominal height of 800 nm, and a nominal width of the step height of 20 µm. It is made in silicon and silicon oxide and covered with a metallic layer of PtIr.

4.3.3 Calibration and measurement procedures

For the two major comparisons Nano 4 and Nano 2 the same general approach for combined calibration and measuring procedure (A-B-A) has been used. As mentioned earlier a calibration and measuring procedure based on the A-B-A sequence is very useful as a concept for comparable measurements. All calibrations correspond to the **A**-B-**A** sequences (and measurements on the unknown specimen correspond to A-**B**-A).

For the procedure used in the pre-key comparisons a number of parameters have been changed to ensure the validity of the measurements and the robustness of the results. Between measurements the following conditions are changed:

- The tip - sample interaction.
- Gain.
- Orientation and location of sample.
- Investigated spot on sample.
- Time, temperature and humidity.

This includes all the necessary changes of conditions in order to measure an unknown sample (B). By changing the tip we achieve different Abbé offset. The environmental condition, temperature and humidity, are influence parameters that change the permeability of the air which affects the capacity of the linearization sensors [47].

4.4 Pre-key comparison - Nano 4

The aim of this pre-key comparison[27] was to compare pitch measurements of 1D gratings in the nanometre range. The standards should meet the requirements of different measuring methods such as SEM, STM, AFM or laser diffraction [74].

The comparison was held as a pre-key comparison due to the fact that this is the first larger intercomparison into the nanometre range. If the results show good agreement the comparison will be accepted as a real key comparison [74].

4.4.1 The unknown 1D-gratings

The transfer standards used were two holographic gratings, manufactured by Moxtek, with pitches of nominally 290 nm (EAM G/300-1) and 700 nm (EAM G/700-1). The direction of the pitch was defined to be orthogonal to the ribs of the grating (see Figure 49).

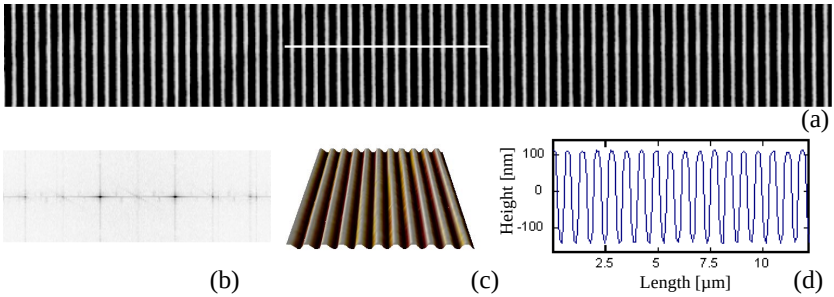

Figure 49: Nano4: The pictures above are typical measurement of the unknown line specimen. The distance between the ribs is ≈ 700 nm and the height ≈ 200 nm. ***(a)*** *50 µm x 6.25 µm scanned area.* ***(b)*** *Fourier transformation of (a).* ***(c)*** *3D-view of rib structure (zoomed).* ***(d)*** *Profile along the line in (a) [47], [48].*

[27] *Nano4, started in February 1999 with the Swiss Federal Office of Metrology as the pilot laboratory.*

The measurand for this comparison was defined to be the average pitch distance over the central surface of 1 mm × 1 mm at 20°C. The participants should deliver the average pitch values with the standard uncertainty u_c and the degree of freedom ν_{eff}*.used to obtain* u_c *[74],[75].*

4.4.2 Experimental methods

A rectangular area of 50 µm x 6.25 µm with a resolution of 512 × 64 pixels was used for all the measurements. The 2D reference lattice was orientated so that its ***a*** and ***b*** directions were approximately parallel to the scanning X and Y-axis, respectively, see Figure 47. It is along the fast scanning X direction the best calibration of the AFM is obtained. For the line specimen the lines were always oriented approximately parallel to the Y-axis.

The central part of the unknown 1D gratings were measured in five different spots as shown in Figure 50. For the line specimen the lines were always oriented approximately parallel to the Y-axis (see Figure 49) [47], [48].

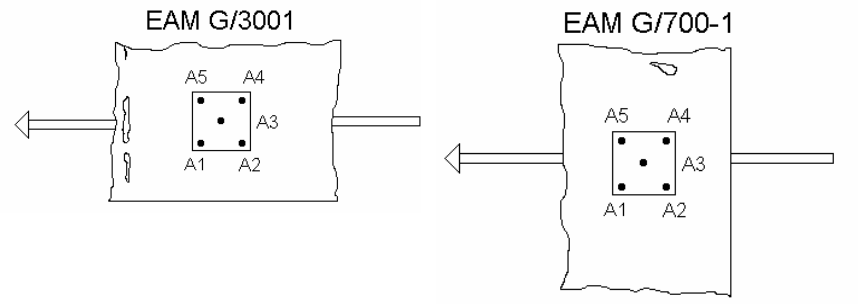

(a) (b)

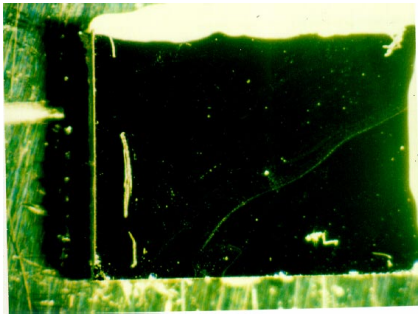

(c)

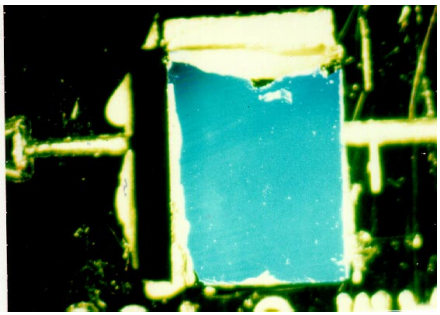

(d)

*Figure 50: **(a)** and **(b)** indicates the measuring position on the unknown line specimen. **(c)** and **(d)** are polaroid pictures of the unknown line specimen [76].*

Four cycles of measurements were performed on each of the five spots on each line standards. The cycles started at area one and ended at area five. More than eight hundred measurements were performed.

4.4.3 Data analysis

During the data analysis two different procedures were used. The first procedure is to calculate the correction parameters, C_x, C_y and C_{xy}, based on the reference measurements (See section 3.1.3 for theory). Three steps are required to estimate these parameters:

1. Slope correction
2. The unit cell vectors $\underline{a}$ and $\underline{b}$ are estimated based on the Fourier transformation.
3. The correction parameters and associated uncertainties are calculated

The second procedure is to correct the observed image of the unknown specimen and find the pitch distance, L. Four steps are required to estimated the line spacing

1. The observed image is corrected with the linear transformation given by the three correction parameters (C_x,C_y and C_{xy}).
2. Slope correction
3. The wave vector for the lines is calculated based on the Fourier transformation
4. The length *L* and the associated uncertainty is calculated.

It was chosen only to use the Fourier Transformation during the analysis to obtain comparability between methods.

To determine the periodic distance *L* of an unknown line specimen, the distorted image is transformed into the corrected image by applying the linear transformation matrix $\underline{\underline{C}}$ *and* $\overline{e'}$*. L* can then be obtained using equation (21) [76]:

$$L = \sqrt{\left(C_x \cdot e'_x + C_{xy} \cdot e'_y\right)^2 + \left(C_y \cdot e'_y\right)^2} \tag{21}$$

where $\overline{e}' = \left(e'_x, e'_y\right)$ is the vector connecting perpendicular two adjacent rips in the corrected image.

4.4.4 Results and uncertainties

The model functions given by (12) - (15) and (21) are used to calculate the correction parameters, line spacing and the associated uncertainty[28].

Two representative examples of uncertainty budgets are shown in Table 18. The uncertainty budgets correspond to one series of measurements.

[28] *All uncertainty calculations for the comparisons are documented in [77].*

i	*Quantity*	*Distribution*	x_i	$u(x_i)$	ν_i	c_i	$u_i(y)$	$r(x_i,y)$
1	L_a [nm]	Normal	895	0.5	infinity	1.21E-07	6.07E-08	8.46E-05
2	L_b [nm]	Normal	895	0.5	infinity	1.12E-03	5.59E-04	7.79E-01
3	γ [°]	Normal	91.106	0.033	infinity	7.94E-05	2.62E-06	3.65E-03
4	d_x [-]	Normal	0	0.0003	21	-1.00E+00	-3.00E-04	-4.18E-01
5	d_y [-]	Normal	0	0.0198	21			
6	a'_x [nm]	Normal	-24.15	0.30	infinity	5.09E-06	1.53E-06	2.13E-03
7	a'_y [nm]	Normal	-910.62	2.40	infinity	-1.56E-08	-3.75E-08	-5.23E-05
8	b'_x [nm]	Normal	895.05	0.30	infinity	-1.12E-03	-3.35E-04	-4.67E-01
9	b'_y [nm]	Normal	-4.15	2.40	infinity	3.44E-06	8.24E-06	1.15E-02
	C_x	**Normal**	**0.9999**	**0.0007**	**infinity**			

Table 18: Uncertainty budget for correction parameter C_x = (0.9999 ± 0.0014) (k = 2). This uncertainty budget corresponds to one series of measurements. [47], [48], [76].

For the presented uncertainty budget are the:

- x_i = Estimate (input)
- $u(x_i)$ = Standard Uncertainty (input)
- ν_i = Degrees of Freedom (input)
- c_i = Sensitivity Coefficient (output)
- $u_i(y)$ = Contribution to Uncertainty (output)
- $r(x_i,y)$ = Correlation coefficient (output)

Quantities 1, 2 and 3 are from the certificate of the reference calibration standard. Quantities 4 and 5 are the reproducibility and the uncertainty is estimated based on the calibration history of the AFM. Quantities 6, 7, 8 and 9 are the values obtained from the observed unit cell vector. They represent the repeatability and the uncertainties include, for example the finite number of samples and the number of observed pitches. The expanded uncertainty U_{Cx} is found to be 0.14% at a confidence level of 95%. The main contribution to the uncertainty is the certified reference value of the calibration standard. The uncertainties for C_y and C_{xy} can be estimated in

a similar way. They are found to be U_{Cy} = 4.1% and U_{Cxy} = 0.15% [47], [48], [76].

i	*Quantity*	*Distribution*	x_i	$u(x_i)$	ν_i	c_i	$u_i(y)$	$r(x_i,y)$
1	C_x	Normal	0.99992	0.0007	infinity	6.99E+02	4.89E-01	9.97E-01
2	C_y	Normal	0.98919	0.0205	infinity	4.59E-07	9.41E-09	1.92E-08
3	C_{xy}	Normal	-0.01342	0.0008	infinity	-1.80E-02	-1.35E-05	-2.75E-05
4	e'_x [nm]	Normal	698.62	0.0350	16	1.00E+00	3.50E-02	7.14E-02
5	e'_y [nm]	Normal	0.018	0.0030	16	-1.34E-02	-4.03E-05	-8.23E-05
	L [nm]	**Normal**	**698.6**	**0.49**	**infinity**			

Table 19: Line spacing L = (698.6 ± 0.98) nm (k = 2) of the unknown line specimen. This uncertainty budget corresponds to one series of measurements [47], [48], [76].

The model function of the line spacing (21) has the correction parameter and the observed line spacing $\underline{e'}$ as input parameters. The expanded uncertainty U_L is found to be 0.2% at a confidence level of 95%. The main contribution of uncertainty is the uncertainty of the correction parameter C_x.

Quantities 1, 2 and 3 are from the determination of the correction parameters. Quantities 4 and 5 are the values obtained from the observed line space vector.

The expanded uncertainty U_L for EAM G-300/1 and EAM G-700/1 is found to be 0.14% at a confidence level of 95%. The main contribution of uncertainty is from the uncertainty of the correction parameter C_x.

The final result as reported to the pilot laboratory can be seen in Table 20. The results obtained in the five spots are summarized in Appendix 3.

Id. no.	Measured average Pitch (over 1mm^2) P [nm]	Uncert. (1σ) u_c [nm]	Eff. deg. of freedom $\nu_{eff.}$
EAM G-300/1	287.47	0.20	Infinity
EAM G-700/1	700.38	0.48	Infinity

Table 20: The final values reported to the pilot laboratory of Nano4 [76].

The pre-key comparison ended in the summer of 2000. The complete result of the comparisons was presented by the pilot laboratory in 2001. A summary of the comparison is shown in Table 21 and Table 22.

Gratings:	G-300	G-700
P_{ref}	287.5961 nm	700.7607 nm
u_c	0.0011 nm	0.0023 nm
ν_{eff}	146	159
U_{95}	0.0021 nm	0.0046 nm

Table 21: Reference value of Nano4 P_{ref}, the combined standard uncertainty u_c, the resulting degree of freedom ν_{eff} and the expanded uncertainty U_{95} obtained from all measurements with EN < 1 [75].

Participants	*dp* (nm)	E_N	*dp* (nm)	E_N
First loop[29]:	G-300/1		G-700/1	
Pilot lab1	0.0001	0.01	0.0017	0.18
Pilot lab2	0.0123	0.78	0.0297	0.30
DFM	**-0.1261**	**0.32**	**-0.3807**	**0.40**
P2	-0.0038	0.57	0.0349	2.18
P3	0.0039	0.39	-0.0067	0.07
Second loop:	G-300/3		G-700/3	
Pilot lab1	0.0011	0.13	0.0066	0.58
Pilot lab2	0.0081	0.63	0.0272	0.85
P4	-0.5861	0.82	-0.6607	0.33
P5	0.0009	0.11	0.0043	0.10
P6			0.0393	0.13
P7	-0.1961	0.48	-1.0607	0.63
P8	-0.0011	0.29	0.0073	0.19
P9	-0.0101	0.07	0.0533	0.11
P10	-0.1961	0.09	-2.6607	0.51
P11	-0.0062	1.37	-0.0073	0.87

Table 22: Deviations from the comparison Reference value dp and En values for the G-300 and G-700 gratings. The result obtained by DFM is highlighted [75].

4.4.5 Summary and conclusions - Nano 4

The aim of the Nano4 comparison was to determine an average pitch distance in the nanometre range. The two 1D-

[29] *There have been 2 loops in Nano4. The unknown line standards were contaminated / damaged and therefore exchanged.*

gratings transfer standards used were two holographic gratings, manufactured by Moxtek, with pitches of nominally 290 nm (EAM G/300-1) and 700 nm (EAM G/700-1). The direction of the pitch was defined to be orthogonal to the ribs of the grating.

The final result for the pre-key comparison showed the values reported by DFM had an E_N-value below 1 and DFM therefore successfully completed the comparison.

During the participation in Nano4 the MAFM has successfully been calibrated based on an oblique reference lattice. For the calibration an expanded uncertainty in the X-direction of U_{Cx} = 0.15% (k = 2) was achieved. The calibration was done for a particular measurement area of 50 µm x 6.25 µm.

Measurement conditions were changed during calibration measurements, ensuring a high degree of confidence in the measurements of the unknown samples.

The Consultative Committee for Length under BIPM accepted to upgrade the preliminary key-comparison to a key-comparison [51].

4.5 Pre-key comparison Nano2

The proposal for this pre-key comparison is to establish agreement about the definition of step heights. The step height standards cover the range from nanometers to several micrometers. Furthermore the measurand should make it possible that different instrument, for example stylus instruments, interference microscopes and other optical instruments as well as scanning probe microscopes could be used [50].

4.5.1 The unknown step height standards

The three transfer step height standards possess nominal step heights at 20 nm (SH20), 70 nm (SH70) and 800 nm (SH800). The measurand defined for this comparison is the average

height obtained from different measurements within the reference area R1 [50] (see Figure 51).

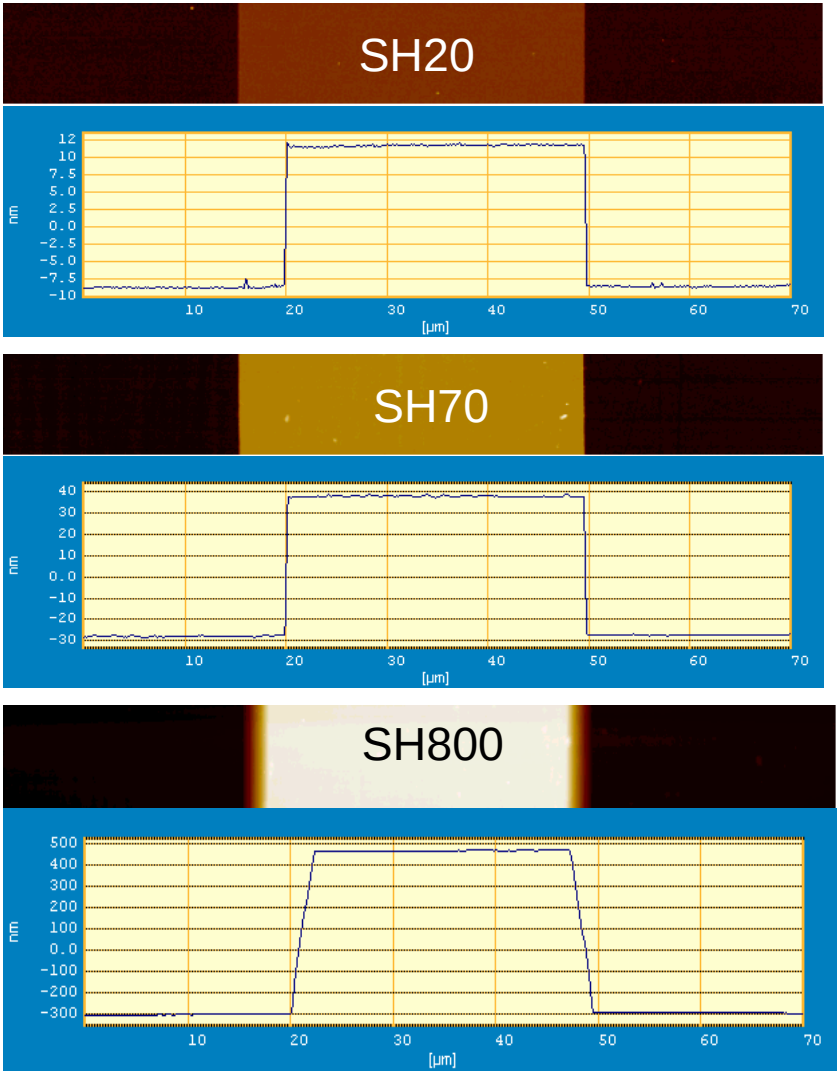

Figure 51: Representative examples of the three unknown step heights to be measured in Nano2.

4.5.2 Experimental methods

For the vertical calibration the reference step height standards are measured and evaluated from images of 64 lines with 512 points corresponding to 70 µm × 8.75 µm, with the edge / groove parallel to the Y-axis. The surfaces were imaged for different average Z-positions (offsets) and at different angles to determine sensitivity and image bow for different ranges of the Z-scale. The same spot of the reference standard was used during all calibrations (see Figure 48).

The unknown transfer step height standards were measured and evaluated at four different spots S1, S2, S3 and S4 along the step height in the square R1 (see Figure 52) from images of 70 µm × 8.75 µm.

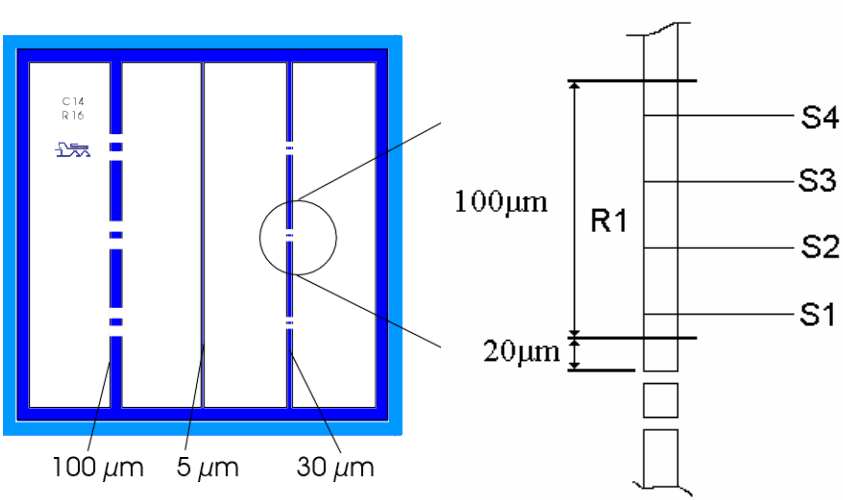

Figure 52: The line used for the comparison has a width of 30 µm and is located on the right side. The field R1 which should be used for the measurements is shown on the right hand side of the figure.

The spot S1 was ≈ 20 µm from the top of the square, S2 ≈ 40 µm, S3 ≈ 60 µm and S4 ≈ 80 µm. On each spot two to four images were recorded with the same tip. The

measurements on spot S1, S2, S3 and S4 were repeated three to four times with different tips. The average step height for the four spots S1, S2, S3 and S4 were then calculated and the average step height, that is the measurand, was calculated. This procedure takes into account a possible significant variation of step heights over the measurement area [78].

4.5.3 Data analysis

The design of SH20, SH70 and SH800 contains one single step height (see Figure 52) which is to wide for the MAFM if the ISO standard has to be followed. The pilot laboratory suggested an analogy definition as shown in Figure 53. The correct definition can be found in section 3.2.3.

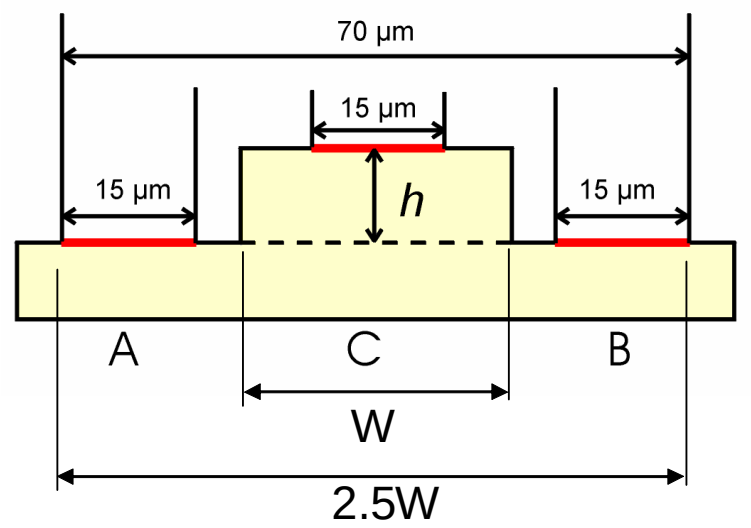

Figure 53: The analogy step height definition after ISO 5436 that was followed in the comparison Nano2 [50]. The total length to be measured corresponds to 2.5W and not 3W as stated in ISO 5436.

A large experimental test was performed to determine the three correction terms as described in section 3.2.4.

The outcome of the test showed:

Correction terms	Error determined by experiment	Residuals after correction.
(A) Thermal drift causes height level differences up to:	≈20 nm	± 0.1 nm
(B) The "out of plane" motion in the X-direction was:	6 ± 0.4 nm for an offset within ± 1 µm	0 ± 0.4 nm
(C) The remaining non-linear error of the vertical capacitive distance sensors has a contribution to the Z-coordinate of up to:	≈50 nm per ≈5 µm	0 ± 0.1 nm

Table 23: The determined correction terms used for step height estimations. The residuals after corrections will be treated as uncertainty contributions. The "out of plane motion" is depending on the X-scan range.

Further description can be found in [59], [60].

An artificial surface containing the reversal superimposed bow[30] (ax^2 = 0.00448) was added to the uncorrected image to compensate for correction term (B). A least squares fitted first order line was subtracted from each recorded line to eliminate thermal drift (correction term (A)), and an average profile was then calculated. A specially developed software algorithm identified the edges of the step and fitted two parallel lines, one line to the profiles A and B segment and the other line to the C segment of the profile (see Figure 53). The Z-coordinate

[30] *The proposel to find the superimposed bow is described in section 3.2.4.*

distance between the two parallel lines is the estimate of the step height *h*, which is the measurand of the comparison. To compensated for the contribution of non-linearity In the Z-scale (Correction term (C)) all measurements were performed symmetrically to the zero point of the Z-scale (0 ± 0.5 µm).

4.5.4 Results and uncertainties

During the preliminary uncertainty estimation of the vertical calibrations the achievable uncertainty was strongly dominated by the stated uncertainties of the reference standard (H800). Table 24 shows the average measured step height Δz_m as function of the reference step height Δz_{ref}. It is seen that the uncertainty of the reference heights of 13 nm (H24) and 80 nm (H80) are much larger than the experimental standard deviation $S(\Delta z_m)$ for the MAFM measurements [59].

Sample	Δz_m [a] [nm]	$S(\Delta z_m)$ [b] [nm]	Δz_{ref} [c] [nm]	E_N
H800	759.7 (4.2)[d]	0.98	759.7 (4.1)	NA
H80	81.7 (0.7)	0.20	81.4 (2.3)	-0.06
H24	12.9 (0.5)	0.07	13.2 (1.6)	-0.09

Table 24: The observed step height Δz_m and reference values Δz_{ref}. [a] The calibrated average step height estimated from the average profile from more than ten different images with more than two different tips. [b] The experimental standard deviation of the observed average step height. [c] The reference step height. [d] The calibration is done by setting Δz_0 for H800 equal to Δz_{ref} for H800. Value presented in braces indicate the combined standard uncertainty for k = 1.

In order to avoid a relatively high uncertainty for measuring on the small step height standards the Z-scale was subdivided because the stated uncertainty on the small transfer standards is relatively high (12.1%). The subdivision is performed on the basis of the H800 step height standard with a stated uncertainty of 0.6%. This means that the relative low

uncertainty stated for H800 compared to H24 can be transferred to the smaller step height standard (H24) by setting Δz_m for H800 equal to Δz_{ref} for H800. The correction factor $C_{z(H800)}$ and corresponding relative uncertainty are then used on all step height measurements. The subdivision leads to an uncertainty on small step height standards (H24) that is more than three times smaller than the stated uncertainty on the standard (H80 and H24).

The validity of the subdivided Z-scale based on the result obtained on the three traceable step height standards (H24, H80 and H800) is expressed as a E_N-values (see Table 24). The absolute value of all E_N-values is smaller than 1 which means that at a confidence level of 95% the AFM measurements are consistent with the reference values [60].

Furthermore the linearity of the Z-response was investigated by performing measurements on the H800 step height standard in different positions of the Z-range. This might give more robust guess of the linearity due to the relatively high uncertainty on the small step height standards (H24 and H80).

The investigations described above lead to the following equations to calculate the step height of the unknown step height standards and the corresponding uncertainties [78]:

$$H_{SHunknown} = \left(\delta H'_{C-SH} \cdot \frac{\delta H_{Traceablity}}{\delta H'_{Traceablity}} \right) \tag{22}$$

where

$$\delta H'_{C-SH} = \delta H'_{SHunknown} + \left(\delta h_1 + \delta h_2 + \delta h_3 + \delta h_4 + \delta h_5 \right) \tag{23}$$

The description of the quantities is given in Table 25.

Quantity X_i	Descriptions	Estimate x_i
$H_{SHunknown}$	Is the corrected step height of $SH_{unknown}$	See budget Table 26
$\delta H'_{SHunknown}$	Is the observed step height of $SH_{unknown}$.	See budget Table 26
$\delta H_{Traceability}$	Is the reference step height of the traceable standard.	759.7 ± 4.1 nm
$\delta H'_{Traceability}$	Is the observed step height of the traceable standard.	733.77 ± 1 nm
δh_1	Error due to thermal drift and mechanical vibrations.	0 ± 0.1 nm
δh_2	Error due to the remaining coupling between the height *z* and the position *x*. This coupling is referred to as “image bow error”.	0 ± 0.4 nm
δh_3	Error due to the difference in projected step height for the tilted profile segment A, B, and C and the step height *perpendicular* to the surface.	0 ± 0.01 nm
δh_4	Error due to the difference between the observed average step height and the average step height of the area R1 due to roughness and lack of uniformity of the surface	0 ± 0.15 nm
δh_5	Is the error due to remaining nonlinearity of the Z-scale.	0 ± 0.1 nm

Table 25: Quantities and uncertainty estimation of step height measurements [78].

The standard uncertainties of $\delta H'_{SHunknown}$ is a result of the difference between the average step height and the fit due to errors caused by

- the limited number of pixels, and recorded lines
- imperfections in horizontal alignment of the grooves in the image before the average profile is calculated
- imperfections in estimation of the edge position and thereby the A, B and C segment of the average profile

An example of the uncertainty calculation is shown in Table 26: The final report has not yet been submitted to the pilot laboratory. Therefore the results can be considered as best guess from the author.

Result and uncertainty for SH20

i	*Quantity*	*Distribution*	x_i	$u(x_i)$	ν_i	c_i	$u_i(y)$	$r(x_i,y)$
1	$\delta H_{Traceability}$ *[nm]*	Normal	759.7	4.1	infinity	2.70E-02	1.13E-01	2.40E-01
2	$\delta H'_{Traceability}$ *[nm]*	Normal	733.77	1	8	-2.80E-02	-2.00E-02	-6.00E-02
3	$\delta H'_{SH20}$ *[nm]*	Normal	20.26	0.02	48	1.03E+00	2.00E-02	4.40E-01
4	δh_1 *[nm]*	Normal	0	0.1	infinity	1.00E+00	1.00E-01	2.10E-01
5	δh_2 *[nm]*	Normal	0	0.4	infinity	1.00E+00	4.00E-01	8.60E-01
6	δh_3 *[nm]*	Normal	0	0.01	infinity	1.00E+00	1.00E-02	2.00E-02
7	δh_4 *[nm]*	Normal	0	0.15	infinity	1.00E+00	1.50E-01	3.20E-01
8	δh_5 *[nm]*	Normal	0	0.10	infinity	1.00E+00	1.00E-01	2.10E-01
	H_{SH20} *[nm]*	**Normal**	**≈20**	**0.47**	**infinity**			

Table 26: Example of the result and uncertainty calculation for the unknown step height SH20.

The expanded uncertainty for SH70 and SH800 is shown in Table 27 and Appendix 4. A given uncertainty only makes sense where it is given with respect to a measurement result.

The final result is classified until the pre-key comparison has ended. The expanded uncertainty is shown in Table 27.

Height	Step height nm	**Uncertainty (k = 2) u_c /nm**	**Eff. deg. of freedom $\nu_{eff}(h)$**
SH20	≈20nm	0.9	Infinity
SH70	≈70nm	1.2	Infinity
SH800	≈800nm	8.7	Infinity

Table 27: The uncertainties for the three unknown step height SH20, SH70 and SH800.

4.5.5 Summary and conclusions - Nano2

The aim of the pre-key comparison Nano2 was to estimate an average step height after an analogy to the ISO 5436.The three transfer step height standards had nominal step heights of 20 nm (SH20), 70 nm (SH70) and 800 nm (SH800). The measurand is the average height obtained from different measurements within a reference area. The results obtained on the unknown step height are classified until the pre-key comparison has ended.

The measurements were obtained by following an A-B-A sequence. The calibrations and measurements on the unknown transfer step height standard were performed for a specific measurement area of 70 µm × 8.75 µm. During the measurements many conditions were changed to ensure a high degree of confidence of the measurements.

The MAFM has successfully been calibrated in the vertical direction during the participation in Nano2. The vertical calibration is based on a subdivision of the Z-scale from a step height at 800nm and verified on several other step height standards covering the whole Z-scale.

Based on the investigation of flat surfaces and tilted step heights the nonlinearity and measurement uncertainty of the system has been assessed and estimated.

Through the subdivided Z-scale the achievable uncertainty on the three measurands has been improved to be in the order of 0.5 - 5 %.

4.6 Performance verification of MAFM

In the last part of this chapter, the results obtained during the participation in pre-key comparisons will be summarized according to the final validation and performance verification of the MAFM. Some results have already been presented as illustrations and examples in the previous chapters.

Many performance parameters can be used to verify the MAFM. For this project the approach is mainly focused on verifying the metrology head trough an establishment of traceability by performing calibration on traceable transfer standards.

The performance verification has been split into three main parts (see Figure 54) regarding:

- *Part 1:* Parameters for X,Y-direction.
- *Part 2*: Parameters for Z-direction.
- *Part 3:* other test, which have been performed.

according to the specifications listed in Table 15.

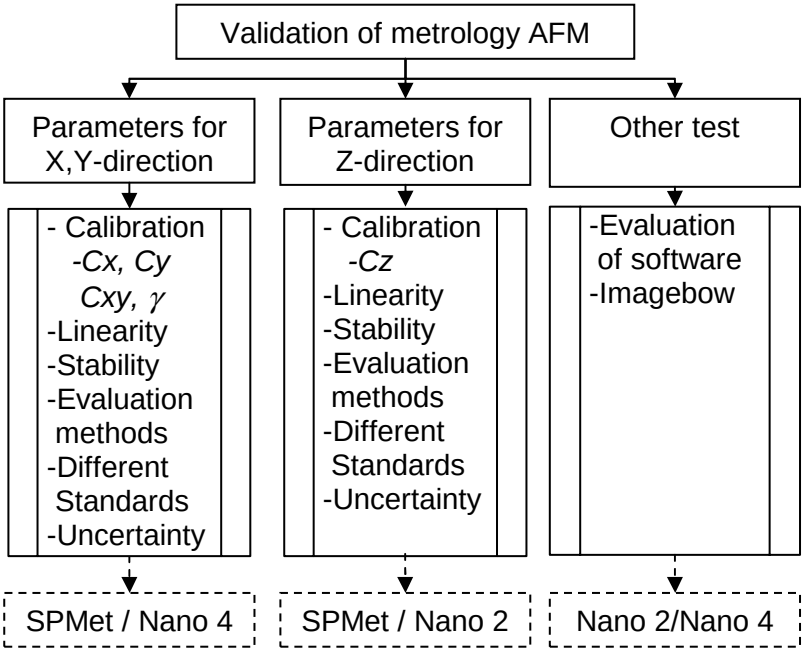

Figure 54: Main parameters to be identified during this project.

4.7 Validation of the performance in the lateral direction (x,y).

The major contribution to this chapter is established trough participation in Nano4. The investigations were focused on performing traceable calibrations, but the non-linearity was evaluated as well. The primary set of data obtained under Nano4 is a non-squared image (50 µm × 6.25 µm). The performances of the lateral direction of the MAFM are here expressed in a set of correction parameters (C_x, C_y and C_{xy}), the non-linearity (mean position error) and angle γ between X and Y-direction.

The effect on the calibration result of using non-squared images leads to a reduced number of periodical structures in the Y-direction which causes a higher uncertainty on

estimation of the unit cell for this particular direction. To ensure a more robust result for parameters in the Y-direction a large series of squared images was measured subsequently (50 µm × 50 µm).

It is expected that the error corresponding to the lateral calibration and non-linearity of the MAFM is small. The MAFM uses an online feedback control system based on the signals from the capacitive distance sensors. The controlling system ensures an equidistant step all over the lateral plane.

The calibration results first presented are obtained according to the Nano4 key-comparison. It is based on a Fourier transformation of 23 independently calibrations of more than 670 measurements. The result is shown in Table 28.

Correction parameters Fourier Transformation	Mean	Uncertainty or Stdev.
Correction factor C_x	0.9999 [-]	0.0007 [-]
Correction factor C_y	0.9872 [-]	0.0066 [-]
Couplings factor C_{xy}	-0.00778 [-]	0.0164 [-]
Angle γ	90.64 [°]	0.94 [°]
n	23 independent calibrations (674 measurement)	

Table 28: Summary of the calibration result obtained from Nano4. The calibration results have stated uncertainties of k = 1. The obtained angle γ has a stated experimental standard deviation of 1σ. Information of the traceable lateral calibration standard can be found in Table 16.

The results show a very stable and accurate correction of the X axis with a small uncertainty. The correction parameter of the Y-axis has a slightly larger than correction parameter of the X-axis and are above the expected. The larger uncertainty is mainly caused by the effect of the non-squared image and

drift. A relative large angle deviation compared to the certified value at 91.106° is observed which also is caused by the effect from non-squared images.

In order to estimate a more robust set of correction parameters for the Y-direction and the lateral non-linearity a series of squared images were analyzed. The determination of correction parameters and the contribution of non-linearity of the lateral plane are based on combined Fourier transformation and cross correlation methods as described in section 3.1.7. The results are shown in Table 29 and Table 30.

Correction parameters Cross Correlation	Mean	Stdev.
Correction factor C_x	1.0002 [-]	0.0004 [-]
Correction factor C_y	1.024 [-]	0.016 [-]
Couplings factor C_{xy}	0.0105 [-]	0.0064 [-]
Angle γ	91.25 [°]	0.055 [°]
n	40	

Table 29: Calibration results obtained from 40 squared images of 50 µm × 50 µm. The result is obtained on the basis of trace direction and equal amount of up trace and down trace. The calibration- and non-linearity results have a stated experimental standard deviation of 1σ.

The results shown in Table 29 indicate a small change of the X-axis correction parameter compared to the parameters obtained by Fourier Transformation but the difference is not larger than the estimated uncertainty. The values of the correction parameters of the Y-axis have changed to a more reliable result but lies still above the expected value. The C_y is now higher than the C_x which is normally expected because of thermal drift. The thermal drift also has an influence on the experimental standard deviation for the result obtained for the Y-direction. The coupling term C_{xy} and the corresponding

angle γ are very stable. The estimated angle γ on the squared images is closer to the certified values compared to the non-squared images.

The observed differences between the calibration results presented in Table 28 and Table 29 is mainly caused by the differences on image configurations (squared or non-squared) and the used calculation methods (Fourier Transformation or / and cross correlation) as described earlier in section 3.1.7.

As shown in Table 30 the obtained non-linearity contributions of the lateral plane expressed as the mean position error is very small. It is much better than one pixel. This corresponds to a mean position error smaller than 10 nm for the whole scan range (for illustration an example can be seen in section 3.1.7).

Non-linearity	Mean (Stdev.) [Pixels]	Mean (Stdev.) [µm]
Mean position error (total)	0.081 (0.12)	0.8 (0.01)
Mean position error (X-direction)	0.045 (0.08)	0.4 (0.007)
Mean position error (Y-direction)	0.059 (0.09)	0.6 (0.009)
n	40	40

Table 30: Results of the non-linearity analysis obtained from 40 squared images of 50 µm $\times$ 50 µm (512 $\times$ 512 pixels).

The small deviations between X, Y are mainly caused by the thermal drift.

The angle deviation of γ has to been compensated for the effect due to the zig-zag scan motion[31] of the MAFM during measurement (see Figure 55).

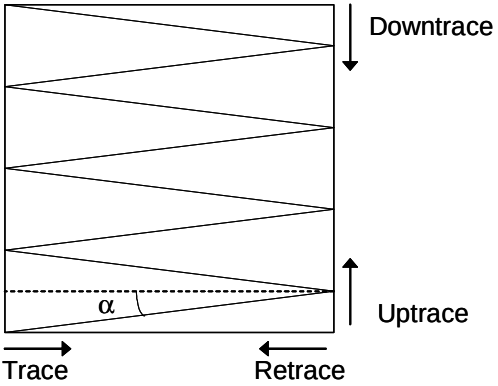

Figure 55: The scan pattern of the MAFM. If the scan has 512 x 512 pixels, $\alpha = 0.11°$. Modified after [62].

The zig-zag scan motion introduces a systematical angle error (α) correlated to the scan directions (see Figure 55) and the number of pixels of the measurement. An image containing 512 x 512 pixels introduces an angle error (α) in the order of 0.1°. The angle error can be eliminated by using the same amount of images covering the scan directions. For this particular case the results are obtained only from the trace direction and an equal number of up trace and down trace images. The observed angle deviation has to be corrected for $\alpha \approx 0.1°$.

4.7.1 Summary of the performance verification in the lateral direction

The performance of the MAFM in the lateral direction is expressed as a set of correction parameters (C_x, C_y and C_{xy}),

[31] *See also section 1.4.*

the non-linearity (mean position error) and angle γ between X and Y-direction. In general the result shows a system with a high degree of accuracy and reliability. This can be seen in the small uncertainty of the presented parameters.

The observed larger deviations are mainly caused by the experimental setup, environmental conditions or calculation methods rather than the system performance.

During the investigations the behaviour of Y-axis showed a larger error corresponding to the correction parameter compared to the X-direction. A thorough investigation has not been performed yet but is desirable.

A final comparison between the obtained results and the specification can bee seen in section 4.8.3.

4.8 Validation of the performance in the vertical direction (z).

The primary set of data has been obtained under Nano2. All measurements are non-squared images (50 µm $\times$ 6.25 µm or 70 µm $\times$ 8.75 µm). By performing non-squared images the effect of thermal drift is minimized. The performances of the vertical direction of the MAFM are here expressed in a correction parameter (C_z) and the non-linearity.

As for the lateral direction the vertical axis of the MAFM contains a capacitive distance sensor. The capacitive distance sensor is used to read out the “true” scale value during measurement.

The calibration results that regard the vertical axis have already been presented (in Table 24) under the discussion of subdivision the Z-scale. During the subdivision all the observed reference values were corrected by the $C_{z(H800)}$ estimated for step height standard H800 (see Table 31). Information on the specification of the traceable vertical calibration standard can be found in Table 17.

ISO 5436	Correction factor
Correction factor $C_{z(H800)}$	1.0353 [-]

Table 31: Calibration result for H800 step height standard.

The obtained correction factor $C_{z(H800)}$ is higher than expected due to the linearization facility of the Z-scale.

During the investigation several step height standards were measured (see Table 32), covering step heights in the range from 20nm to 2.4µm. For two of the standards (V180) the traceability can be traced back to NIST (USA). The other standards were calibrated in Europe. All the step heights were evaluated after ISO 5436 and corrected with reference to H800 as shown in Table 31.

Sample	Δz_m [nm]	Δz_{ref} [nm]	U_{Zm}[32] k=2	E_N
$H2400^F$	2312.3	2322 (17)	17.1	-0.40
$H800^F$	757.9	759.7 (8.2)	8.3	-0.16
$H800^S$	759.7	759.7 (8.2)	8.3	NA
$H240^F$	257.1	258.7 (5.4)	3.0	-0.26
$V180^F$	180.8	175.9 (2.6)	2.2	1.44
$V180^S$	182.8	179.8 (2.2)	2.2	0.95
$H80^S$	81.7	81.4 (4.6)	1.3	0.06
$H24^S$	12.9	13.2 (3.2)	1.0	-0.09
$H24^{SU}$	13.4	13.2 (3.2)	1.0	0.09

[32] *The uncertainties reported in Table 32 are an approach like the PUMA methods.*

$H24^{FIT}$	*13.1*	*13.2 (3.2)*	*1.0*	*-0.05*

Table 32: Step heights obtained over a time period at more than one year. S = spring, F = fall, SU=Summer, FIT = Corrected with a new "out of plane motion" factor. All step heights are corrected with reference to $H800^{S}$. NA means not actual.

The first set of measurements was performed in $spring^{S}$ 2001. The second set in $fall^{F}$ 2001 (a slightly lower number of measurements was performed).

The two results obtained on the H24 step height standard ($H24^{S}$ and $H24^{F}$) have systematically changed by an amount of 0.5 nm in that period which is much higher than the reproducibility of the measurement (in the order of 0.1nm). Further investigations showed that the observed superimposed bow was different for the two time periods. By correcting the $H24^{F}$ result with a new 2^{nd} order polynomial approach for the superimposed bow the value ($H24^{FIT}$) change to be closer to the first observed values $H24^{S}$. This indicates that the Z-scale is not stable in time[33] resulting in different contributions of coupling terms for the superimposed. Small changes can also be seen on the H800 standard, but these differences can be more difficult to separate from the stated uncertainty of the reference. Therefore is it important to verify the "out of plane motion" before performing a vertical calibration after ISO 5436.

The second observation of the analysis regards the relative large deviation on the result obtained on the V180 step height standards which are traceable to NIST. The first set of measurements had an E_N - value close to 1. The second set of measurements has an E_N larger than 1. A clear explanation has not been found, but the V180 step height standard is not designed to follow ISO 5436 and the step heights were difficult to calculate.

[33] *This drift might be cased by the transportation between DFM and DTI.*

However the results obtained during this investigation shows a system / Z-scale that works very well after a correction with a rather large $C_{z(H800)}$. This indicates a good linear response of the Z-scale.

The non-linear behaviour of the Z-scale was detected by following the procedure suggested by the manufacturer [53]. The procedure prescribes a sequence of measurements performed at the same spot of the step height standard. By changing the position in the Z-scale (offset from zero point) the non-linear behaviour of the Z-scale can be expressed as the deviation of the observed correction factor as shown in Figure 56. The values were determined after ISO 5436 (not included in the procedure) from measurements performed on step height standards H80 and H800.

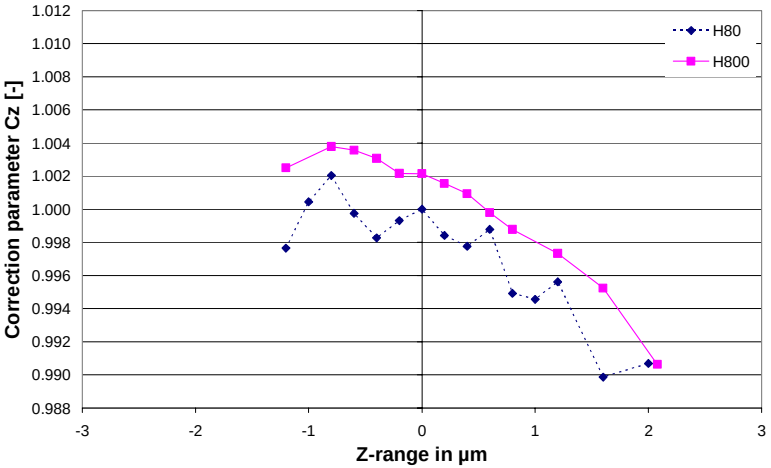

Figure 56: The measured correction factor C_z as function of the average observed Z-coordinate. The squares indicate correction factors for calibrations on H800 with a nominal step height of 800 nm; the diamonds indicate correction factors for calibration on H80, with a nominal step height of 80 nm. The observed non-linearity is in the order of 1.3% for the whole scan range. [60].

The observed non-linearity is in the order of 1.3% for the whole scan range. By taking the non-linearity into account during the measurement the remaining contribution of non-linearity will be in the order of 0.1% (not shown in this thesis)

4.8.1 Summary of the performance verification in the vertical direction

The performance of the vertical axis of the MAFM is here expressed as a correction parameter C_z and non-linearity. These parameters were evaluated during the work on pre-key comparison Nano2. As for the lateral direction the performance verification has mainly been focused on performing suitable calibrations.

The Z-axis was successfully calibrated on several step height standards. By subdividing the Z-scale the achievable relative uncertainty for the Z-calibration is in the range of 0.5% for step heights above 200 nm. For step heights below 50 nm the standard uncertainty is in the range of 0.5 nm corresponding to 3 - 4%. That is approximately an order of magnitude lower for the small step heights than the stated uncertainties on the certified values.

In general the results show a very stable and reliable system over shorter times. During the investigation a systematical drift of the Z-axis is observed on small step heights which might be caused due to the transportation of the MAFM between DFM and DTI.

4.8.2 Other tests

In order to determine the three mentioned correction terms (see 3.2.4) for calibration after ISO 5436 a large test was performed on flatness standards. The measurement mainly consisted of non-squared images (70 µm $\times$ 8.75 µm) as used in the Nano2 comparison. A set of measurement on squared images was performed as well (50 µm $\times$ 50 µm) to verify the

superimposed bow for the Y-direction. The result is shown in Table 33.

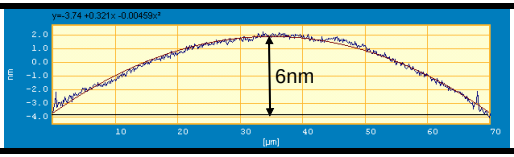	Flatness translation (superimposed bow)
Superimposed bow X-direction	6 ± 1 nm
Superimposed bow Y-direction	10 ± 5 nm

Table 33: Investigation on superimposed bow for X and Y-direction. The presented result covers the full scan range at 70 µm × 70 µm.

The superimposed bow concerning the Y-direction was extended to cover the whole scan range at 70 µm. It was strongly dominated by thermal drift which introduced curvatures different from the 2nd order polynomial approach as used for the X-direction. Therefore the size of the superimposed bow is very difficult to separate from other error sources as thermal drift.

4.8.3 Summary and Conclusions – Performance verification

The main purpose of this chapter was to verify the specifications of the MAFM. The performance verification was accomplished by participating in two large pre-key comparisons. Table 34 summarizes the results of the performance verification of the MAFM. The instrument specifications are listed for comparison in the same table.

Not all results are directly comparable to the specifications mainly due to the missing explanation from the manufacturer. Another disturbing factor is the terminology used by the manufacturer.

The calibration was performed on the instrument as delivered to DFM. This means that when the calibration result show

higher parameter values than the specification, the instrument does not meet the specifications.

Parameters	Results		Manufacturer's specifications	Better-B Equal-E Worse-W
Linearity (X,Y)	<0.02%		±0.10 % for X,Y	B
Linearity (Z)	<1.3%		±1.2 %	B
Orthogonally (X,Y)	0.14°		<0.1° for X,Y	E
Repeatability	<1.5 nm for X,Y <0.25 nm for Z		1.5 nm(1σ) for X,Y 0.25 nm(1σ) for Z	B B
Flatness translation	6 ± 1 nm 10 ± 5 nm		±5 nm for X ±10 nm for Y	B
	Correction parameter [34]	Uncert. or stdev.		
Accuracy (X)	0.01% 0.02%	0.14% 0.04%	±0.3% for X	B
Accuracy (Y)	1.28% 2.4%	1.3% 1.6%	±0.3 % for Y	W
Accuracy (Z)	3.53%	1.1%	±1.2 % for Z	W/B

Table 34: Result of performance verification of the MAFM.

[34] A correction parameter describe the relative differences between the observed- and reference value which correspond to a percentage deviation by |(1-correction parameter)|·100%.

On basis of the obtained results during the investigation the following conclusions can be drawn:

- The linearity of the three axes is in general better than the specifications.
- The orthogonality between X-Y direction lies just above the specification but due to the effect from the scanner motion (zig-zag) it can be difficult to give a clear statement.
- The observed repeatability (short term stability) of all performed measurements is very good and better than specified.
- The obtained average accuracy for the X-axis (calibration factor C_x and uncertainty) is very good and within the specification (see Table 28 and Table 29). The obtained reproducibility (long term stability) is also very good and is in the order of few parts per thousand. These results do not change due to the used calculation methods.
- The obtained average accuracy for the Y-axis (calibration factor C_y and standard deviation) does not meet the specification (see Table 28 and Table 29). The obtained reproducibility (long term stability) is in the order of few percent which approximately is one order of magnitude higher than the specification. Investigations of the Y-direction have not during this project had the same focus as the X-axis. This might have some influence on the result. Nevertheless the result shows an significant different behaviour compared to X and Z.
- The obtained average accuracy for the Z-axis (calibration factor C_z and uncertainty) does not meet the specification (see Table 31). However when the Z-axis is calibrated it provides very consistent and reliable results with a good reproducibility.
- The observed flatness translation (superimposed bow) is below the specified limits. Regarding the Y-direction the

flatness translation has to be found under other condition then used here due to eliminate the effect of thermal drift.

As a general conclusion the instrument fulfils the main part of the specification (see Table 34). Some misinterpretation of the terms in the specifications is likely because of their bad definition. The Y-axis seems to have a significant worse behaviour than X and Z.

As a general approach for the acceptance test for the instrument it is very important to agree on how the instrument can be validated. The procedures and calculation methods used by the manufacturer and buyer have to be the same. Furthermore a consistent interpretation of the terms used in the specification is necessary.

4.9 Summary and Conclusions Validation of MAFM

The validation and performance verification test of the MAFM is based on participation in intercomparisons. Three comparisons covering the nanometre range of length measurement has been held in this project period.

The parameters concerning the X and Y directions have been established during the work on the intercomparison Nano4 (see section 4.4), the Z-direction on Nano2 (see section 4.5).

The aim of Nano4 was to compare the pitch measurements of two 1D gratings with nominal distances at 290nm (EAM G/300-1) and 700 nm (EAM G/300-1). The final result of this key comparison shows E_N-values below 1 for the two 1D-gratings. The results indicated no significant differences compared to the references. This leads to a successful participation for DFM. It indicated furthermore that the used calibration- and measuring procedures (A-B-A) and analysis methods were adequate and formed a good basis for accreditation in the field. Finally due to the good results for all the participants this pre-key comparison was upgraded to a key-comparison.

The purpose of the Nano2 pre-key comparison was to establish agreement onto the definition of step heights after a analogy to ISO 5436. The three transfer step height standards possess nominal step heights at 20 nm (SH20), 70 nm (SH70) and 800 nm (SH800). During the work three important correction terms regarding calibration after the ISO 5436 were quantified (see section 3.2.4 and 4.5.3). The results can not be published in this thesis due to the fact that the comparison is still ongoing.

During the calibrations for the intercomparisons traceability was established to the MAFM by the use of traceable transfer standards, covering X, Y and Z.

In general the preparation work for an intercomparison covering a new field is not straight forward. This has lead to the test of many possible solutions of the identified problems before handing in the final results to the pilot laboratory.

A successful validation and performance verification of the MAFM (see section 4.6) was performed on the basis of the participation in the two intercomparisons mentioned above.

As a general conclusion the instrument fulfils the main part of the specification (see Table 34). Some misinterpretations of terms in the specification are likely because of their bad definitions. The Y-axis seems to have a significant worse behaviour than X and Z.

As a general approach for the acceptance test for an instrument it is very important to agree on how the instrument should be validated. The procedures and calculation methods used by the manufacturer and the buyer in principle have to be the same. Furthermore a consistent interpretation of the terms used in the specification is necessary.

Chapter 5
INTEGRATION OF AN AFM ON A CMM

Characterization and quantification of surface texture is an area of big interest presenting a number of problems [79], [80], [81]. In particular, the topographic characterization of fine surfaces on mechanical workpieces with complex geometry and relatively big dimensions is not a trivial task. Instruments available for measurement of fine surfaces usually have a limited vertical and horizontal range [80] and a limitation as to the maximum size of the workpiece that can be investigated. This chapter describes the construction, calibration and use of an integrated system for topographic characterization of fine surfaces on parts having relatively big dimensions by the use of surface mapping.

5.1 Design of the integrated system

An AFM was mounted on a manual three-coordinate measuring machine (CMM) achieving free positioning of the AFM probe in space. This means that the limited measuring range of the AFM can be extended by positioning the AFM probe using the movements of the CMM axes. The integration of an AFM on a CMM opens up for the possibility of using AFM technology in connection with larger workpieces [1], [82].

Besides functioning as an ordinary AFM[35], the instrument also works as an optical microscope. This means that it is possible to observe the surface during positioning and measurement by the AFM probe. The specification is shown in Table 35.

[35] *This AFM is constructed as a piezo electrical tube scanner where the tip is moving relatively to the sample.*

AFM	
Scanning mode:	Non-contact (AC)
Max. Scanning area:	$40 \times 40\ \mu m^2$
Max. Vertical movement:	2.7 µm
Vertical resolution	1.5 pm
Non-linearity horizontal	< 2 %
Non-linearity vertical	< 10 %
Optical system	
Magnification	25 X
Optical axis	Infinite corrected
Transmission bandwidth	400 - 600 nm

Table 35: Specifications of the AFM used in the integrated system

The CMM is a three-coordinate measuring machine on which movement and detection of axis positions are performed manually in this first generation. The CMM guideways are supported by journal bearings. The CMM has a working volume $X \times Y \times Z$ max 400 mm $\times$100 mm $\times$ 75 mm and is essentially used as a stage for the AFM probe. The AFM can then be positioned arbitrarily.

A special fixture was constructed in such a way that it can be mounted in the existing probe holder on the CMM. The two parts of the fixture are equipped with conical flanks so that the fixture is locked relatively to the CMM when the two parts are screwed together (see Figure 57). The AFM is mounted on the lower part of the fixture, which has been manufactured in brass. A photograph of the integrated system is shown in Figure 58.

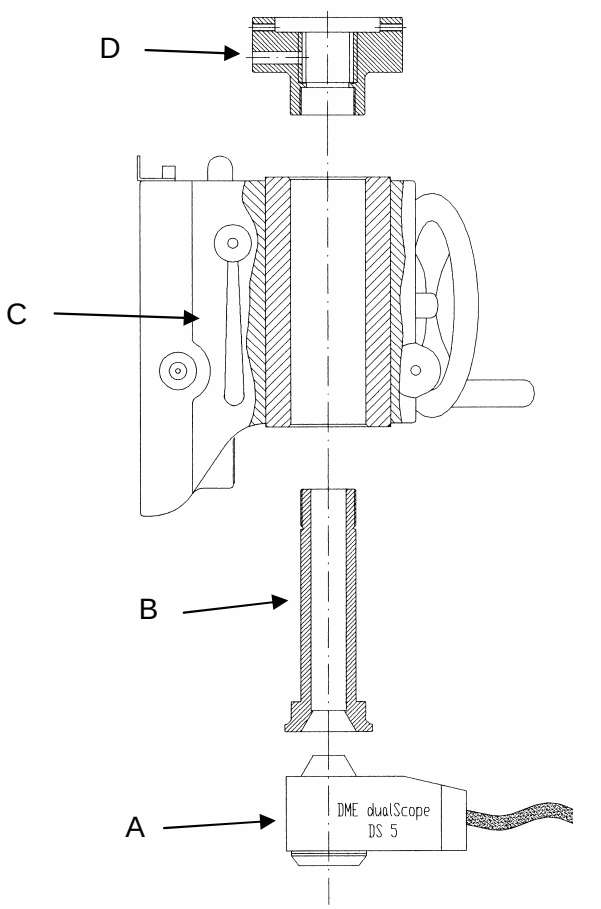

Figure 57: The special fixture developed for mounting the AFM on the Z-axis. (a) AFM, (b) lower part of fixture, (c) Z-axis and probe holder and (d) upper part of fixture.

Due to the construction of the fixture and probeholder, only surfaces lying underneath the AFM probe can be measured. The optical possibilities of the AFM can be used to monitor the surface under investigation by means of a CCD camera. The light source uses fibers not introducing heat to the system (Figure 58).

The development and the first results of applying the system are reported in [1], [82]. Basically the integrated system can be used in three different ways:

- The CMM positions the AFM probe and a measurement covering max 40 µm × 40 µm is performed (corresponding to the maximum scan area of the AFM).
- The CMM positions the AFM probe at different places for spotwise investigation of larger areas within the CMM working volume (X × Y × Z max 400 mm ×100 mm × 75 mm).
- The CMM is used to reposition the AFM probe in between surface roughness measurements to cover continuous areas larger than 40 µm × 40 µm (called surface mapping).

These different modes of application create relatively high demands to the calibration and performance verification of the system. The initial results [1] have indicated that an improvement of the instrument was necessary especially concerning an implementation of electronic scales. The next chapter describes some major improvements made to the system and the resulting increase in performance.

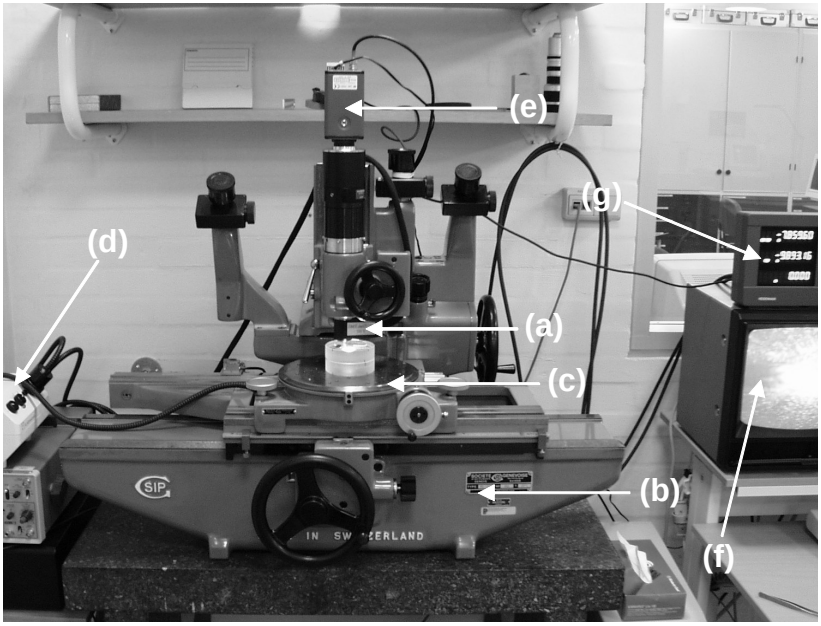

Figure 58: The integrated system. ***(a)*** *the AFM probe,* ***(b)*** *the CMM,* ***(c)*** *rotary table, (d)light source,* ***(e)*** *CCD-camera and optical parts,* ***(f)*** *monitor and* ***(g)*** *display for the reading the X,Y-positions.*

5.2 Performance of the system

The integrated system was improved by mounting electronic scales on the X and Y axes of the CMM (see Figure 59). No scales were mounted on the Z axis because this axis is only used for the rough positioning of the AFM probe as described in section 5.1.

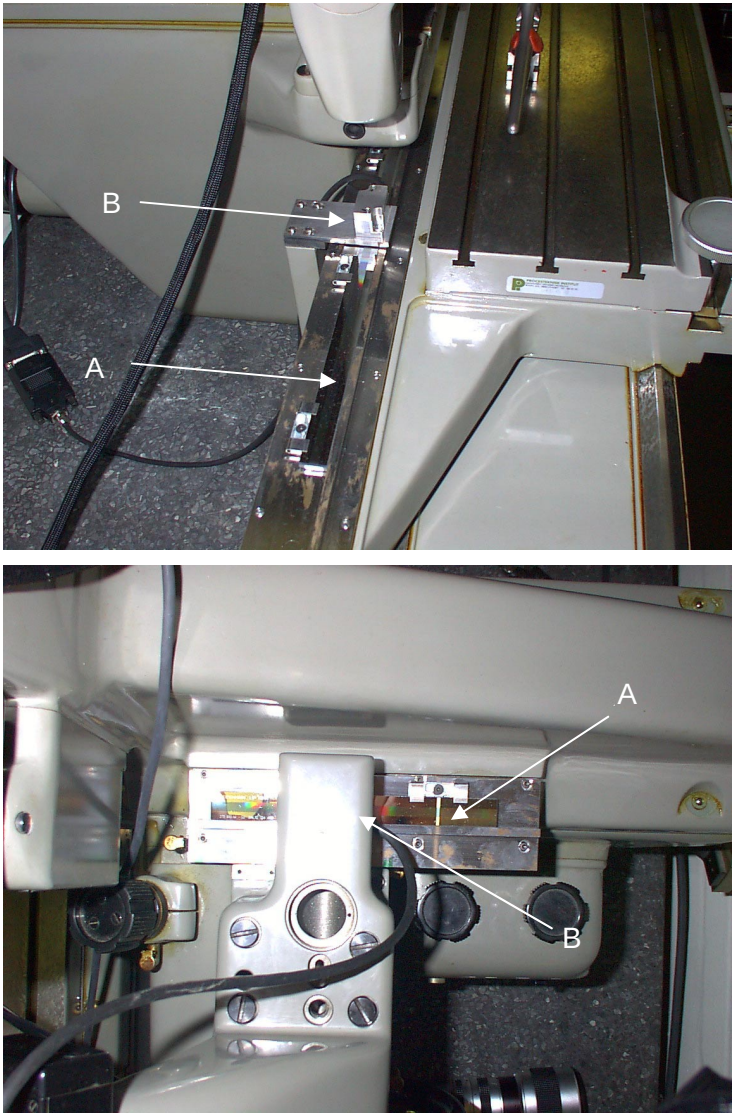

Figure 59: The electronical scales are mounted directly above the existing scales. Upper picture indicates position for X-axis, lower picture the Y-axis. A indicates the scales. B indicates the scanning unit.

The exposed linear encoders[36] operate with no mechanical contact between the scanning head and the scale. They have a fine signal period of 2 µm which permits measuring steps down to 5 nm [84]. They were mounted directly on the fixtures for the original machine scales to ensure optimal alignment and compatibility.

To improve the facility of the CMM according to the final adjustment of the specimen (in X and Y direction) a rotary table was mounted on the measuring plane of the CMM (see Figure 58, c).

5.3 Test and validation of the integrated system

The integrated system was calibrated using the following approach:

- The AFM was calibrated separately as stand-alone instruments using state-of-the-art calibration methods.
- The CMM was calibrated using laser interferometer after guidelines described in VDI/VDE 2617
- The performance of the integrated system was verified using a newly developed calibration procedure.

In the following sections the results of the individual calibrations as well as of the total calibration are described.

5.3.1 Calibration of AFM

The motivation for a very thorough calibration of the AFM is to find in the use of the integrated system for surface mapping. In order to achieve the optimal performance for surface mapping a series of parameters are investigated (see Table 36). Due to the fact that not all investigated corrections terms

[36] *The scales are manufactured by Heidenhain, produced in Zerodur material (LIP-series). The X-scale has a total length of 370 mm and the Y-scale is 120 mm.*

can be implemented into the instrument facilities the different contributions have to be taken into account during the measuring procedures.

Parameters	Influence on surface mapping
Correction terms C_x, C_y	The lateral calibration directly influences the measuring procedure and the following data analysis. A missing lateral calibration can lead to lack of surface information or huge overlap between measurements.
Correction terms C_z	Has influence on all vertical parameters but not directly on surface mapping.
Orthogonality between X -Y (γ)	Directly influences the surface mapping due to a necessary re-rotation of measurements. It can be needed to compensate for lack of surface by perform overlapping measurements.
Background noise	Has no direct influence on performing surface mapping. It describes a general behaviour of the particular instrument.
Tip approach facility (inchworm)	The tip is positioned automatically on the surface. The behaviour of this approach facility can directly influence the surface mapping procedures.

Table 36: Investigated parameters on the AFM and their influence on surface mapping.

The AFM was calibrated using a 2D-grating standard with a certified 2.12 µm pitch distance (Figure 60, a), and a set of three standard step height standards containing nominal step heights at 22 nm, 100 nm and 485 nm respectively (Figure 60, b). The calibrations were performed over a period of five weeks. Calibration factors were determined for all three

directions X, Y and Z for a number of different scan ranges summarized in Figure 61 and Table 38.

The calibration factors were determined as described earlier in this thesis. The lateral correction parameters deduced in Chapter 4 are based on a linear expression and therefore the observed measurement might be considered as linear. For the AFM a residual non-linearity of the image better than one pixel for the applied measurement conditions is acceptable. This leads to necessary pre operation procedures where the non-linearity effects caused by hysteresis and creep necessarily must be reduced before the determination of calibration factors. The non-linearity effects of each measurement are reduced using the 3rd order polynomium approximation expressed in equations (17) and (18). This is an iterative process and three to four runs might be needed. Thereafter the final correction parameters can be calculated. For the vertical calibration the histogram method was used.

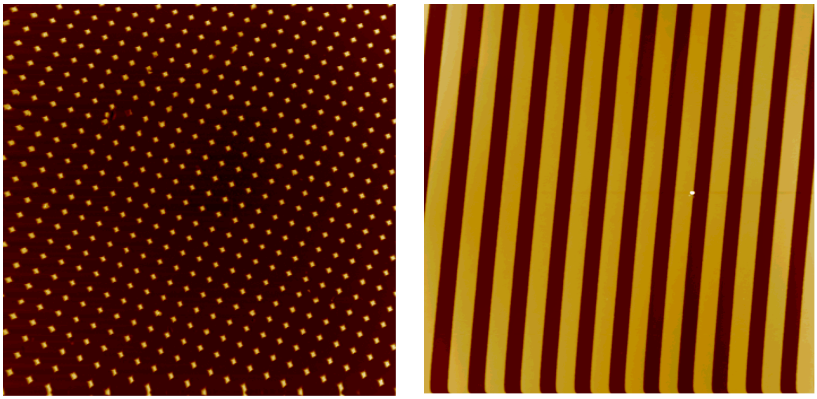

(a) (b)

*Figure 60: Examples of performed measurements on **(a)** 2D-calibration grid with a pitch distance of 2.12 µm and **(b)** step height standard with a nominal height at 100 nm.*

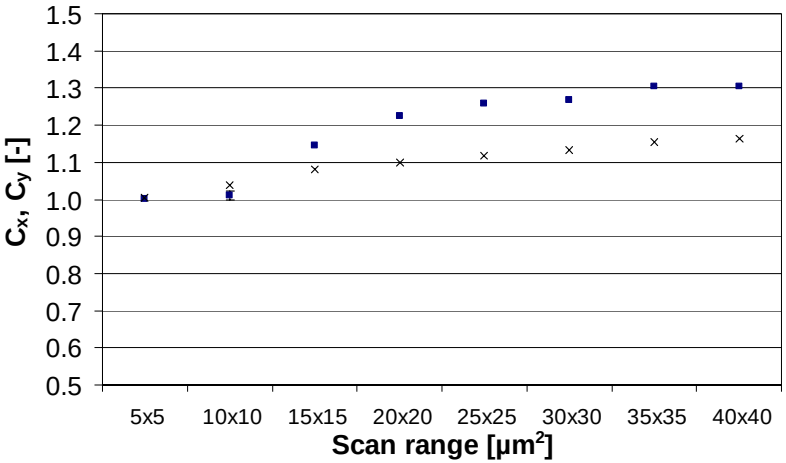

Figure 61: Calibration results for X and Y direction of the AFM. The results are only presented by the average values determined by cross correlation method. Crossed markers: X-axis. Squared markers Y-direction.

Standard deviation for Correction factor C_x and C_y		
Scan range	Stdev. for C_x (1σ)	Stdev. for C_y (1σ)
5 µm × 5 µm	0.109	0.067
10 µm × 10 µm	0.014	0.012
15 µm × 15 µm	0.024	0.088
20 µm × 20 µm	0.007	0.095
25 µm × 25 µm	0.004	0.077
30 µm × 30 µm	0.002	0.020
35 µm × 35 µm	0.002	0.011
40 µm × 40 µm	0.005	0.016
n	4 (for each scan range)	

Table 37: The standard deviations for the calibration result presented in Figure 61.

To verify the performance of the lateral calibration the deduced correction factors were implemented into the AFM. The re-calibration of the AFM shows a residual error in the order of 3 - 5% with respect to the scan range and scan direction (X or Y).

Table 38 summarizes the results from the vertical calibration.

Step height	Correction factor C_Z	
	Average [-]	Stdev 1σ.
22 nm	0.31	0.005
100 nm	0.40	0.005
485 nm	0.47	0.004
n	12 (on each step height)	

Table 38: Vertical calibration results expressed as the correction term C_z. The values are calculated by using the histogram method as described in section 3.2.5 [84].

As is clearly seen from Figure 61 and Table 38, the scan range has an influence on the calibration factors C_x and C_y and thereby on the size of the measured area. However a tendency towards stable calibration factors is seen for large scan ranges. The calibration factor C_z was investigated and it was shown not to be significantly dependent on the scan range. However the calibration factor varies according to the nominal step height presenting a challenge to the user of the system to choose an appropriate step height relative to the workpiece surface. The AFM has a C_z in the order of 0.5 which is not optimal, but the instrument leaves no possibility of improvement with respect to this.

Furthermore the angular error XY was determined as a function of the scan range (See Figure 62).

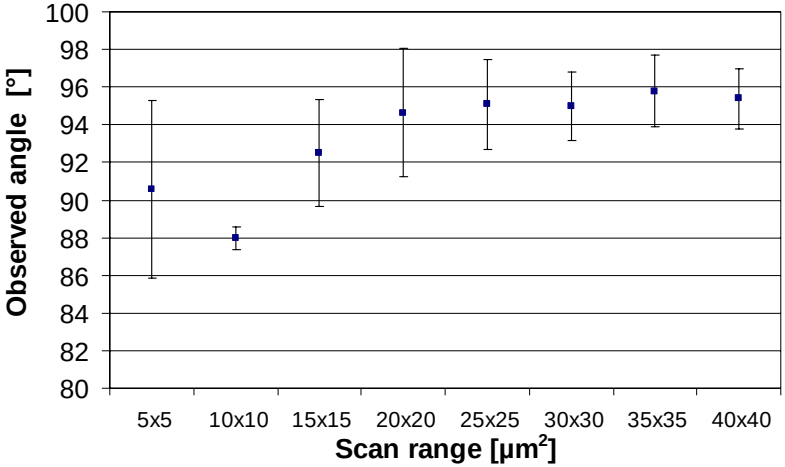

Figure 62: The observed angle γ of a 2D calibration grid versus the scan range. The bars indicate $\pm$ one standard deviations [84].

The angular error XY is significantly changing when the scan area is varied (see Figure 62). The largest deviation is seen for small scan area, which can be explained by the relatively low number of periodical structures used for the calculation. However a tendency towards stable angular errors is seen for large scan ranges. A change over two degrees for larger scan areas is still observed.

In order to test the integrated system as one instrument, the background noise was determined as the Sa value [79] measured on an optical flat. More than 100 separate areas were scanned on the optical flat over a time period of 4 weeks. During these measurements the AFM was positioned using the CMM, but only scan areas up to $40\ \mu m \times 40\ \mu m$ were investigated. Figure 63 summarizes the results obtained on the optical flat. Five different square scan areas were investigated and the background noise was determined to be at a level of 1 - 2 nm (Sa value), independent of the scan area for the four smallest areas. Values in the order of 10 - 20 nm

were found for the corresponding Sz [79]. The standard deviation of the measurements was observed to be at the level of 0.5 nm for all areas. The background noise was observed to be stable over a time period of 4 weeks for all scan areas. During the measurements, the cantilever was replaced several times without any observed influence on the background noise [82].

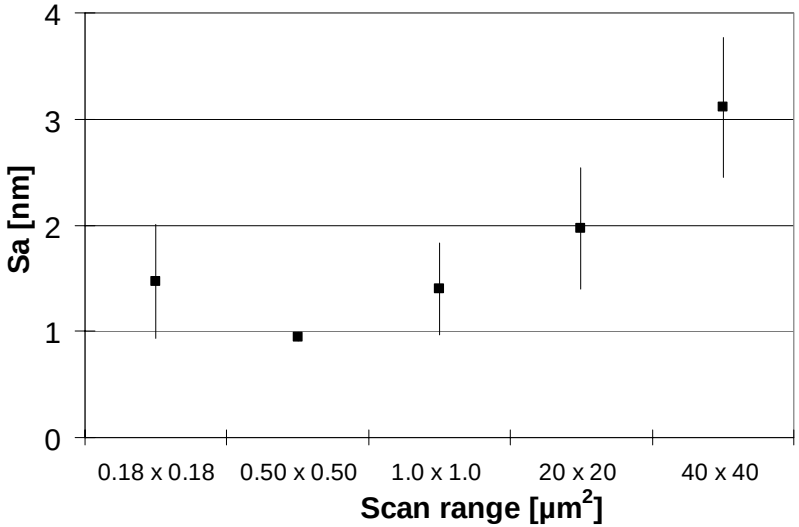

Figure 63: Background noise (expressed as Sa) as a function of scan area. Dot indicates mean value, lines indicate ± one standard deviation.

The AFM contains a so called inchworm for an automatic approach of the tip to the surface and to retract the cantilever to a secured position between measurements (parked position or view-distance). The inchworm has a maximum travel of ≈ 2 mm. When shifting between two consecutive measurements the AFM moves up to a view distance using the inchworm. A test was performed to investigate the influence of the inchworm movement of the AFM scanner on

the lateral position of the scanned image when approaching the tip on the surface (see Figure 64).

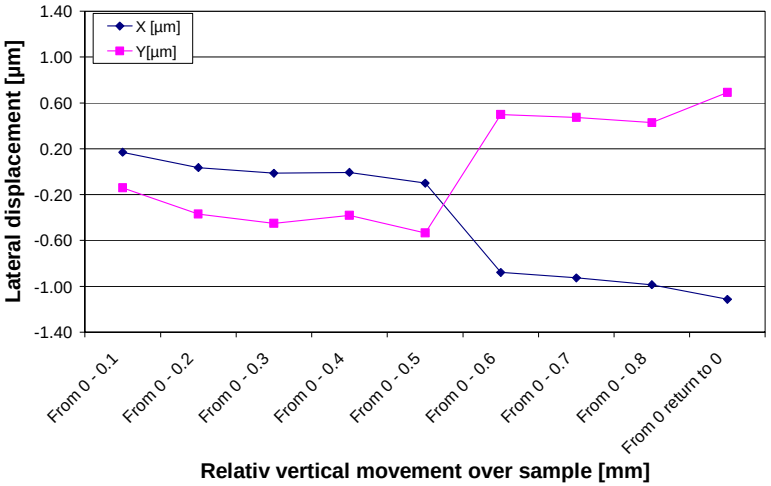

Figure 64: The maximum effect due to changing the vertical distance of the AFM above the specimen.

The measurement was performed on a 2D-grating standard in different Z-heights on the CMM (by moving the CMM Z-axis). The lateral translation was determined by using cross correlation method of two consecutive images in different height. The influence was determined to be 1 µm for a maximum tip movement of 0.8 mm. This result is a sum of errors mainly caused by the approaching tip and the vertical movement of the Z-axis of the CMM in steps of 0.1 mm. The contribution of the inchworm on short distances (no vertical movement of the CMM) is in the order of 0.2 µm.

The inchworm and Z-axis on the CMM do have some effect expressed as the lateral translations of image in the order of 0.2 µm up to 1 µm. The effect has to be considered for measuring sequences for surface mapping where it is necessary to move the AFM upwards or downwards to follow the form of the specimen (on non flat or tilted specimens).

5.3.2 Calibration of CMM

The scales and axes of the CMM were calibrated [85] using a commercial laser interferometer. The positioning error, pitch and yaw were determined for each axis according to VDI 2617 [86].

VDI/VDE 2617 is a series guidelines developed in Germany concerning verification of CMMs. For this project VDI/VDE 2617: part 3 is used. It describes methods for evaluating and determining guideway errors of a CMM according to a rigid-body model. This model assumes that each guideway is a rigid body having six degrees of freedom as illustrated in Figure 65. Combining three orthogonal axes will give a total of eighteen parametric errors and three squareness errors [68].

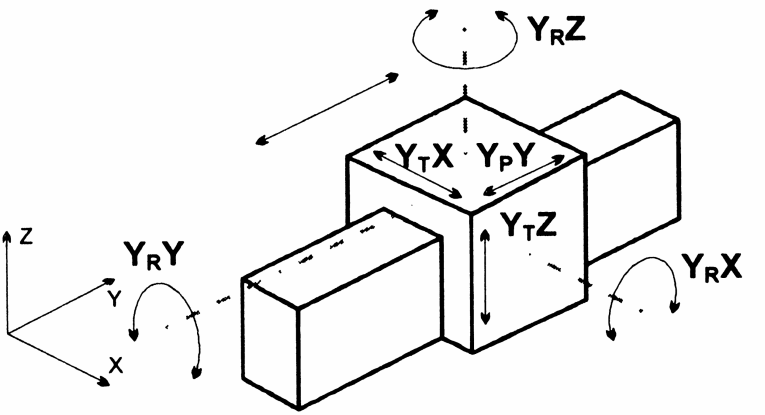

Figure 65: Rigid body error model of one axis [68].

The convention for naming the error components is shown in Table 39.

Y_PY	Positioning error Y-axis	[µm]
Y_RX	Pitch Y-axis	[µrad]
Y_RY	Roll Y-axis	[µrad]
Y_RZ	Yaw Y-axis	[µrad]
Y_TX	Translatory error of Y-axis in X-direction	[µm]
Y_TZ	Translatory error of Y-axis in Z-direction	[µm]

Table 39: The convention for naming the error components of the rigid body model according to VDI/VDE 2617 [68]. The table contains only error components for the Y-direction.

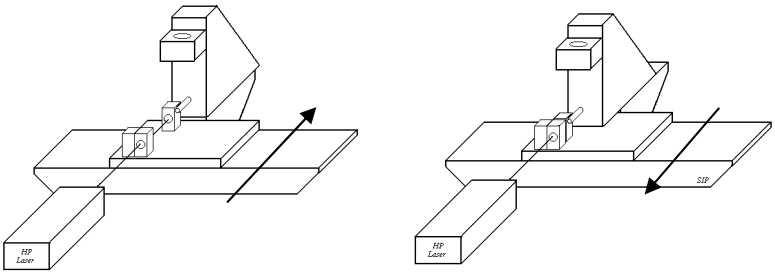

(a) (b)

Figure 66: Calibration of the Y-axis of the CMM using laser interferometer. During the calibration the axis is moved forwards (b) and backwards (a) in incremental steps to certain positions.

During the calibration the axis is moved forwards (Figure 66(b)) and backwards (Figure 66(a)) in incremental steps to certain positions. The particular position of the CMM and laser interferometer is then recorded. Due to the differences between the obtained values the positioning error can be determined. The relative angle deviations as a function of position on the respective axis (pitch and yaw) are determined from relative length differences between two laser beams [1].

Each axis was calibrated over its entire length and in more detail over the part of the working volume were the calibration

and performance verification procedure was applied. The results are summarized in Table 40 and Table 41 and Figure 67 and Figure 68.

X-axis (total range 400 mm)		
Error	Range [mm]	Mean error [µm]/[µrad]
Position	60 - 360	1.5 µm
Position	180 - 220	0.5 µm
Position	180.000 – 180.300	0.1 µm
Yaw	60 - 360	5.6 µrad
Pitch[37]	60 - 360	2.8 µrad

Table 40: Calibration result of X-axis

Y-axis (total range 100 mm)		
Error	Range [mm]	Mean error [µm]/[µrad]
Position	10 – 100	0.8 µm
Position	45 - 75	0.7 µm
Yaw	10 – 100	2.1 µrad
Pitch	10 – 100	1.9 µrad

Table 41: Calibration result of Y-axis.

[37] *See Figure 69*

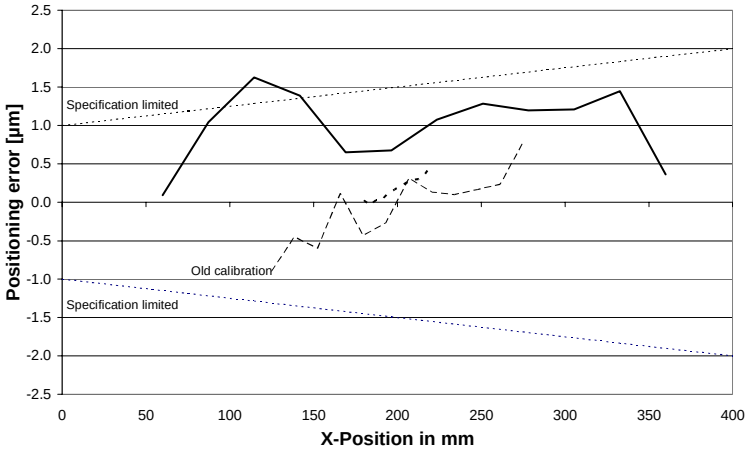

Figure 67: The average positioning error of the whole X-axis (full line). The result obtained over 40 mm is presented (dotted line). Comparison of the new scales versus the original scales of the CMM an old calibration result is indicated as well.

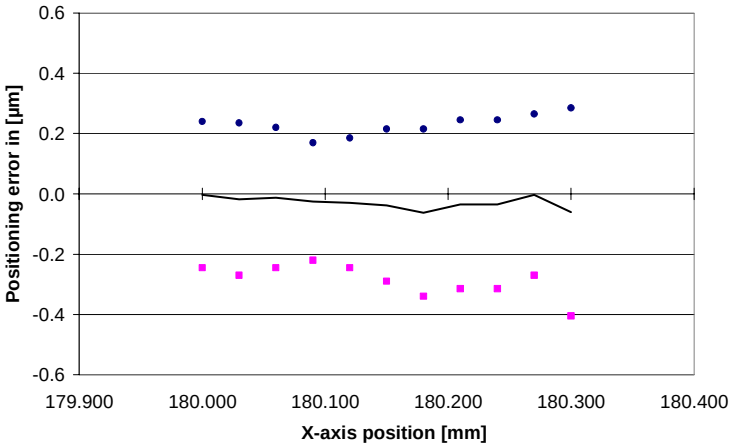

Figure 68: Positioning error of X-axis in the range from 180.000 mm to 180.300 mm (0.03 mm steps). Full line indicates average positioning error. Dots indicate error relative to "forward" movement. Squares indicate error relative to "backward" movement.

An average positioning error of 1.5 µm over the entire length was determined for the X-axis with a repeatability better than 0.1 µm. A significantly better performance was observed for limited ranges of the X-axis, 40 mm and 0.3 mm respectively. For example, a positioning error better than 0.1 µm was determined for a range of 0.3 mm starting at 180 mm on the X-axis (Figure 68). Surface mapping is typically performed in an area of this size. The results of the Y-axis are comparable to the ones obtained for the X-axis.

During the calibration with the laser interferometer the angle error (pitch and yaw) were determined for the X and Y-axes (summarized in Table 40, Table 41 and Figure 69). The results show good accordance with previous results indicating high stability of the CMM.

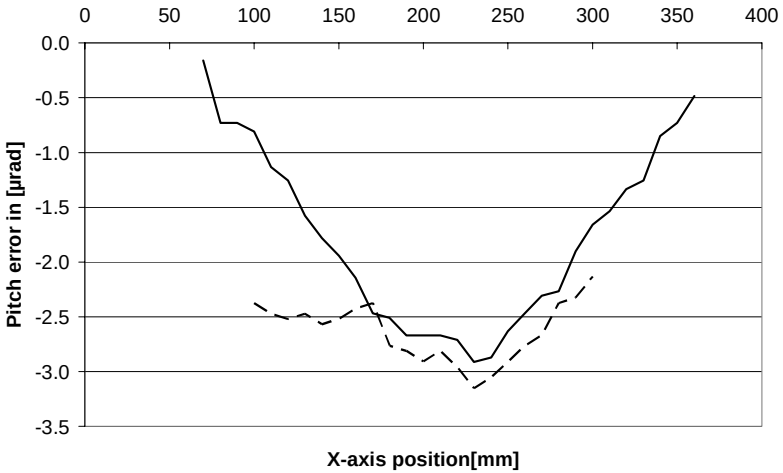

Figure 69: Pitch error of the whole X-scale (full line). For the comparison of the new scales versus the original scales of the CMM an old pitch result (dotted line) is indicated as well.

The squareness error of the XY-plane was determined to be in the order of 25 µm over a length of 85 mm (see Figure 70).

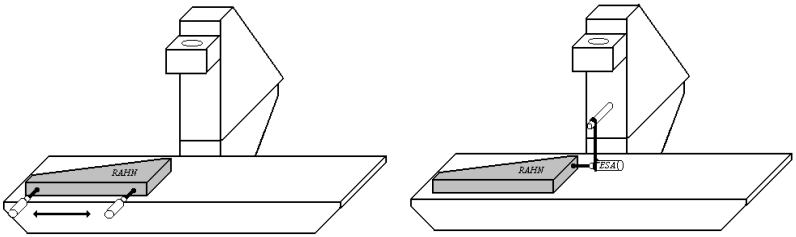

(a) (b)

Figure 70: The principle of measuring the squareness error between X and Y axes on the CMM using a straight edge and a probe. ***(a)*** *The one side of the straight edge is aligned parallel to the X-axis. The angle deviation can then be measured on the orthogonal side of the straight edge* ***(b)****. The observed angle deviation has to be corrected due to the certified values of the angle.*

The calibration results allow for a mathematical modelling of the CMM errors according to e.g. [68], [69], [70]. The error propagation model shown in equation (24) to (29) covers the 2D-problem.

$$\underline{E} = \underline{P} + \underline{A} \cdot \underline{X} + \underline{A_P} \cdot \underline{X_P} \tag{24}$$

where $\underline{A}$ concerns the rotatorical errors, $\underline{A_P}$ the rotatorical errors influencing probe offset, $\underline{X}$ the position of reference probe, $\underline{X_P}$ the probe offset vector and $\underline{P}$ the translational errors (see (25)-(29)).

$$\underline{A} = \begin{bmatrix} 0 & -xrz - xwy \\ 0 & 0 \end{bmatrix} \tag{25}$$

$$\underline{A_p} = \begin{bmatrix} 0 & -xrz - yrz \\ xrz + yrz & 0 \end{bmatrix} \tag{26}$$

$$\underline{X} = \begin{bmatrix} x \\ y \end{bmatrix} \tag{27}$$

$$\underline{X_P} = \begin{bmatrix} x_P \\ y_P \end{bmatrix} \tag{28}$$

$$\underline{P} = \begin{bmatrix} xtx + ytx \\ yty + xty \end{bmatrix} \tag{29}$$

The mathematical simulation is especially interesting if the instrument is used to measure specific separate areas located relative to each other on the workpiece.

The error propagation model has been used to investigate the errors introduced during small steps in the order of 30 µm - 40 µm (when performing surface mapping the steps are quite small).

The calibration of the X and Y scales are performed in the same horizontal plane as the working plane of the AFM probe. This leads to a probe offset vector equal to zero. The translational errors *ytx* and *xty* have not been determined but their effect is expected to be very small. The following equation was expressed:

$$\begin{bmatrix} E_X \\ E_Y \end{bmatrix} = \begin{bmatrix} xtx + y(xrz - xwy) \\ yty \end{bmatrix} \tag{30}$$

A simulation of the CMM errors was performed. The X and Y-axes were moved arbitrarily in small steps no larger than 30 µm. The difference in error vectors ($\Delta\underline{E_X}$, $\Delta\underline{E_Y}$) was calculated and all results were below 5 nm. Therefore the CMM leads to no introduction of significant errors when the CMM axes are moved in small steps during the surface mapping procedure.

During the investigation and measurements a thermal drift in the order of 20 - 30 nm over 24 hours is observed (Table 42).

To determine the re-positioning error on arbitrary lateral movements of the CMM as seen through the glasses of the AFM a set of AFM measurements was performed. The AFM

was moved between measurements up to 10 mm in X and Y from the same spot. The same area was measured and the re-positioning error was determined by using cross correlation methods indicating the deviation between measurements on the basis of images. The results shown in Table 42 indicate a maximum observed error in the order of 0.5 µm for the two axes. The result shows good agreement compared with the results obtained by laser interferometer (see Table 40 and Table 41).

Thermal drift in X-direction	<30nm
Thermal drift in Y-direction	<30nm
Re positioning error arbitrary in the X, Y direction in the mm-range	<0.5µm

Table 42: Experimentally determined error components for the CMM.

The calibration results indicate that the error components of the CMM are not of an order of size requiring error compensation for surface mapping when the CMM movements are relatively small, typically less than 100 µm in both X and Y directions. However relatively large reversal errors were observed (Figure 68) indicating the importance of designing the calibration and performance verification procedure for surface mapping in a proper way. The stability of the CMM has been demonstrated to be very high [1], [82].

The AFM and CMM have been calibrated individually with focus on the performance when used for surface mapping. In Table 43 the deduced parameters are listed according to their influence on surface mapping.

Error components				Influence on surface mapping	
	Parameter	Size	Figure / Table	Horizontal plane	Z-direction
AFM	C_x [-]	Var.[1]	Fig.61, Table 37	√	
	C_y [-]	Var.[1]	Fig.61, Table 37	√	
	C_z [-]	Var.[2]	Table 38		√
	γ [°]	Var.[1]	Fig.62	√	
	Stability of C_x and C_y	3-5%		√	
	Backgrond noise (Sa)	Var.[1]	Fig.63		√
	Tip approach	0.2µm[3]	Fig.64	√	
CMM	$X_P X$	Var.[4]	Fig.67,68, Table 40	√	
	$Y_P Y$	Var.[4]	Table. 41	√	
	$X_R Y$ (Pitch X)	Var.[4]	Fig.69, Table. 40	√	
	$X_R Z$ (Yaw X)	Var.[4]	Table. 40	√	
	$Y_R X$ (Pitch Y)	Var.[4]	Table. 41	√	
	$Y_R Z$ (Yaw Y)	Var.[4]	Table. 41	√	
	XWY	0.017°		√	
	Thermal drift	20-30nm	Table. 42	√	
	Re-positioning test X and Y (performed by AFM)	0.5µm	Table. 42	√	

Table 43: Summarizing the error components identified during the calibration of AFM and CMM. The error components have different effects on surface mapping indicated by "√". The majority of the parameters are variable due to a particular movement: ***[1]:*** *corresponds to scan range,* ***[2]:*** *step heights,* ***[3]:*** *will be larger by using the Z-axis up to 1µm,* ***[4]:*** *the position of the X or Y axes. Var. = Variable.*

5.3.3 Calibration of the integrated system

The purpose of the proposed calibration and verification procedure is to demonstrate and quantify the capability of the system to perform surface mapping.

The proposed procedure makes use of two calibration artefacts. One is a standard optical flat used to determine the background noise. The other is a commercially available optical artefact (chromium lines on glass) with a repetitive line pattern (Figure 71). The pattern consists of 9 areas each with 15 chromium lines with pitch distances varying from 1.6 µm to 10 µm as shown in Figure 71.

For establishment of traceability into the integrated system the pitch distances of the optical artefact has to certified by a traceable measuring system. This can be accomplished by letting the MAFM characterize the line pattern of the optical artefact[38].

[38] *During this project these measurements have not been performed due to instrument problems..*

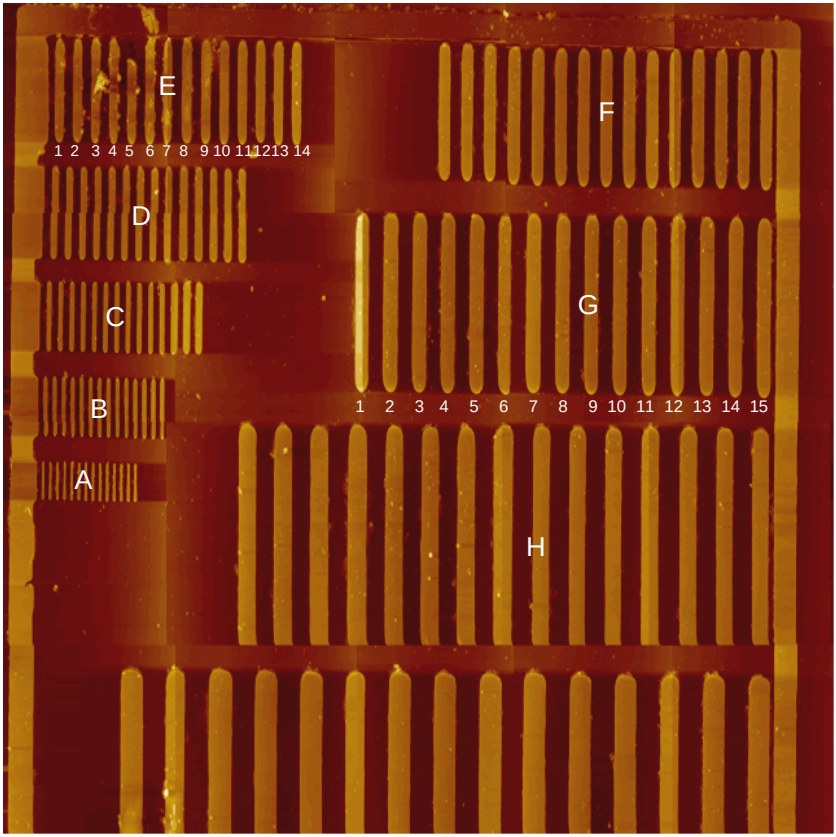

Figure 71: The optical standard used for verification of the integrated system. Result of surface mapping using an "overlapping" measurement strategy and stitching process.

The pattern allows for an exact identification of measured areas when stitching measurements together. The two-dimensional pattern allows for a verification and calibration in both X and Y directions. The proposed procedure consists in measuring 5×5 areas of 35 µm $\times$ 35 µm, covering a total area of 175 µm $\times$ 175 µm. The areas are measured in the sequence indicated in Figure 72 to minimise the reversal errors of the CMM axes (refer to axes' directions in Figure 72).

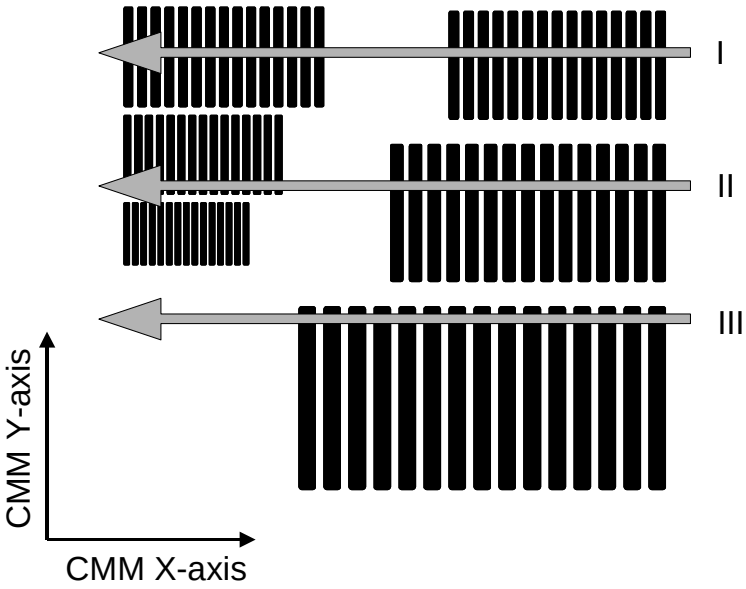

Figure 72: Principle of optical standard used for calibration. Arrows and numbers indicate measurement sequence.

The principle of the procedure is to cover an area that corresponds to the area to be measured on a workpiece. The procedure is quite time consuming since the measurement of 5×5 areas takes approximately 7 hours. Two measurement strategies can be chosen:

- Areas are measured edge-to-edge, i.e. no overlap.
- Areas are measured with a defined overlap.

The first measurement strategy immediately reveals problems of the integrated system when stitching areas together. The first visual evaluation is based on the image of the stitched areas (positioning errors, squareness errors and not-intended overlap etc.), and the results are quantifiable as shown later. The second approach requires a software evaluation of each measured area and a correct alignment of each area relative to each other. The chosen calibration artefact possesses

repetitive features that enable the user to perform such an evaluation. A simple software algorithm was developed and tested during this investigation. The result of such data manipulation no longer makes it possible to separate system performance and software algorithm performance (shown in Figure 71).

After measurement of the 5×5 areas, the raw data were filtered using a first order least mean squares plane, and the 25 areas were stitched together edge-to-edge without further data manipulation. This means that the CMM axes where moved 35 µm between each area following the path indicated in Figure 72. The visual result is shown in Figure 73 (only the first 5×3 areas are shown in Figure 73).

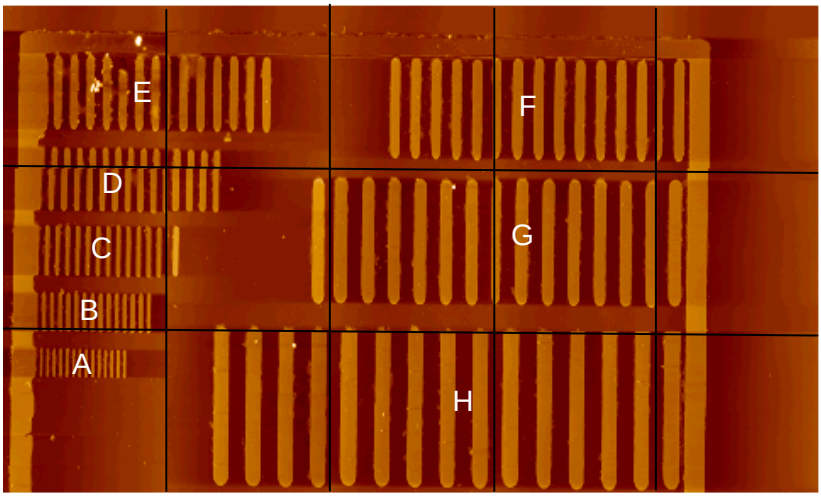

Figure 73: The optical standard used for verification of the integrated system for surface mapping using a edge-to-edge measurement strategy and stitching process. The full line indicates the border between the single measurements.

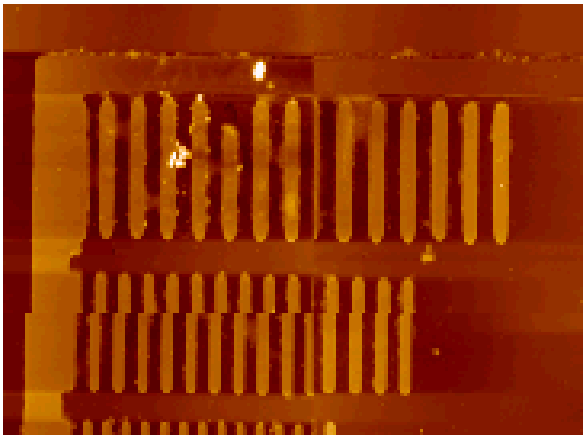

Figure 74: A zoom of the top left corner of Figure 73. Areas D and E are presented in the zoom.

It is seen that certain dislocations occur, which is particularly clear in the top left corner on Figure 73. Knowing the performance of the CMM and AFM, these errors are interpreted as a result of the poor performance of the AFM. Although the long-term stability of the calibration factors C_x and C_y was documented, some short-term variations are clearly seen here. The pattern of the calibration artefact is clearly recognisable and no squareness error is visible. The calibration results were evaluated by means of profile analysis. Each pitch area was analysed using FFT analysis on the profiles. In this way variations in pitch distances within each area of the artefact were quantified (see Table 44 and Table 45). From Table 44 and Table 45 it is seen that especially the small pitch distances show very good accordance with the artefact values whereas there are some differences with respect to the larger pitch distances. This is due to the fact that the larger pitch distances cover more than two areas and thereby reveal the errors introduced by the integrated system. However, the results are satisfactory and demonstrate the good performance of the integrated system.

The same analysis was carried out on results from a measurement where the calibration artefact was rotated 90°. These results are also reported in Table 44 and they are comparable to the first results. As seen from Figure 73, the areas A, B and C are not interrupted when measuring 35 µm × 35 µm, whereas D, E, and to some extent F, G and H, are interesting to analyse. The consequence for the calculated surface roughness parameters of areas containing interruptions in the horizontal plane is relatively small in the case of amplitude roughness parameters.

Pitch distance	Position 1		Position 2 (90° rot.)	
	Avg.[µm]	Std.[%]	Avg.[µm]	Std.[%]
A: 1.6 µm	1.6	0.0	1.6	0.2
B: 2.0 µm	2.0	0.6	2.0	0.2
C: 2.5 µm	2.5	0.8	2.5	0.0
D: 3.2 µm	3.2	1.8	3.1	0.9
E: 4.0 µm	4.2	6.9	4.0	0.1
F: 5.0 µm	5.1	0.2	5.0	1.5
G: 6.4 µm	6.3	0.3	6.3	0.1
H: 8.0 µm	8.1	0.2	8.0	0.1
n	1 stitched area of15 single measurements		1 stitched area of15 single measurements	

Table 44: The observed pitch distances from the optical artefact. In the table, values from to different direction are presented (position 1 and 2).

In Table 45 the average pitch distances and standard deviations of all the performed surface mappings are presented (four complete sets of surface mapping). The deviation between the obtained results and nominal values of the optical artefact are presented as well. The measurement

has been carried out over two mounts and more than 200 measurements have been performed to obtain the four stitched areas.

Pitch distance	All surface mappings		Deviations
	Avg.[µm]	Std.[%]	[µm]
A: 1.6 µm	1.6	1.1	0
B: 2.0 µm	2.0	0.8	-0.0
C: 2.5 µm	2.5	1.3	0.0
D: 3.2 µm	3.2	2.3	-0.1
E: 4.0 µm	4.2	5.6	0.2
F: 5.0 µm	5.1	1.1	0.1
G: 6.4 µm	6.3	0.5	-0.1
H: 8.0 µm	8.0	3.1	-0.0
n	4 stitched areas containing > 200 single measurements		

Table 45: The average pitch distances obtained from all measurements. The deviations between observed and nominal pitch distance are presented.

One set of data for surface mapping was obtained by following the overlapping measuring strategy. The overlap was in the order of 20% (corresponds to ≈ 7µm). A very time consuming stitching process was performed where the single measurements where fitted together as shown in Figure 71. Even though this large stitching process was performed, certain dislocations can still be seen particularly in the top left corner (area D). No difference on the pitch distances compared to the edge-to-edge strategy was observed.

In order to automatically detect large dislocations or other defects of the surface mapping results the geometry of each

single line structure was analysed by using grain analysis (see Figure 75) the following geometry parameters could be determined for each line structure.

- Area
- Volumen
- Perimeter
- Average length

The Grain analysis detects image “grains” in a certain level of the particular measurement, therefore this can only be useful on relatively flat surfaces as the used optical artefact

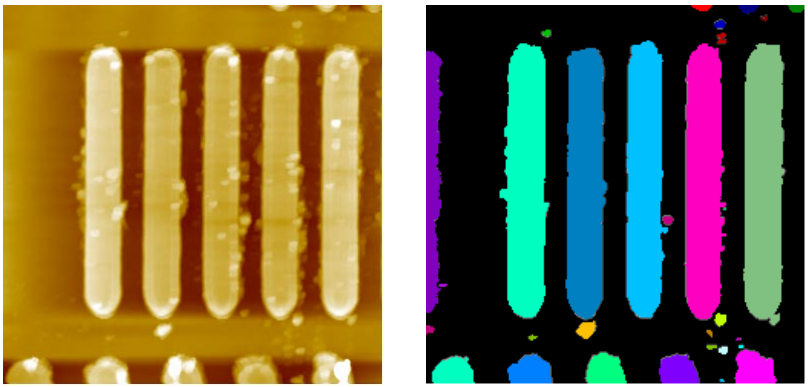

(a) (b)

Figure 75: (a) A measurement obtained on the standard. (b) the corresponding grain analysis.

In order to detect and quantify the deviations for a particular geometry parameter all values obtained for one single area (e.g. C which contains 15 lines) is normalised to the lowest recorded value. Differences will be seen as peaks in the graphs (see Figure 76 and Figure 77).

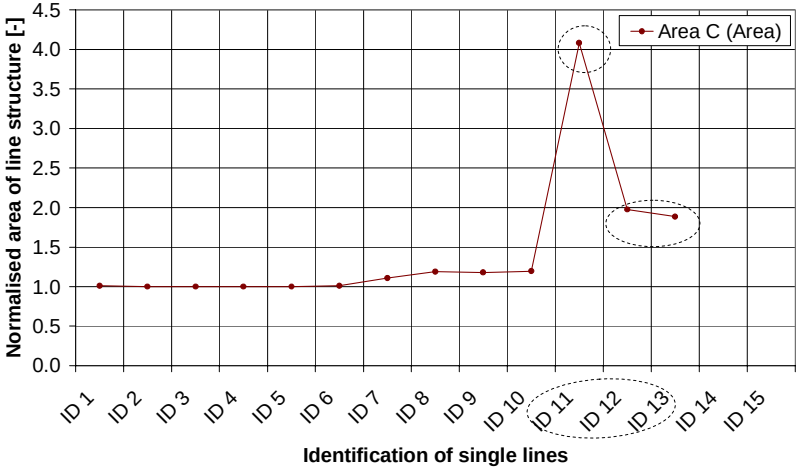

Figure 76: Grain analysis of line structure. Normalised area of line structure of area C. Dotted circles indicate area deviations between the single line structures.

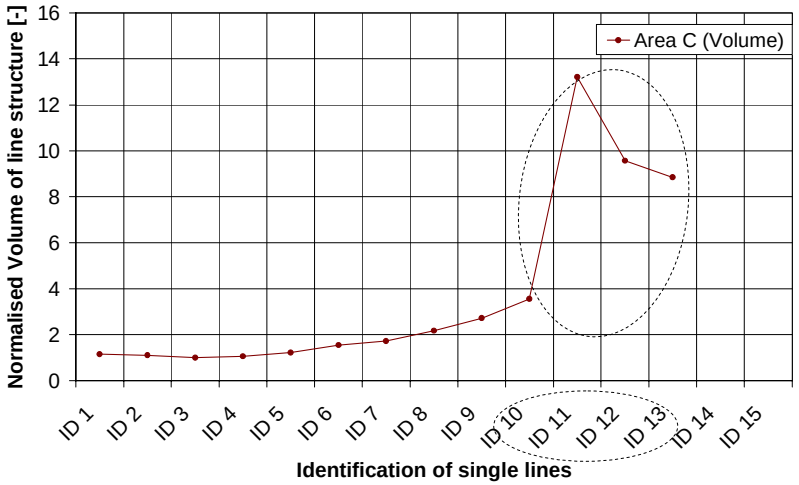

Figure 77: Grain analysis of line structure. Normalised volume of line structure of area C. The dotted circles indicate volume deviation between the single line structures.

By comparing the particular area visually as shown on Figure 78 against the peaks in Figure 76 and Figure 77 an identification of the same defects is possible.

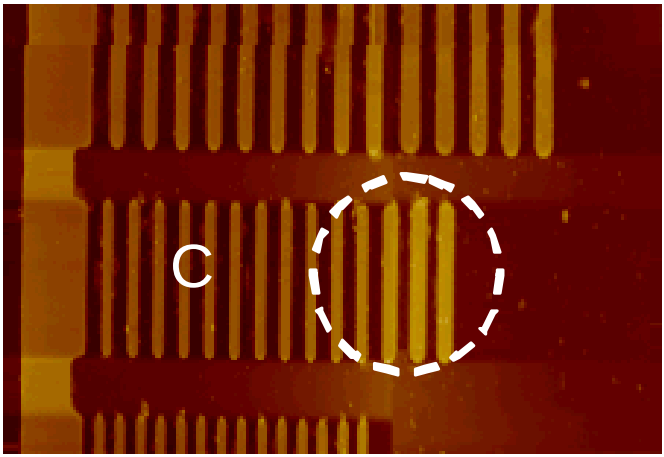

Figure 78: Grain analysis identifies deviations in line 11 - 14.

Grain analysis is a useful tool for detection and identification of relatively large deviation between line structures based on geometrical parameters. It can be difficult to separate small deviations. To quantify dislocations the grain analysis methods is not especially good. Therefore other methods may be developed for this particular error. The grain analysis method is relatively time consuming and has to be improved for further use.

5.3.4 Summary calibration of integrated system

The integrated system has been passing through two phases of calibrations. The first concerns the individual systems (AFM and CMM), the second the integrated system.

The system performance has been quantified using an optical artefact containing a two-dimensional pattern that allows for an exact identification of measured areas when stitching measurements together.

Two methods of stitching processes are introduced (overlapping- or edge-to-edge strategy). The method based on overlapping measurements is very time consuming and the results are not significantly better than the edge-to-edge method. In order to using the edge-to-edge method the individual systems have to be calibrated in order to avoid missing information about the surface. The edge-to-edge method is preferred due to the relative good results compared to the overlapping strategy and the smaller costs in terms of measuring and analysis time. For the integrated system the stability of the CMM has been proved to be very high. The poor short and long-term stability of the AFM makes a calibration before each surface mapping necessary.

To investigate the quality of the stitched images the average pitch distance (of each group of lines) and the geometry of each line structure was determined. The average pitch distance was determined by the use of FFT. The line geometry was determined by using grain analysis. This method is useful for detection of large deviation between lines structures in the same group. Dislocation of line structures can not be proved in this way and a visual inspection is therefore needed.

The system performance has now to be demonstrated on a real surface. A hip joint prosthesis was measured using surface mapping based on an edge-to-edge strategy.

5.4 3D roughness measurements of hip joints

After having verified the performance of the system as described above a hip-joint implant was investigated using surface mapping. The implant is a steel sphere (approximately 58 mm diameter), and due to its size it is suitable for measurement using the integrated system. Other conventional AFMs would require a destruction of the workpiece in order to be able to perform measurements.

Four 25 µm x 25 µm areas were measured edge-to-edge as shown in Figure 79.

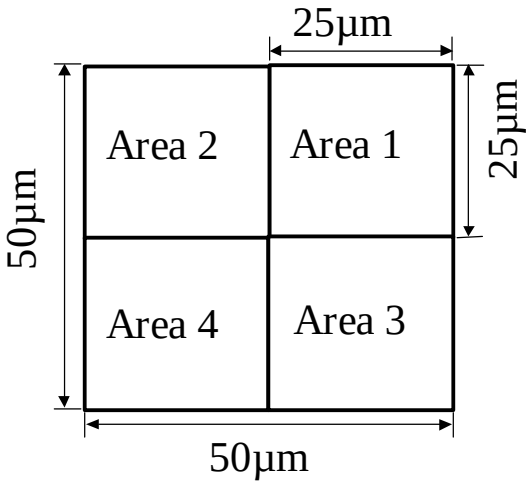

Figure 79: Sequence of scans for surface mapping on the hip joint

A total of three measurements were performed in order to test the repeatability of the integrated system on this type of surface. Each area was aligned using a least squares plane of first order and the four areas were then stitched together. In order to suppress the shifts between the stitched areas (caused by the differences in mean plane of the single areas) a phase correct filter was applied to the stitched area and roughness parameters calculated.

The filter and filter configuration was chosen on the basis of a test. The test couples the loss of information versus the used cutoff length for a particular filter (see Figure 80). The minimum loss of data is obtained when the curve converges for a particular cutoff length. In this particular case the Robust filter was chosen due to a fast convergence for a cutoff in the order of 1/4 to 1/5 of the scan length corresponding to a cutoff at 10-12.5 µm. Further information about the filter can be found in [55].

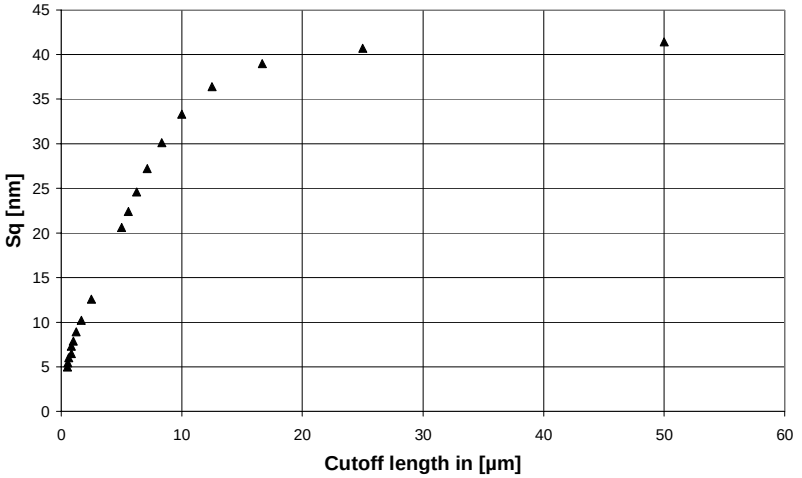

Figure 80: The graph expresses the convergence of Sq as a function of the cutoff length.

The filter has a characteristic that suppresses high peaks and low valleys thus minimizing possible differences in height between the four mean planes of the measured areas as shown in Figure 81.

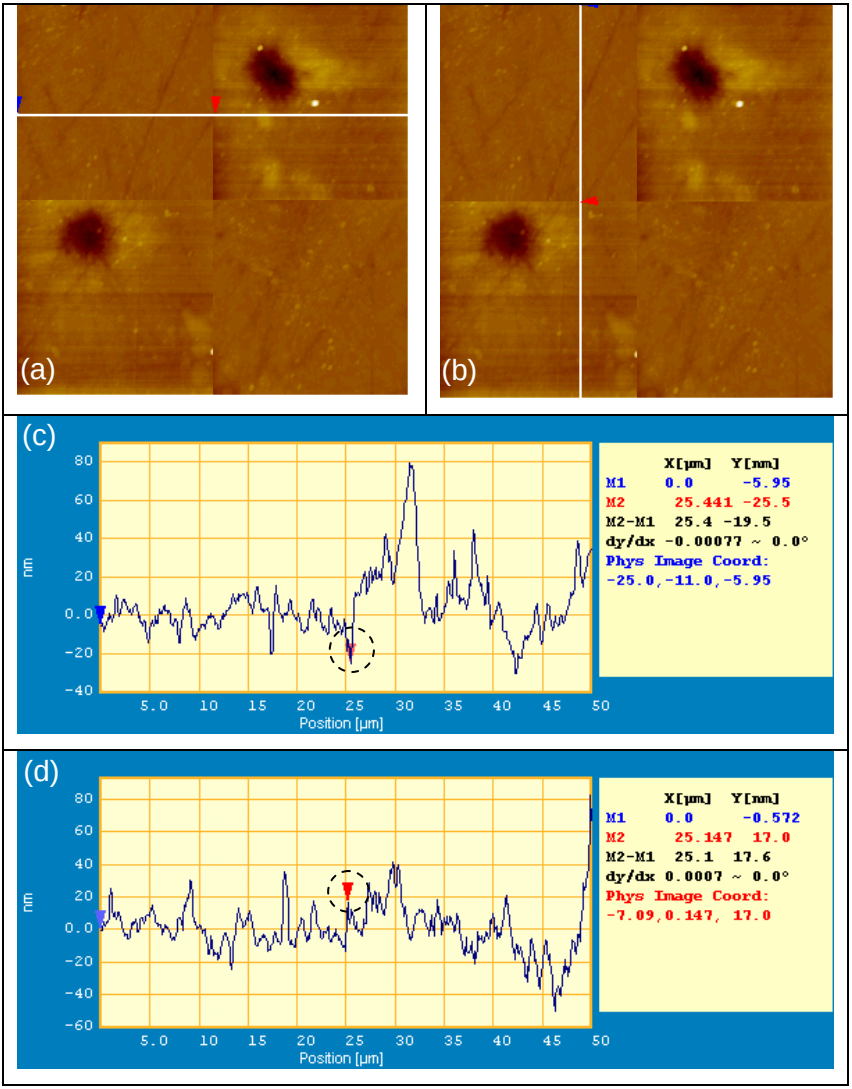

Figure 81: By using a robust filer the remaining effect caused by different mean planes of the single measurements is minimized. The white lines on (a) and (b) indicate the position of the shown profiles. The triangles on profiles (c) and (d) indicate the remaining shift between the stitched areas.

As seen in Figure 82 the four areas vary considerably, each of the areas 1 and 4 contain a large pit, whereas areas 2 and 3 are relatively fine. The borders between the four areas are clearly identified on the image, yet the fine features of the surface indicated with dotted circles are well recognizable between the stitched areas.

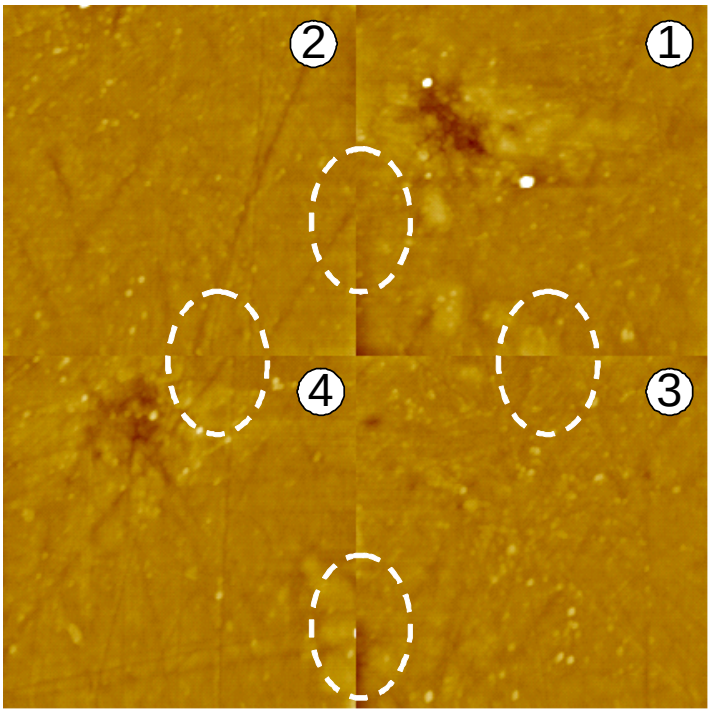

Figure 82: Surface mapping of hip joint implant. Four 25 µm × 25 µm areas measured edge-to-edge and stitched together. Numbers indicate sequence of measurement.

The calculated surface roughness parameters are summarized in Table 46.

	Area 1	Area 2	Area 3	Area 4	Stitched
Sq [nm]	4.3	2.5	2.6	3.4	6.0
Std. [%]	1.6	6.6	1.2	1.5	0.8

Table 46: Results from surface mapping. Stdev. Based on three measurements.

The areas can be grouped into two categories, one with a smaller average roughness than the other. The repeatability of the integrated system is satisfactory with standard deviations per measured area in the order of 5 - 10 %. The average roughness of the stitched area is in the order of 6 nm. As seen in Table 46 there is a relative large difference between the stitched area and the single area measurements. This difference is mainly caused by the remaining displacement between the mean planes of each single measurement despite the filtering process.

The same specimen was measured previously on the MAFM [59], [60], the results obtained in these investigations being based on a single scan area of 40 µm x 24 µm. A Sq value of 2.9 nm was obtained in [59], [60] and this is comparable to the values of areas 2 and 3 in Table 46.

5.5 Conclusions

An integrated system for the characterization of fine surfaces on large workpieces consisting of an atomic force microscope (AFM) mounted on a coordinate measuring machine (CMM) was developed and improved by mounting electronic scales on the X and Y axes of the CMM.

A calibration and performance verification procedure for the integrated system was proposed and applied. The CMM and the AFM were calibrated separately as stand-alone instruments using state-of-the-art calibration methods. Thereafter the performance of the integrated system was

verified using a new procedure developed in this industrial researcher project.

The calibration procedure involves a glass artefact featuring chromium lines with a two-dimensional pattern that allows for an exact identification of measured areas when stitching measurements together.

The system was calibrated in both X, Y and Z directions and used to surface map a hip-joint prosthesis consisting of a steel sphere with a polished surface having 3 nm roughness (Sq).

Chapter 6
SUMMARY AND CONCLUSION

The main conclusions of this industrial researcher project are summarized in the following five paragraphs which refer to the five chapters in this thesis.

Besides the problem identification of this project, *Chapter 1* contains a description of the history, technology and working principle of Scanning Probe Microscopy especially the Atomic Force Microscope. The description is mainly focused on the tube scanner design. Furthermore methods for uncertainty estimation after GUM are summarized.

The aim of *Chapter 2* is to give a short description of state-of-the-art within the area of establishment of traceable standards regarding calibration and performance testing of SPMs. The link between the measurements and the scale on the images from a SPM may in general be performed by measurements on transfer standards. There exists number of different commercial artefacts which are used as calibration standards. In most cases the standards are not specifically designed for use with SPMs. An important design criterion for the standards has been that they should cover the whole range of scan areas of SPM microscopes, but also possess dimensions suitable for classical measurement instruments. The methods normally used to calibrate transfer standards are based on optical principles. Lateral calibration standards are typically calibrated by optical diffraction, vertical calibration standards typically by interference microscopy.

The calibration of AFMs has been a central activity in this industrial researcher project. Therefore, *Chapter 3* gives a general approach for calibration of AFMs and describes the corresponding theory and calibration procedures developed under this project. The method described in this chapter is mainly developed for a metrological atomic force microscope

equipped with capacitive distance sensors. To perform a calibration of an AFM a certain number of steps have to be considered to get the optimal outcome of the work. Depending on the purpose of the calibration and the accuracy level different procedure can be chosen, e.g. A, A-B, A-B-A sequences or other methods. The lateral calibration method is based on an oblique two dimensional grid characterized by its lattice constants in the X and Y direction along with the angle between the two directions. A linear transformation of the scanned and uncorrected image into a corrected image can be defined by a correction parameter C_x for the x-direction, a correction parameter C_y for the Y-direction and a coupling term C_{xy} between the scanned x and y axes. Several methods for determination of the lateral correction parameters and the non-linearity have been demonstrated. The vertical calibration method is based on step height standards after the principle described in ISO 5436. In addition to the implementation of ISO 5436, a thorough analysis was performed and the three most important correction terms were identified. These are thermal drift, “out of plane motion” and the remaining non-linearity of the vertical distance sensor. The histogram and manual point to point methods for step height estimation were presented and evaluated as well.

The validation and performance verification test of the MAFM as described in *Chapter 4* is based on the participation in intercomparisons. In the project period three intercomparisons (SPM*et*, Nano4, Nano2) covering the nanometre range of length measurement have been held. In this thesis only results obtained in the pre-key- and key comparisons are presented (Nano2 and Nano4). Until now one pre-key comparison is finished (Nano 4) and Nano 2 is still running. The parameters concerning the X and Y direction have been established during the work on the intercomparison Nano4 and the parameters concerning the Z-direction on Nano2. The aim of Nano4 was to determine an average pitch distance of two 1D-gratings. The result reported for the pre-key comparison

showed a E_N-value below 1 and therefore the participation in the comparison resulted in a satisfactory result. Finally Nano4 was upgraded to a real key-comparison. The aim of Nano2 was to determine an average step height after an analogy to the ISO 5436 on three transfer step height standards. The microscope was successfully calibrated based on a subdivision of the Z-scale. The subdivision of the Z-scale has improved the uncertainty especially for low step heights. The final results of Nano2 have still to be reported to the pilot laboratory. However the preliminary results indicate good performance. Traceability was established by means of traceable transfer standards covering X, Y and Z. A successful validation and performance verification of the MAFM was performed on behalf of the participation in two intercomparison. As a general conclusion the instrument fulfils the main part of the specification. Some misinterpretations of terms in the specification are likely because of their bad definitions. The Y-axis seems to have a significantly worse behaviour than X and Z. As a general approach for the acceptance test of an instrument it is very important to agree on how the instrument is validated. The procedures and calculation methods used by the manufacturer and the buyer have in principle to be the same. Furthermore a consistent interpretation of the terms used in the specification is necessary. Based on the work on the MAFM and the participation in intercomparisons the first approach for an accredited service with AFM measurement has been established at DFM.

Chapter 5 describes an integrated system for the characterization of fine surfaces on large workpieces consisting of an atomic force microscope mounted on a coordinate measuring machine. The performance of the integrated system have been developed and improved by mounting electronically scales on the X and Y axes. The Z-axis is only used for a rough positioning of the AFM above the surface. A calibration and performance verification procedure

for the integrated system was proposed and applied. The CMM and the AFM were calibrated separately as stand-alone instruments using state-of-the-art calibration methods. All calibration results for the AFM show that the scan range is an important parameter to investigate due to the effect caused by hysteresis and creep. The AFM leave a remaining correction error for the X and Y direction in the order of 3-5% which is the largest error source when performing surface mapping. The CMM has a very small positioning error especially for small steps (30µm-40µm). The performance of the integrated system was verified using a newly developed procedure. The calibration procedure involves a optical flat and a glass artefact featuring chromium lines with a two-dimensional pattern that allows for an exact identification of measured areas when stitching measurements together. Two methods for stitching process were proposed, one using “overlapping measurements” strategy and one based characterization as edge-to-edge strategy. The overlapping strategy is very time consuming and the obtained image seems not to be significantly better then the image created by edge-to-edge. To quantify the quality of the stitched images two methods were used. A Fourier analysis was used to calculate the pitch distance of the glass artefact. The geometry of each single line structure was estimated by the use of grain analysis. The grain analysis is useful for verification of large errors caused by the stitching process. The system was calibrated in both X, Y and Z directions and used to surface map a hip-joint prosthesis consisting of a steel sphere with a polished surface having 3 nm roughness (Sq).

Outcomes of the project for DFM:

- DFM has developed calibration and measuring procedures for a metrology AFM and knowledge about the calibration by using transfer standards. By participating in international key-comparisons DFM has built up reliability regarding its measurements.

- DFM has created knowledge about industrial application of the metrology AFM and thereby recognized tasks where the instrument is relevant to use. Through these tasks knowledge of stating uncertainties for AFM measurements has been established.
- Development of knowledge into the field of applications, measuring procedures, international comparisons and uncertainties has created the necessary basis for DFM to establish an accreditation of AFM measurements.

Outcomes of the project for IPL:

- IPL has developed an integrated system dedicated for performing surface mapping on products which normally not are measurable for AFMs.
- To investigate the behaviour of the integrated system a calibration procedure has been developed. Furthermore a suitable calibration artefact and procedure covering the integrated system have been suggested.

FURTHER WORK

This industrial researcher project has achieved results in the field of calibration of AFMs as well as in the field of integration of an AFM on a CMM. The results have been described in this thesis. During the finalisation of the work a couple of points for further investigation were identified. These points may be seen as new projects or simply as extra experiments to be carried out.

Calibration of Metrology AFM

- Further investigations on the correction parameter covering the Y-direction of the Metrology AFM (C_y).
- Further development of the calibration and measurement procedure based on traceable transfer standards.
- Optimisation of the procedure for measurement uncertainty calculation.

Integrated system

- Establishment of traceability to line standard. This can be done by transferring the traceability from the metrology AFM to the line standard.
- Further development of the calibration procedure to comprise a total uncertainty budget for the integrated system.
- Improvement of the optical system in a way so it is possible to receive a clear image in the normal working position.
- Use of the integrated system in dedicated fields / applications where this special type of instrument is useful, e.g. in the field of micro/nano manufacturing.

REFERENCES

[1] N. Kofod, “Three dimensional characterization of surfaces with focus on AFM”, M.Sc-theses, MM98.50, Department of Manufacturing Enginnering (IPT), The Technical University of Denmark (DTU), 1998 (in Danish).

[2] H. K. Wickramasinghe, ”Progress in Scanning Probe Microscopes”, Acta mater 48 (2000), pp. 347 - 358, Pergamon.

[3] M.G. Heaton, F.M. Serry, “Scanning Probe / Atomic Force Microscope: Technical overview and update”, Application note 48, Digital Instruments, Veeco Metrology Group.

[4] K. Dirscherl, “Online correction of Scanning Probe Microscopes with pixel accuracy”, Ph.D-thesis, IMM-PHD-2000-76, 08-2001, Technical University of Denmark.

[5] The Materials Information Society (ASM), ”Ceramics and Glasses – Engineered Material Handbook, volume 4, ISBN 0-87170-282-7, 1991, US.

[6] N. Kofod, “PZT-Based electro ceramics”, Afløsningsopgave, F97 C3535 Keramiske processer og Materialer (1997) (in danish).

[7] G. Binnig et al,”Atomic Force Microscope”, Phys. Rev. lett., 56(9): pp. 930-933, 1986.

[8] A.A. Baker,”High resolution Atomic Force Microscopy of Polyaccharides”, Ph.D. thesis, University of Bristol, May 1998.

[9] ISO/BIPM, ”ISO Guide to Expression of Uncertainty in Measurement”, Corrected and reprinted, 1995, 1993(E).

[10] J. Pauwels, A. Lamberty, H. Schimmel, “The determination of uncertainty of reference material certified by laboratory intercomparison”. Accred Qual Assur (1998)3: pp.180-184, Spring-Verlag.

[11] Course material for Geometrical metrology and machine testing, 2001 (42215 at DTU).

[12] T. Doiron, J. Stoup, “Uncertainty and Dimensional Calibrations”, J. Res. Natl. Stand. Technol. Vol.102, No. 6, pp. 647-676(1997).

[13] EAL-R2, “Expression of the Uncertainty of Measurement in Calibration”, Edition 1, April 1997.

[14] B.N. Taylor, C.E. Kuyatt, “Guidelines for Evaluating and Expressing the Uncertainty of NIST measurement result” , Technical Note 1297, 1994 Edition National Institute of Standard and Technology (1994).

[15] EAL-R2-S1, “Supplement 1 to EAL-R2, Expression of the Uncertainty of Measurement in Calibration, Examples”, Edition 1, November 1997.

[16] ISO 14253:2, “Geometrical Product Specifications (GPS)-Inspection by measurement of workpieces and measuring equipment-Part 2: Guide to the estimation of uncertainty in GPS measurement, in calibration of measuring equipment and in product verification”, 1st edition 2000-04-10.

[17] P. Bennich, “Tools for uncertainty estimation-GUM, PUMA ect”, Script in Danish. www.bennich.dk/

[18] International vocabulary of basic and general terms in metrology, International Organisation of standardization (ISO), 1993.

[19] EAL-G12, “Traceability of measuring and Test equipment to National standards”, Edition1, Nov. 1995.

[20] L. Koenders, R. Krüger-Sehm, G. Wilkening," Calibration of transfer standards for SPM", Proceedings of the 4th seminar on Quantitative Microscopy QM 2000 Dimensional measurements in the micro- and nanometre range, 2000, PTB-Bericht, pp. 25-29 January 2000

[21] J. Garnaes, N. Kofod, J. F. Jørgensen, A. Kühle, P. Besmens, O. Ohlson, J. B. Ramussen, G. Wilkening, L. Koenders, W. Mirande, K. Hasche, J. Haycocks, J. Nunn, M. Stedman, "Standards for Scanning Probe Microscopes", pp.632-633, proceedings for the 10th international conference on Scanning Tunneling Microscopy / spectroscopy and related Techniques, Seoul, Korea, July 1999.

[22] J. Garnaes, N. Kofod, J. F. Jørgensen, A. Kühle, P. Besmens, O. Ohlson, J. B. Rasmussen, G. Wilkening, L. Koenders, W. Mirande, K. Hasche, J. Haycocks, J. Nunn, M. Stedman, "Nanometer scale transfer Standards", Vol. 2, pp. 134-137, Shaker-Verlag, Paper for the 1st EuSPEN conference May-June 1999.

[23] G. Wilkening," State of the art review on metrology SPMs and calibration means", published by the "EU Network on the Calibration of SPMs". Updated 10-2001.

[24] J. Garnaes, N. Kofod, A. Kühle, P. Besmens, O. Ohlsson, J.B. Rasmussen, G. Wilkening, L. Koenders, W. Mirande, K. Hasche, J. Haycocks, J. Nunn, M. Stedman, "Standards for the calibration of SPMs:design - traceable calibration - application", X. International Colloquium on Surfaces, 31st January to 2nd February 2000.

[25] VLSI Standards Inc.; 3087 North First Street; San Jose, CA 95134-2006, USA; (www.supersite.net/semiH2/vlsi)

[26] Moxtek Inc. Orem, UT 84057, USA; (www.moxtek.com)

[27] MDT-NT Co. Zelenograd Research Institute of Physical Problems; 103460 Moscow, Russia; (www.ntmdt.ru)

[28] NanoSensors Dr. Olaf Wolter GmbH; Wacholderweg 8, 71134 Aidlingen 3, Germany; (www.ourworld.compuserve.co/homepages/nanosensors)

[29] MikroMasch, Silicon-MDT Ldt. POB 50, 1003305 Moscow, Russia.

[30] J.I. Mosley, M.G. Heaton, Application Notes, Veeco Metrology Groupe. WWW.di.com

[31] L. Koenders, Website of Physikalisch-Technische Bundesanstalt regarding “Scanning probe microscopy (SPM), Standards for the calibration of scanning probe microscopes”(www.ptb.de/en/org/5/51/512/espm_nor.htm) last update 09.08.2001.

[32] Measurement performed according to SPMet comparison, European Commission funded research contract SMT4-CT95-2018 "Transfer standards for calibration of scanning probe microscopes".

[33] J.S. Villarrubia (1997) Algorithms for Scanned Probe Microscope, Image Simulation, Surface Reconstruction and Tip Estimation, J. Nat. Inst. Stand. and Technol. 102, pp. 435-454.

[34] P. M. Williams, K. M. Shakesheff, M. C. Davies, D. E. Jackson, C. J. Roberts (1996) Blind reconstruction of scanning probe image data, JVST B 14(2), pp. 1557-62.

[35] J. Nunn , ”Calibration of 2 dimensional magnification standards for SPMs and SEMs through optical diffraction: Method, traceability and uncertainties”,

Proceedings of the 4th seminar on Quantitative Microscopy QM 2000 Dimensional measurements in the micro- and nanometre range, 2000, PTB-Bericht, pp. 17-24, January 2000.

[36] Swiss Federal office of Metrology – specification from website. www.metas.ch

[37] U. Brandt, W. Hillmann, “Calibration of step height standards for nanometrology using interference microscopy and stylus profilometry”, Precision Engineering 17:pp. 22-33, 1995.

[38] K.J. Gasvik, ”Optical Metrology”, ISBN 047191246B, 1987.

[39] W. Hillmann, U. Brandt, M. Krystek, “Capability and limitations of interference microscopy for two- and three dimensional surface measuring technology”, Measurement vol. 19, No. 2, pp. 95-102, 1996.

[40] K.J. Stout, L. Blunt, ”Three dimensional Surface Topography” Second edition, ISBN 1 85718 0267,. 2000.

[41] PTB certificates.

[42] European Commission funded research contract SMT4-CT95-2018 "Transfer standards for calibration of scanning probe microscopes".

[43] Surfstand, “Development of a basis for 3D Surface Roughness Standards”, EC Sponsored project (No. SMT4 CT98-2209).

[44] J.F. Jørgensen, C.P. Jørgensen, J. Garnaes, ”Lateral Metrology using scanning probe microscopes, 2D pitch standards and image processing”, Appl. Phys. A 66, pp. 847 - 852 (1998)

[45] J.F. Jørgensen et al., “Calibration, drift elimination and molecular structure analysis”, JVST B, 12(3), pp.1698-1701 (1994).

[46] J. Garnaes et al, “Two-dimensional nanometer-scale calibration based on one-dimensional gratings”, Appl. Phys. A 66, pp.831-835(1998).

[47] N. Kofod, J. Garnaes, J.F. Jørgensen, “Method for lateral calibration of Scanning Probe Microscopes based on two dimensional transfer standards”, Proceedings of the 4th seminar on Quantitative Microscopy QM 2000 Dimensional measurements in the micro- and nanometre range, 2000, PTB-Bericht, pp. 36-43 January 2000.

[48] N. Kofod, J. Garnaes, J.F. Jørgensen, ”Calibrated line measurements with an Atomic Force Microscope, 1st Topical EuSPEN conference, Lyngby, pp. 373-381, Denmark May 2000.

[49] F. Meli, R. Thalmann, “Das Metrologie-Raserkraftmicroskop”, OFMET info, Vol. 6 no. 1, pp. 1-8, 1999 – Switzerland.

[50] L. Koenders, “WGDM-7 Preliminary comparison on nanometrology, According to the rules of CCL key comparisons, Nano 2: Step height standards” 7. sep. 2000, Germany.

[51] J. Pekelsky, ”Chairman’s Report on the 5th WGDM Meeting”, Consultative Committee for Length – CCL, Working Group on Dimensional Metrology – WGDM, 19-20 Sept 2000, Sèvres, CCL/WGDM/00-46.

[52] R. Breil, T. Fries, J. Garnaes, J. Haycocks, D. Huser, J. Joergensen, W. Kautek, L. Koenders, N. Kofod, K.R. Koops, R. Korntner, B. Lindner, W. Mirande, A. Neubauer, J. Peltonen, G.B. Picotto, M. Pisani, H. Rothe, M. Sahre, M. Stedman and G. Wilkening,

"Intercomparison of Scanning Probe Microscopes", Euspen 2001, Vol 1, pp. 510-513, Turin, Italy.

[53] Dimension™ 3100 system equipped with a metrology head , Digital Instruments Homepage, WWW.di.com

[54] Scanning Probe Image Processor (SPIP), Developed by Imagemetrology APS. www.imagemet.com

[55] J. F. Jørgensen, "Scanning Probe Microscopy image resortion and analysis", Ph.D thesis 1993. The Technical University of Denmark.

[56] National Physical Laboratory (NPL), "Certificate of calibration - IBSEN 2D 1000 Prototype Standard", Reference: LR0304/99001/DR1/116, Date of issue: 08 January 1999 - UK.

[57] J.F. Jørgensen, Imagemetrology Aps (personal reference).

[58] F. Meli, "Z-calibration of a metrology AFM scanner using an interferometer and a tilting device together with a linear displacement stage", Proceedings of the 3rd Seminar on Quantitative Microscopy, November 1998, Lyngby, Denmark, PTB-F-34 pp. 61-67 (1998).

[59] J. Garnaes, N. Kofod, A. Kühle, C. Nielsen, K. Dirscherl, L. Blunt, "Treaceable step height and roughness measurements with atomic force microscopes", 2nd International Conference in euspen, May 2001 Italy, Vol 1, pp. 514-517.

[60] J. Garnaes, N. Kofod, A. Kühle, C. Nielsen, K. Dirscherl, L. Blunt, "Treaceable step height and roughness measurements with atomic force microscopes" (accepted for publication in Precision Engineering).

[61] Measurement carried out for the NANO2 pre key comparison (2001).

[62] C. J. Jensen, ”Calibrated atomic force microscope measurements of Vickers hardness indentations and tip production and characterization for scanning tunnel microscope”, Ph.d. thesis, DFM and IPL (1998).

[63] Griffith et al, “Dimentional metrology with scanning probe microscopes”, J. Vac. Sci. Technol. B 13(3), May 1995, pp. 1100-1105.

[64] DS/ISO 5436:1987, Calibration specimens - Stylus instruments Types, calibration and use of specimens.

[65] H. Edwards et al, “Vertical metrology using scanning-probe microscopes: Imaging distortions and measurement repeatability”, J. appl. phys, Vol. 83, No.8 (April 1998), pp. 3952-3971.

[66] H. Edwards, New method to estimate step heights in scanning-probe microscope images, Nanotechnology 8 pp. 6-9 (1997).

[67] H. Edwards, J .F. Jørgensen, J. Dagata, Y. Strausser, J. Schneier, Influence of data analysis and other factors on the short-term stability of vertical scanning-probe microscope calibration measurements, J. Vac. Sci. Technology. B 16(2) Mar/Apr (1998).

[68] H. N. Hansen, ”Verification and calibration of coordinate measuring machines”, Ph.d thesis, IPT, DTU, Publ. nr. MM97.06 - 1997, Denmark.

[69] E. Trapet, F. Wäldele, “The Virtual CMM concept”, Oral presentation at the Euroconference” Advanced mathematical tools in metrology”, Lady Margaret Hall, Oxford, England, 27.-30. September 1995.

[70] K. Busch, H. Kunzmann, F. Wäldele, “Calibration of coordinate measuring machines”, Precision Engineering Vol. 7, No. 3, July 1985, pp. 139-144.

[71] EU-project SMT4-CT95-2018, ”Transfer standards for calibration of Scanning Probe Microscopes”.

[72] Dimension 3100 SPM with metrology AFM head, Digital Instrument. WWW.DI.com.

[73] National Physical Laboratory (NPL)”Certificate of calibration - IBSEN 2D 1000 Prototype Standard”, Reference: LR0304/99001/DR1/116, Date of issue: 08 January 1999 - UK.

[74] F. Meli, “Final instructions for WGDM-7: Preliminary comparison on nanometrology According to the rules of CCL key comparisons Nano4: 1D-Gratings”, OFMET EAM UFMET, Nov.1998 – Switzerland.

[75] F. Meli,” International comparison in the field of nanometrology: Pitch of 1D gratings (Nano4)”, 2nd International Conference in euspen, May 2001 Italy, Vol 1, pp. 358-361.

[76] N. Kofod, J. Garnaes, “Measurement Report” for participating in WGDM-7: Preliminary comparison on nanometrology According to the rules of CCL key comparisons Nano4: 1D-gratings.-DFM 2000.

[77] Software called “DFM-GUM, version 2.1” Danish Institute of Fundamental Metrology- for uncertainty calculation after GUM– Denmark.

[78] N. Kofod, J. Garnaes, “Preliminary Measurement Report” for participating in WGDM-7: Preliminary comparison on nanometrology According to the rules of CCL key comparisons Nano2: Step height - Not published yet.

[79] Lonardo P.M., Trumpold H., De Chiffre L., 1996, Progress in 3D surface microtopography characterization, Annals of the CIRP, 45/2: pp. 589-598.

[80] Vorburger T.V. et al, 1997, Industrial uses of STM and AFM, Annals of the CIRP, 46/2: pp. 597-620.

[81] De Chiffre, L. et al, 2000, Quantitative characterization of surface texture. Annals of the CIRP, 49/2: pp. 635-652.

[82] De Chiffre, L., Hansen, H.N., Kofod, N., 1999, Surface topography characterization using an atomic force microscope mounted on a coordinate measuring machine. Annals of the CIRP, 48/1: pp. 463-466.

[83] N. Kofod, H. N. Hansen, L. De Chiffre, "Characterization of fine surfaces using an atomic force microscope mounted on a coordinate measuring machine", 1st EuSPEN conference, Vol. 2, pp. 278-281, Shaker-Verlag, May-June 1999.

[84] H.N. Hansen, N. Kofod, L. De Chiffre, T. Wanheim, "Calibration and Industrial Application of Instrument for Surface Mapping based on AFM", Annals of the CIRP, 2002, in press.

[85] H. Kunzmann et al," Scales vs. Laser Interferomters - Performance and Comparison of two Measuring systems", Keynote papers, Annals of the CIRP Vol. 42/2/1993, pp. 753 - 767.

[86] VDI/VDE 2617. Accuracy of coordinate measuring machines, 1989, Characteristic parameters and their checking. Part 3, Components of measurement deviation of the machine, Verein Deutscher Ingenieure, Düsseldorf, Germany.

[87] Kofod N., Hansen H.N., De Chiffre L., 1998, Integration of atomic force microscope on coordinate measuring machine, Proceedings of the 3rd seminar on quantitative microscopy (QM'98), Lyngby, Denmark.

APPENDIX LIST

Appendix 1: The effect of alignment techniques on the measurable values.

- *Graph 1: Effect on X and Y-values. 50µm×50µm measurement on a VLSI grating. Measured with the MAFM.*
- *Graph 2: Effect on Mean position error (lateral). 50µm×50µm measurement on a VLSI grating. Measured with the MAFM.*
- *Graph 3: Effect on Z-values. 50µm×50µm measurement on a VLSI grating. Measured with the MAFM.*
- *Graph 4: Effect on Sa roughness. 20µm×20µm measurement on a polished hip joint. Measured with the MAFM.*

Appendix 2: Test of new algorithms

- *Graph 5: No. of periodical structures vs. deviation on pitch distance.*
- *Graph 6: No. of image pixels vs. deviation on X,Y-pitch distances.*

Appendix 3: All results obtained in Nano4.

Appendix 4: Uncertainties obtained in pre-key comparison Nano2

Appendix 1 - The effect of alignment techniques on the measurable values.

Graph 1: Effect on X and Y-values. 50µm×50µm measurement on a VLSI grating. Measured with the MAFM.

Graph 2: Effect on Mean position error (lateral). 50µm×50µm measurement on a VLSI grating. Measured with the MAFM.

Graph 3: Effect on Z-values. 50µm×50µm measurement on a VLSI grating. Measured with the MAFM.

Graph 4: Effect on Sa roughness. 20µm×20µm measurement on a polished hip joint. Measured with the MAFM.

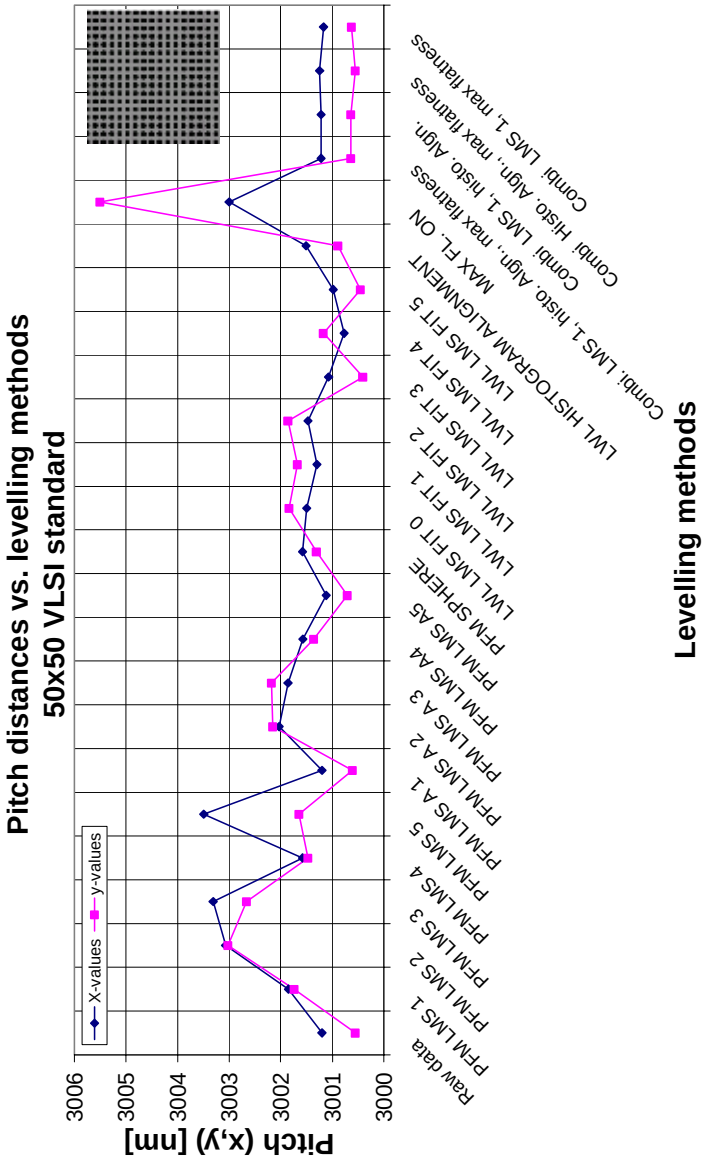

Graph 1: Pitch vs. different levelling techniques.

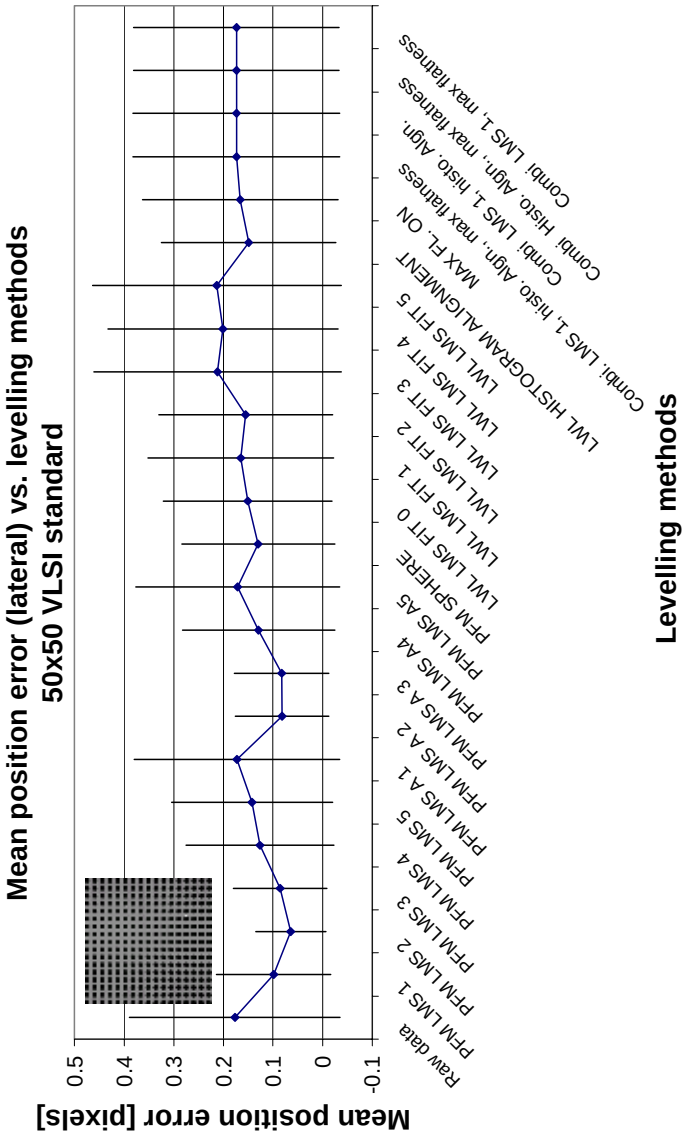

Graph 2: Mean position error different levelling techniques.

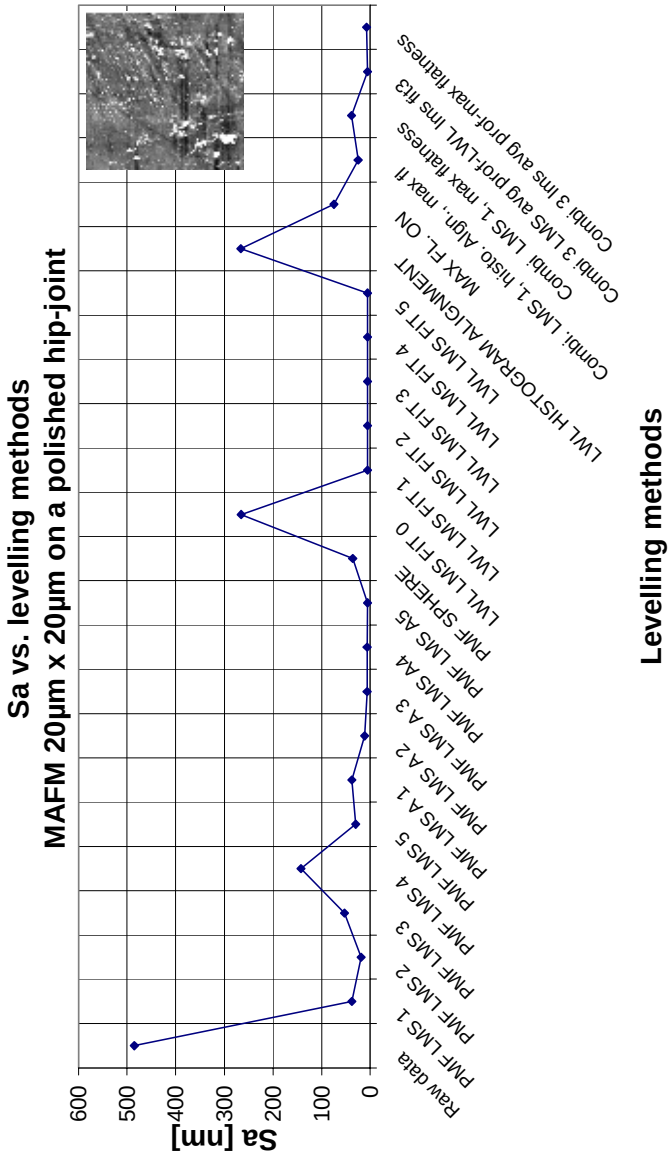

Graph 3: Sa roughness vs. different levelling techniques.

Appendix 2 - Test of new alogithms

Graph 5: No. of periodical structures vs. deviation on pitch distance.

Graph 6: No. of image pixels vs. deviation on X,Y-pitch distances.

Behaviour of analytical and numerical solution (example)

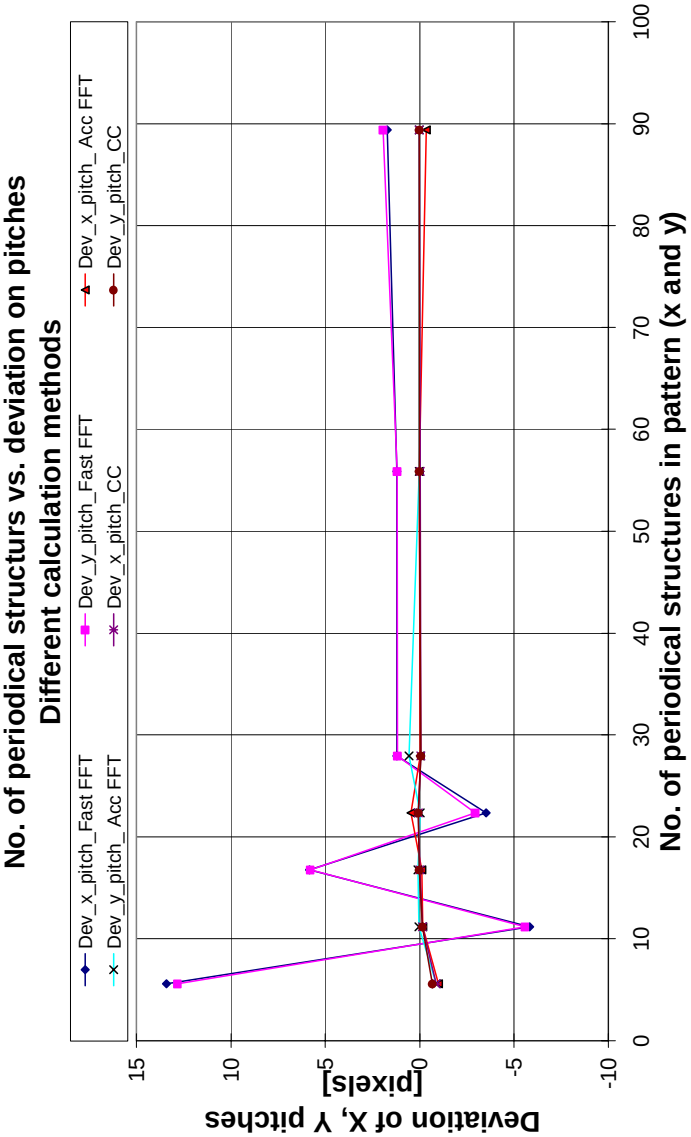

Graph 4: No. of periodical structures vs. deviation on pitch distance.

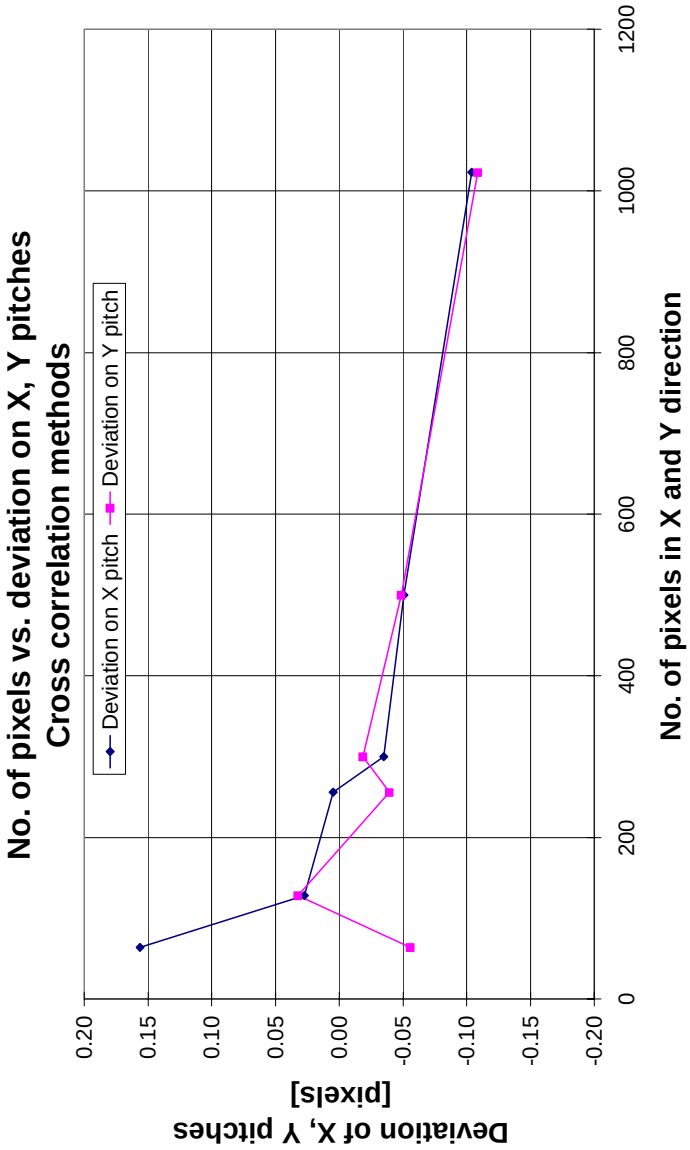

Graph 5: No. of image pixels vs. deviation on X,Y-pitch distances.

Appendix 3: All results obtained in Nano4

All results from measuring on EAM 700/1

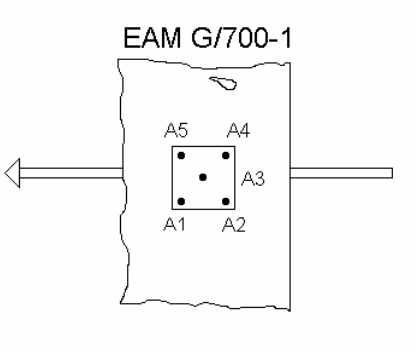

Area	EAM700 Average-1	U (k=1)
1	700.61	0.493
2	700.639	0.477
3	700.393	0.477
4	700.093	0.479
5	700.509	0.479
1-1L	700.235	0.478
1-1M	700.474	0.479
2-1L	700.376	0.479
2-1M	700.366	0.479
.4-1	700.21	0.481
5-1L	700.337	0.478
5-1M	700.361	0.478
Average	700.384	0.480

All results from measuring on EAM 300/1

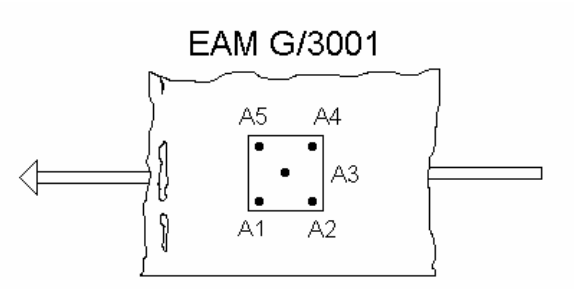

Area	EAM300 Average-1	U (k=1)
1	287.52	0.196
2	287.459	0.196
3	287.47	0.196
4	287.479	0.196
5	287.436	0.196
Average	287.473	0.196

Appendix 4 Uncertainties obtained in pre-key comparison Nano2

For SH70

Quantity (unit)	Distribution	x_i	$u(x_i)$	ν_i	c_i	$u_i(y)$	$r(x_i,y)$
Reference step height h_{ref} [nm]	Normal	759,7	4,1	infinity	0,0897368	0,3679209	0,5886896
Observed height of reference $h_{obs,ref}$ [nm]	Normal	733,768	0,5	6	-0,092908	-0,046454	-0,074329
Observed average step height Δz_o [nm]	Normal	65,846	0,05	42	1,0353409	0,051767	0,0828295
Error due to thermal drift δz_d [nm]	Normal	0	0,1	infinity	1	0,1	0,1600044
Error due to image bow δz_c [nm]	Normal	0	0,4	infinity	1	0,4	0,6400175
Error due to tilt of sample δz_t [nm]	Normal	0	0,02	infinity	1	0,02	0,0320009
Error due to roughness δz_r [nm]	Normal	0	0,2	infinity	1	0,2	0,3200088
Error due to nonlinearity of z-scale δz_l [nm]	Normal	0	0,2	infinity	1	0,2	0,3200088
	Normal	= 80	0,6249829	infinity			

Conf. level =	95,45%	k =	2,0000
Result =	= 80	U =	1,2

For SH800

Quantity (unit)	Distribution	x_i	$u(x_i)$	ν_i	c_i	$u_i(y)$	$r(x_i,y)$
Reference step height h_{ref} [nm]	Normal	759,7	4,1	infinity	1,0304273	4,224752	0,9662807
Observed height of reference $h_{obs,ref}$ [nm]	Normal	733,768	0,5	6	-1,066844	-0,533422	-0,122004
Observed average step height Δz_o [nm]	Normal	756,0946	0,2	42	1,0353409	0,2070682	0,0473604
Error due to thermal drift δz_d [nm]	Normal	0	0,4	infinity	1	0,4	0,0914876
Error due to image bow δz_c [nm]	Normal	0	0,4	infinity	1	0,4	0,0914876
Error due to tilt of sample δz_t [nm]	Normal	0	0,1	infinity	1	0,1	0,0228719
Error due to roughness δz_r [nm]	Normal	0	0,6	infinity	1	0,6	0,1372314
Error due to nonlinearity of z-scale δz_l [nm]	Normal	0	0,5	infinity	1	0,5	0,1143595
	Normal	= 800	4,3721786	infinity			

Conf. level =	95,45%	k =	2,0000
Result =	= 800	U =	8,7